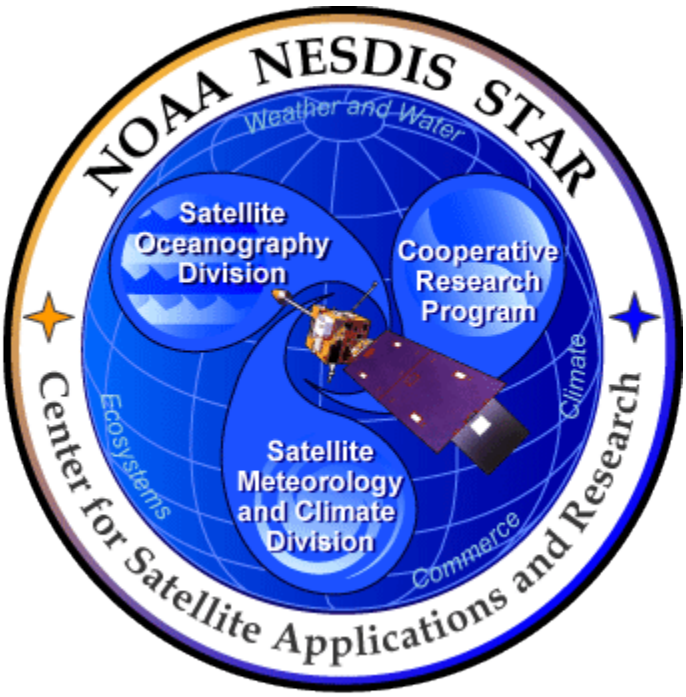

NOAA NESDIS
CENTER for SATELLITE APPLICATIONS and RESEARCH

GOES-R Advanced Baseline Imager (ABI) Algorithm Theoretical Basis Document For Derived Motion Winds

Jaime Daniels, NOAA/NESDIS/STAR
Wayne Bresky, IMSG, Inc.
Steve Wanzong, Chris Velden, Howard Berger, UW/CIMSS

Version 3.1
February 2019

TABLE OF CONTENTS

LIST OF FIGURES

LIST OF TABLES

LIST OF ACRONYMS

ABI – Advanced Baseline Imager
AIADD – Algorithm Interface and Ancillary Data Description
AIT – Algorithm Integration Team
AQC - Automatic Quality Control
ASCII - American Standard Code for Information Interchange
ATBD – Algorithm Theoretical Basis Document
AVHRR - Advanced Very High Resolution Radiometer
AWG – Algorithm Working Group
CC – Cross Correlation
CONUS – Continental United States
CRTM – Community Radiative Transfer Model
CTP – Cloud-top Pressure
NWP – Numerical Weather Prediction
DMW – Derived Motion Winds
DMWA – Derived Motion Winds Algorithm
EE – Expected Error
EUMETSAT - European Organization for the Exploitation of Meteorological Satellites.
FD – Full Disk
F&PS – Functional and Performance Specification
GFS – Global Forecast System
GOES – Geostationary Operational Environmental Satellite
GPO – GOES-R Program Office
IGFOV – Instantaneous Geometric Field of View
INR – Image Navigation and Registration
IO – Input/Output
IR – Infrared
LWIR – Longwave Infrared
LZA – Local Zenith Angle
MRD – Mission Requirements Document
MSG – Meteosat Second Generation
MODIS - Moderate Resolution Imaging Spectroradiometer
MVD – Mean Vector Difference
MSFC – Marshall Space Flight Center
NASA – National Aeronautics and Space Administration
NCSA – National Center for Super Computing Applications
NCEP – National Centers for Environmental Prediction
NESDIS – National Environmental Satellite, Data, and Information Service
NOAA – National Oceanic and Atmospheric Administration
NWP – Numerical Weather Prediction
OSDPD – Office of Satellite Data Processing and Distribution
PDF – Probability Distribution Function
PG – Product Generation
PORD – Performance Operational Requirements Document
QC – Quality Control

QI – Quality Indicator
RAOB – Radiosonde Observation
RMSE – Root Mean Square Error
SD – Standard Deviation
SEVIRI – Spinning Enhanced Visible Infrared Imager
SOI – Successive Order of Interaction
SSD – Sum of Squared Differences
STAR – Center for Satellite Applications and Research
SWIR – Shortwave Infrared
TELL – Tracking Error Lower Limit
TOA – Top of Atmosphere
TRR – Test Readiness Review
VAGL - Vendor Allocated Ground Latency
VIS – Visible
WRF – Weather Research and Forecasting

ABSTRACT

This Derived Motion Winds (DMW) Algorithm Theoretical Basis Document (ATBD) contains a description (including the physical basis) of an algorithm for estimating atmospheric winds from images taken by the Advanced Baseline Imager (ABI) flown on the Geostationary Operational Environmental Satellite-Series R (GOES-R) series of National Oceanic and Atmospheric Administration (NOAA) geostationary meteorological satellites. A brief overview of the GOES-R observing system is followed by a more specific description of the Derived Motion Winds algorithm, validation efforts, and planned improvements.

1 INTRODUCTION

1.1 Purpose of This Document

The derived motion wind Algorithm Theoretical Basis Document (ATBD) provides a description of and the physical basis for the estimation of atmospheric wind from observations from the Advanced Baseline Imager (ABI) flown on the GOES-R series of NOAA geostationary meteorological satellites. The Derived Motion Wind Algorithm (DMWA) estimates not only the speed and direction of identified tracers (clouds and/or moisture gradients), but also their height in the atmosphere. This document also provides details on the evaluation of the DMWA performance during the development phase.

The central purpose of this ATBD is to facilitate development of operational Product Generation (PG) software for the derived motion wind product which is to be implemented within the GOES-R Ground Segment product generation subsystem.

1.2 Who Should Use This Document

The intended users of this document are those interested in understanding the physical basis of the algorithms and how to use the output of this algorithm to optimize the use of the derived motion wind output for a particular application. This document also provides information useful to anyone maintaining or modifying the original algorithm.

1.3 Inside Each Section

This document is broken down into the following main sections.

- **System Overview**: Provides relevant details of the ABI DMWA system and gives a brief description of the products generated by the algorithm.

- **Algorithm Description**: Provides a detailed description of the DMWA algorithm including its physical basis, its input and its output.

- **Assumptions and Limitations**: Provides an overview of the current limitations of the approach and gives the plan for overcoming these limitations with further algorithm development.

1.4 Related Documents

This document currently does not relate to any other document outside of the specifications of the GOES-R Ground Segment Mission Requirements Document (MRD) and Functional and Performance Specification (F&PS) and to the references given throughout.

1.5 Revision History

Version 0.1 of this document was created by members of the GOES-R winds algorithm development team and its intent to accompany the delivery of the version 1.0 derived motion winds algorithm to the GOES-R AWG Algorithm Integration Team (AIT). (May 2008)

Version 0.2 of this document was created by members of the GOES-R winds algorithm development team and its intent is to accompany the delivery of the version 3.0 derived motion winds algorithm to the GOES-R AWG Algorithm Integration Team (AIT). (June 2009)

Version 1.0 of this document was created by Jaime Daniels, Wayne Bresky, and Steve Wanzong in response to internal AWG review items. This version of the ATBD still accompanies the version 3.0 of the derived motion winds algorithm to the GOES-R AWG AIT. (September 30, 2009)

Version 1.1 of this document was created by Jaime Daniels, Wayne Bresky, and Steve Wanzong and its intent is to accompany the delivery of the version 4.0 derived motion winds algorithm to the GOES-R AWG Algorithm Integration Team (AIT). (June 2010)

Version 1.2 of this document was created by Jaime Daniels, Wayne Bresky, and Steve Wanzong and its intent is to accompany the delivery of the version 5.0 derived motion winds algorithm to the GOES-R AWG Algorithm Integration Team (AIT). (August 2010)

Version 2.0 of this document was created by Jaime Daniels, Wayne Bresky, and Steve Wanzong in response to internal AWG and STAR review items. This version of the ATBD still accompanies the version 5.0 of the derived motion winds algorithm to the GOES-R AWG AIT. (September 2010)

Version 2.1 of this document was created by Jaime Daniels, Wayne Bresky, and Steve Wanzong to reflect corrections/additional information as a result of technical interactions the winds team had with AER over the past year. (July 2012)

Version 3.1 of this document was created by Jaime Daniels, Wayne Bresky, and Steve Wanzong to update the section on the gross forecast difference test and the cloud top band 8 height assignment method.

2 OBSERVING SYSTEM OVERVIEW

This section will describe the products generated by the GOES-R ABI Derived Motion Winds Algorithm (DMWA) and the requirements it places on the sensor.

2.1 Products Generated

The GOES-R ABI DMWA employs a sequence of images to arrive at an estimate of atmospheric motion for a set of targeted tracers viewed in selected spectral bands. These targets include well defined cloud edges or moisture gradients. Table 1 outlines the specifications for the GOES-R derived motion winds product as defined in the latest version of the GOES-R Ground Segment Project Functional and Performance Specification (F&PS) requirements document.

Table 1: F&PS Requirements for the Derived Motion Winds product

Derived Motion Winds	**Specification**
Geographic Coverage	Full Disk, CONUS, Mesoscale
Vertical Resolution	Cloud Motion Vector winds: At cloud tops; Clear-Sky Water Vapor winds: 200 mb
Horizontal Resolution	10 km *(Changes pending:* *FD: 38km* *CONUS: 38km* *Mesoscale: 38km*
Mapping Accuracy	5 km
Measurement Range	Speed: 0-300 kts (0 to 155 m/s) & Direction: 0 to 360 degrees *(Change pending: Speed 5.83-300 kts (3-155 m/s)*
Measurement Accuracy	Mean Vector Difference: 7.5 m/s
Refresh Rate/Coverage Time (Mode 3)	FD: "60 mins (based on a single set of 3 sequential images 5 or more minutes apart); CONUS: 15 minutes; Mesoscale: 5 minutes)
Refresh Rate (Mode 4)	FD: "15 mins (based on a single set of 3 sequential images 5 or more minutes apart);*Change pending:60mins)* CONUS: 15 minutes; Mesoscale: 5 minutes)
VAGL (Mode 3 or 4)	806s
Measurement Precision	3.8 m/sec *(Change pending to "4.2 m/s")*
Product Qualifiers	
Temporal Coverage	Day and night
Product Extent	Quantitative out to at least 62 degrees LZA and qualitative beyond

Cloud Cover Conditions	Clear conditions down to feature of interest associated with threshold accuracy
Product Statistics	Over specified geographic area

The DMW products will be produced for each of the ABI bands designated in Table 2 over the various ABI Full Disk (FD), Continental United States (CONUS), and Mesoscale scan domains.

2.2 Instrument Characteristics

The GOES-R ABI has been designed to address the needs of many users of geostationary data and products (Schmit, et al, 2005) It will offer more spectral bands (to enable new and improved products), higher spatial resolution (to better monitor small-scale features), and faster imaging (to improve temporal sampling and to scan additional regions) than the current GOES imager.

Table 2. Channel numbers and associated wavelengths for the GOES-R ABI, as well as those channels that will be employed operationally by the DMWA in "Day1" applications

Channel Number	*Wavelength Range (um)*	*Central Wavelength (um)*	*Nominal subsatellite IGFOV (km)*	*Used in DMWA*
1	0.45-0.49	0.47	1	
2	0.59-0.69	0.64	0.5	✓
3	0.846-0.885	0.86	1	
4	1.371-1.386	1.38	2	
5	1.58-1.64	1.61	1	
6	2.225-2.275	2.26	2	
7	3.80-4.00	3.9	2	✓
8	5.77-6.6	6.15	2	✓
9	6.75-7.15	7.0	2	✓
10	7.24-7.44	7.4	2	✓
11	8.3-8.7	8.5	2	
12	9.42-9.8	9.7	2	
13	10.1-10.6	10.35	2	
14	10.8-11.6	11.2	2	✓
15	11.8-12.8	12.3	2	
16	13.0-13.6	13.3	2	

The spatial resolution of the ABI data will be nominally 2 km for the infrared bands and 0.5 km for the 0.64-μm visible band. Table 2 provides a summary of the 16 spectral bands that will be available on the ABI. Those channels that are expected to be used in DMW feature tracking, at least initially for "Day-1" operational production, include the 0.64um, 3.90um, 6.15um, 7.0um, 7.4um, and 11.2um bands. These are the so-called heritage channels that are used operationally today to derive atmospheric motion vectors.
Derived motion winds will be generated separately from each of these six ABI bands.

Collectively, the derived motion winds from each of the six runs are the derived motion winds product.

The ABI will scan approximately 5 times faster than the current GOES imagers. This brings opportunities and flexibility for the collection of more observations that will enable user needs to be better met. At the present time, there are two anticipated scan modes for the ABI. The first is a flexible scanning scenario that will provide one scan of the Full Disk (FD), three scans (5 minutes apart) of the Continental United States (CONUS), and 60 scans (30 seconds apart) over a selectable 1000 km ×1000 km area every 15 minutes. The second mode is continuous full disk scanning where full disk coverage is obtained every 5 minutes. In practice, some combination of both modes may be used. For example, three sequential FD images that are 5 minutes apart may be taken every hour for the generation of DMWs. The flexible scanning mode would then be used for the rest of the hour.

Table 3. Image navigation and registration pre-launch specifications (3σ) for day and night (in black) for the GOES-8-12, GOES-13/O/P, and GOES-R series of satellites. In red are actual computed image navigation and registration performance statistics (in km) for GOES-12 and GOES-13. (Computed values courtesy of G. Jedlovek; NASA/MSFC)

	GOES 8-12 Day/Night	GOES 13,O,P Day/Night	GOES-R Day/Night
Absolute Navigation (km)	**4.0 / 6.0** **(4.5 /5.0)**	**2.3**	**1.0 / 1.5**
Within Image (km)	**1.6 / 1.6**	**2.0**	**1.0**
Image-to-Image (km)			
5-7 min	**--** **(2.3 / 2.3)**	**--** **(0.6/0.6)**	**0.75** **1.0**
15 min	**1.5 / 2.5** **(2.8 / 3.2)**	**1.3** **(1.0/1.3)**	**0.75** **1.0**
90 min	**3.0 / 3.8**	**1.8**	**0.75** **1.0**
24 hr	**6.0 / 6.0**	**4.0**	**--**

Significant improvements in the performance of the image navigation and registration are expected with GOES-R. This is expected to translate to more accurate DMWs. The stability of the frame-to-frame navigation, in particular, is a key factor for deriving accurate atmospheric motion vectors. Table 3 shows the image navigation and registration pre-launch specifications (3σ) in black for the GOES-8-12, GOES-13/O/P, and GOES-R series of satellites. In red are actual computed image navigation and registration performance statistics for GOES-12 (using four 1-week periods of residual data from 2005 and 2006)

and for GOES-13 (using two days from special collection period in December 2006) based on the standard deviation of the residual differences calculated from satellite image navigation and registration (INR) data. It is clear from this table that the image navigation and registration performance has improved with each new series of GOES satellites. The GOES-13 image-to-image registration accuracy, for example, is substantially improved over its predecessors and approaches the GOES-R specifications, which represent even a further improvement. Higher spatial, spectral, and temporal resolution, together with increased radiometric performance and improved navigation/registration performance of the GOES-R ABI is expected to result in better target selection, improved feature tracking, and target height assignment. In addition, new opportunities for applications of very high-resolution (spatial & temporal) winds in severe storm environments and feature tracking of volcanic ash and dust are expected.

The performance of the DMWA is sensitive to any imagery artifacts, instrument noise, and image registration accuracy. The GOES-R ABI channel specifications are given in the MRD section 3.4.2.1.4.0 and it is assumed that the GOES-R ABI will perform within these specifications.

3 ALGORITHM DESCRIPTION

A complete description of the DMWA algorithm at the current level of maturity (which will improve with each revision) is provided in this section.

3.1 Algorithm Overview

The DMWA developed for the GOES-R ABI instrument has its heritage with the DMWA being used operationally today at NOAA/NESDIS for the current GOES series of satellites (Merrill et al, 1991; Nieman et al, 1997, Velden et al, 2005). There are a number of basic steps involved in the process of generating DMWs:

- Obtain a set of at least three precisely calibrated, navigated and co-registered images in a selected spectral channel
- Locate and select a set of suitable targets in the middle image domain
- For each image pair in the image triplet, use a correlation algorithm to derive the motion most representative for the target scene

  When tracking cloudy target scenes using ABI channels 2 (0.64um), 7 (3.9um), 8 (6.15um), or 14 (11.2um) the correlation algorithm is used in conjunction with a nested tracking algorithm where the following steps are performed:

  - Apply the correlation algorithm to smaller sub-targets within each target scene in order to derive a set of local motion vectors for each target scene

- Analyze the local motion field with a cluster analysis algorithm in order to extract the dominant motion within the target scene.
- Assign a height to the derived winds using pixel level information from the dominant cluster.

When tracking moisture gradients in clear target scenes using ABI channels 8 (6.15um), 9 (7.0um), or 10 (7.4um), the nested tracking algorithm is disabled and the following steps performed:

- Assign a height to the tracer using a cold sample of pixels.
- Apply the correlation algorithm to the entire target in order to arrive at a motion vector

- Average the vectors derived from each of the image pairs to arrive at the final set of DMWs
- Perform quality control on the DMWs and assign quality indicators to each of the DMWs

A target scene is represented by an NxN array of pixels that defines a suitable feature in the image whose movement can be tracked in time. The size of this array is a function of the spatial and temporal resolution of the imagery and the scale of the intended feature to be tracked. One of the challenges of deriving atmospheric motion winds operationally from satellites is to determine and utilize imagery taken at frequencies appropriate to the scales resolvable by operational numerical weather prediction systems while at the same time meeting production demands that require routine full disk coverage.

3.2 Processing Outline

In order to estimate motion, one must have a sequence of images separated by some, preferably fixed and relatively short, time interval. The DMW algorithm described here uses a sequence of three images to compute a pair of vector displacements (one for an earlier time step and one for a later time step) that are averaged to obtain the final motion estimate. The current version of the algorithm requires that the three images be equal in size. The DMWA uses the middle image to perform the initial feature targeting, then searches the before and after images for traceable (coherent) features to derive motion estimates.

The basic processing outline for the DMWA is summarized in Figure 1. The algorithm is designed to run on segments of data provided by the framework and consisting of multiple scan lines. Processing begins after a data buffer containing the brightness temperature values from three consecutive images is filled. The data buffer also contains output from the cloud mask and cloud height algorithms which must execute before the DMWA. It should be noted that the cloud data is only required for the middle image time because this is the image that is processed for targets. On the other hand, brightness temperature values

are required for all three image times because this is the quantity being tracked. In practice, the buffer is a data structure holding the 2-dimensional arrays of brightness temperatures for three image times and the cloud information for a single image time.

Once the data buffer is full, the middle portion of the buffer is divided into small "target" scenes NxN pixels and each scene is analyzed to determine if it is a suitable tracer. Only the brightness temperature field from the middle image time is processed for targets and it is these targets that will be tracked over time to derive the motion. Processing only the middle portion of the buffer allows for the features to drift over time but still remain within the domain of the buffer. Within each target scene, the algorithm locates the strongest 2-D gradient in the brightness temperature field and re-centers the NxN target scene at this location. A brightness temperature gradient threshold is used to prevent target selection on very weak gradients.

After the target scene is re-centered on the maximum gradient, tests are performed to determine whether or not the scene would be a suitable tracer. These tests eliminate target scenes that lack the gradients necessary to track reliably while also removing scenes that are suspected to contain multiple cloud layers.

If a potential tracer makes it through the target quality control, a search region, much larger in size than the target scene, is defined in each of the tracking images. At this point, depending on the channel being processed, one of two tracking strategies is employed. Both strategies use the Sum of Squared Differences (SSD) similarity measure to locate the target scene in the preceding and succeeding images.

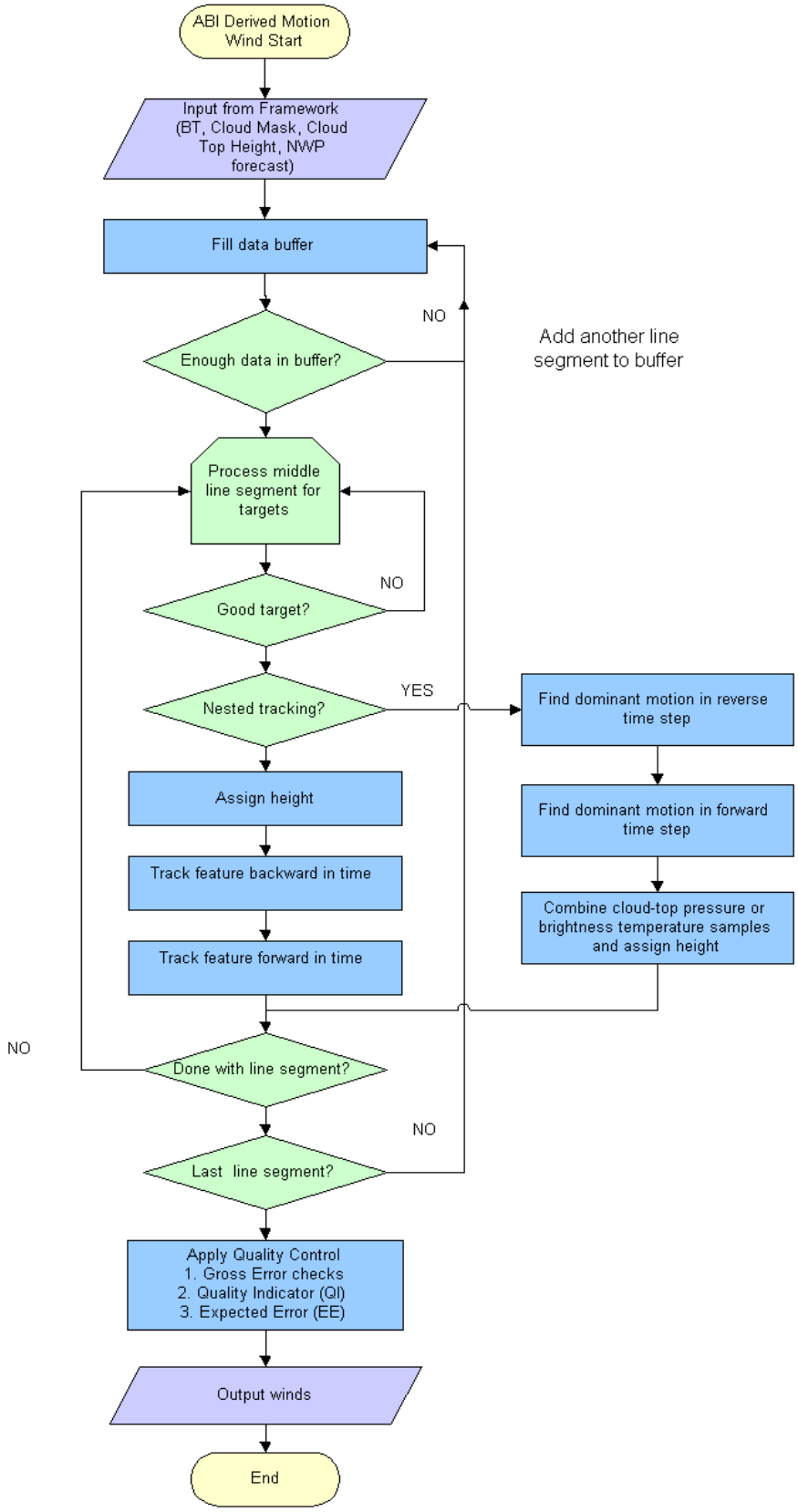

Figure 1. High Level Flowchart of the ABI Derived Motion Wind Algorithm.

When processing cloud-top features from the 0.6, 3.9, 6.2 or 11.2 micron channels, a tracking strategy called nested tracking is used to estimate motion. In this approach, a small 5x5 pixel box is "nested" within the outer target scene and a local motion vector is derived at each interior pixel. A 2-pixel offset is used near the boundary of the outer target scene. The field of local motion vectors that results is then analyzed with a cluster analysis algorithm to find the dominant motion. The dominant motion is computed by averaging the displacements associated with the largest motion cluster found by using a cluster analysis algorithm. The wind vector is then assigned a representative height after examining the cloud top pressure or brightness temperatures associated with the pixels in the largest cluster. When processing the visible, SWIR or LWIR channels, a median cloud top pressure is found by examining the cloud-top pressure values of all pixels in the largest cluster. When processing one of the three water vapor channels the height assignment process is slightly different. Here, the water vapor channel brightness temperature values are examined and a median temperature is found from the pixels in the largest cluster. The median brightness temperature is then compared to a GFS forecast temperature profile to find the pressure where the two values agree. The pressure at which these two values agree serves as the representative height of the derived motion wind.

When processing the clear sky portions of a water vapor (6.2um, 7.0um or 7.3um) image, the strategy for tracking features is more conventional. For these cases, the target is assigned a height before it is tracked. The height is computed using a sample of pixels from the coldest portion of the scene. After the target is assigned a height, a search is performed to find the closest match of the target in the preceding and succeeding images in the image triplet. This conventional approach produces a single motion vector associated with the motion of the entire target scene.

Both tracking approaches use a forecast wind (from the center of the target scene) to locate and place the center of the search region in the next image. This practice of using the forecast to "guide" the search serves two purposes. First, it reduces the number of "false positives" in the tracking step. Secondly, it minimizes the computational expense of the search.

During the tracking process, correlation thresholds are applied to screen out false positives. When nested tracking is employed, only matching scenes possessing a correlation score of 0.8 or higher (1.0 is perfect) are allowed to influence the final solution. For conventional tracking, where nested tracking is not invoked and the larger target scene is tracked, the correlation threshold is reduced to 0.6.

Two sub-vectors are generated in the tracking process, one vector for the backward time step and one vector for the forward time step. Accelerations between sub-vectors exceeding a user defined threshold (5 or 10 m/s depending on band) are not permitted (vectors are discarded). In addition, gross errors in the height assignment and tracking estimates are removed by comparing the satellite-derived motion wind to a numerical forecast wind and discarding those satellite-derived wind vectors which differ significantly from the forecast wind. These gross error thresholds are band-dependent.

Once the last line segment is processed, the entire set of derived winds undergoes a more rigorous quality control process. Two related algorithms will make up the Automatic Quality Control (AQC) of the GOES-R DMW processing. The first one is the quality indicator (QI), based on work done at EUMETSAT (Holmlund, 1998). The second is the Expected Error (EE) principles developed at the Bureau of Meteorology, Australia (LeMarshall et al. 2004).

3.3 Algorithm Input

This section describes the input needed to process the DMWs. While the DMWA uses information at the pixel level (e.g., cloud mask, cloud height), the derived motion is representative of a group of pixels (i.e., a scene within a target box of size NxN pixels). The DMWA is currently designed to process winds only after a data buffer has been filled with brightness temperature data from all three images in the tracking sequence. Cloud height and cloud mask information for the middle image time is also required. The buffer must be large enough to capture the motion of features up or down in the image. Consequently, the DMWA processes only a portion of the buffer (a middle strip the same width as the target box size) for suitable tracers. Processing proceeds from west to east until the earth edge is encountered or no more elements exist in the line segment. The process is repeated until the number of lines remaining in the line segment is smaller than the number of lines that make up the target scene. At this point the extra lines are saved in the buffer and control is returned to the framework until the next line segment is read into memory. The following sections describe the actual input needed to run the DMWA.

3.3.1 Primary Sensor Data

The list below contains the primary sensor data to be used by the DMWA. By primary sensor data, we mean information that will be derived solely from the ABI observations and geolocation information. The sensor data is used at it original resolution.

- Calibrated and navigated radiances for ABI channel 14 (11.2um) for the middle image time of the loop sequence.
- Calibrated and navigated reflectances (percent) for ABI channel 2 (0.64um) and brightness temperatures for ABI channels 7 (3.9um), 8 (6.15um), 9 (7.0um), 10 (7.4um), and 14 (11.2um) for three consecutive images.

3.3.2 Ancillary Data

The following list briefly describes the ancillary data required to run the DMWA. By ancillary data, we mean data that will require information not included in the ABI observations or geolocation data.

- **Land mask / Surface type**

A land mask file is needed such that each ABI pixel can be classified as being over land or water. The details of the dataset that contains this information and the procedure for spatially mapping it to the ABI are described in detail in the Algorithm Interface and Data Description (AIADD) Document.

- **DMWA configuration file**

  A configuration file is needed to set six variables within the DMWA processing algorithm:

  1. GOES-R ABI channel number – Channel number to use for feature tracking
  2. Time step between images
  3. Target box size – In pixel space
  4. Nested tracking flag – to enable or disable nested tracking.
  5. Expected Error (EE) filter flag
  6. Clear-sky WV flag – to enable or disable clear sky processing.

- **Numerical Weather Prediction (NWP) Forecast Data**

  1. Short-term forecast temperature and wind data on pressure surfaces from National Centers for Environmental Prediction's (NCEP) Global Forecast System (GFS) model are used to calculate target heights and for calculating model shear and model temperature gradients used in the Expected Error algorithm described in Section 3.4.2.4.2. Details concerning the preprocessing of NWP forecast data can be found in the AIADD Document.
  2. Short-term GFS forecast wind profiles are also used to center the search box on the predicted locations of targeted features being tracked in the first and last images of the loop sequence

- **Expected Error Coefficients File**

  1. A set of regression coefficients corresponding to a number of predictors used to compute the Expected Error quality flag that is appended to each DMW that is computed. The details of this approach are described in Section 3.4.2.4.2.

3.3.3 Derived Data

This section lists the input data that must be derived before the DMWA is executed. The output of several upstream cloud product algorithms from the GOES-R AWG cloud team are used in the DMWA derivation process and include the following:

- **Cloud Mask**

The cloud mask is used by the DMWA as part of the cloud amount test when selecting which target scenes to process. It is also used to screen out pixels that do not have a cloud top pressure associated with them.

- **Cloud top pressure, cloud top pressure quality, and cloud top temperature**

  This information is used by the DMWA to assign a representative height to the target scene being tracked.

- Cloud top height and temperature error estimates

- **Low level inversion flag**

  This information is used by the DMWA to assign a representative height to the scene being tracked within a GFS model designated low-level inversion.

- **Solar zenith angle**

  This information is used by the DMWA to determine day/night pixels.

3.4 Theoretical Description

3.4.1 Physics of the Problem – Estimation of atmospheric flow from motions in sequential satellite imagery

This section discusses the theory behind the challenge of estimating atmospheric flow from motions in sequential satellite imagery. Atmospheric motion is determined through the tracking of features in time. Identifying features to be tracked is the first step in the process. These features can be clouds, or in the case of clear-sky conditions, moisture gradients.

The DMWA uses the ABI visible and infrared observations shown in Table 3 to extract atmospheric motion. The choice of spectral band will determine the intended target (cloud or moisture gradient) to be tracked, its height in the atmosphere, as well as the scale of its motion. Historically, the coverage of operational GOES DMWs is diurnally consistent in the mid- to upper tropospheric levels (100–600 hPa) through the use of the mid-wave (6.7um – 7.3um) water vapor channels and longwave (10.7um) infrared (LWIR) channel for deriving vectors. In the lower levels (600–950 hPa), DMWs are provided by a combination of the visible (VIS) and IR channels, depending on the time of day. During daylight imaging periods, the VIS channel usually provides superior low-level tracer detection than the LWIR channel due to its finer spatial resolution and decreased susceptibility to attenuation by low-level moisture. During night-time imaging periods, the shortwave (3.9um) infrared (SWIR) channel compliments the LWIR channel to derive DMWs. The SWIR channel is a slightly “cleaner” window channel than the LWIR (less WV attenuation), making it more sensitive to warmer (lower tropospheric) temperature

features (Dunion and Velden, 2002). The SWIR channel is also not as sensitive as the LWIR channel to cirrus clouds that may obscure low-level cloud tracers. These two characteristics make it a superior channel for producing low level DMWs at night.

As described previously, each target is an NxN array of ABI pixel measurements (scene) that encapsulate a suitable feature whose movement is tracked in time. The size of this array is a function of both the spatial and temporal resolution of the imagery and the scale of the intended feature to be tracked. Generally speaking, a small target box yields a noisier motion field than one generated with a larger target box. Conversely, if the target scene is too large, the algorithm will tend to measure the mean flow of the pixels in the target scene (i.e. a spatial average of several motions) rather than the intended instantaneous wind at a single point. These considerations need to be kept in mind when choosing the optimal target box size.

3.4.1.1 Target Selection

The objectives of the target selection process are to select high quality target scenes that: i) capture the intended target (i.e., clouds or clear-sky water vapor gradient), ii) contain sufficient contrast, and iii) do not contain a mix of multi-layered clouds. Target scenes that posses these characteristics are more amenable to precision tracking and height assignment that result in more accurate atmospheric wind estimates.

Target scenes are centered at pixel locations where the magnitude of the brightness temperature gradient is large. In other words, these target scenes are centered over cloud edges or tight moisture gradients in clear-sky conditions. To assure that only high quality targets are selected, all potential target scenes first undergo a spatial coherence and cluster analysis (Coakley & Bretherton, 1982) check. The primary goal of this analysis is to identify the presence of a coherent signal in the target scene that indicates a dominant single layer cloud in the target scene. The spatial-coherence method attempts to identify the presence of cloud layers in each target scene by identifying the portions of the region that exhibit a high degree of local uniformity in the pixel-level emitted radiances. A high degree of uniformity will exist for regions that are cloud-free or for regions completely covered by cloud at a uniform height. For targets that are not completely covered by clouds, the emitted radiances can vary significantly from one pixel to the next.

3.4.1.1.1 Spatial Coherence and Cluster Analysis Methods

The starting point for spatial-coherence and cluster analysis methods is the model of a well-defined, single-layered system of clouds situated over a relatively uniform background. What is meant by the term “well-defined” and “relatively uniform” will be explained below. The emitted radiance observed by a radiometer viewing such a system is given by

$$I = (1 - C)I_{cs} + C(\varepsilon_{cld}I_{cld} + t_{cld}I_{cs}) \quad (1)$$

where I is the emitted radiance, C is the fractional cloud cover for the field of view, I_{cs} is the radiance associated with the cloud-free portion of the field of view, i.e. the radiance observed when C = 0. ε_{cld} is the mean effective emissivity associated with the cloud layer, t_{cld} is the mean transmissivity, and I_{cld} is the radiance that would be observed for overcast regions, i.e. C = 1, if the clouds were black at the wavelength of observation. The emitted radiance, I, is assumed to be at an infrared (IR) window wavelength so that downward emission above the cloud can be neglected. Likewise, the surface is assumed to be black at the wavelength of observation so that all radiation incident on the surface is absorbed, especially that emitted downward by the cloud. It is assumed that no radiation is reflected by the surface. Over a relatively small region the emission of the clear-sky background, I_{cs}, and the height of the cloud layer, and therefore I_{cld}, are assumed to have little variance. That is, the effects of variations in the thermal emissions associated with the clear-sky background and the height of the cloud layer are small when compared with the effects caused by variations in the fractional cloud cover and the cloud optical properties. If these conditions are met, the background is said to be relatively uniform and the layer is said to be well-defined. From (1), the variance of the radiances under such conditions is given by:

$$(I-\bar{I})^2 = [(C-\bar{C})I_{cs} + (C\varepsilon_{cld} - \overline{C\varepsilon_{cld}})I_{cld} + (Ct_{cld} - \overline{Ct_{cld}})I_{cs}]^2 \qquad (2)$$

The variances of emitted radiances over small areas spanning several image pixels is the key to identifying the portions of a region that are cloud-free or overcast by clouds in a well-defined layer. The variance approaches zero when the mean cloud cover in a region approaches zero. If the mean cloud cover is zero, then the fractional cover in every pixel is also zero (i.e. $C=\overline{C}=0$). Where the clouds become sufficiently extensive so that several image pixels are overcast, then for analogous reasons, the variance approaches zero because $C=\overline{C}=1$. Often when cloud systems become sufficiently extensive that they cover several image pixels, they also become opaque. A notable exception can be cirrus. For opaque, overcast clouds the variance again becomes zero because $t^i_{cld} = t_{cld} = 0$ and $\varepsilon^i_{cld} = \varepsilon_{cld} = \varepsilon_{cldmax.}$, where, t_{cld} is the cloud transmissivity and ε_{cldmax} is the emissivity that the clouds obtain when they become opaque (i.e., where r_{cldmax} is the reflectivity). When pixels become overcast with opaque clouds, the variance in emitted radiances also becomes zero. When pixels become overcast by semitransparent clouds, like cirrus, pixel-to-pixel variations in the cloud optical properties, i.e. ε_{cld} and t_{cld}, prevent the variance from dropping to zero. Because clouds appear to vary incoherently on the ~1 km × 1 km scale available to current satellite imagers, (2) indicates that variances in the emitted radiances for regions that are covered by several image pixels will be nonzero when the region contains broken cloud. The variability will be caused partly by differences in the fractional cloud cover from pixel to pixel and partly by variations in the average cloud optical properties from pixel to pixel. The spatial-coherence method identifies pixels that are overcast by layered clouds where the clouds become opaque, and pixels that are cloud-free by relying on the near-zero variances in emitted radiances for localized collections, or clusters, of the pixels. Collections of pixels that are partly covered by clouds or are overcast by clouds that are semitransparent invariably exhibit relatively larger variances. The application of a simple threshold on the variance of emitted radiances over local sub-regions within each target scene is performed as part of the target selection process in order to identify coherent pixels representative of cloud features and the surface.

The cluster analysis method is designed to filter out hard to track multi-layered cloud scenes. It is related to the spatial coherence method in that it starts with the same radiance information (mean and standard deviation values for small sub-regions of the target box), but takes the analysis further to determine if more than one cloud layer is present in the target scene. This analysis involves constructing a histogram of pixel level radiance values within the target scene and then identifying the clusters of warm and cold samples that are assumed to correspond to the surface and the elevated cloud layer, respectively. A second cloud layer is assumed to exist in the target scene if more than a pre-determined percentage (20%) of the radiance values fall outside of the two clusters of warm and cold samples. If a second cloud layer is determined to exist, the target scene is rejected as a suitable target for feature tracking.

Further details about how both of these tests are applied are provided in Section 3.4.2.1.1

3.4.1.2 Feature Tracking

If a target scene survives the selection criteria, then attempts to track this target in the image sequence can commence. Feature tracking involves coherent tracking of clouds or water vapor features over a specified time interval. A key assumption made in this process is that cloud or water vapor features are passive tracers that move with the ambient wind flow. Of course, it is understood that cloud tracers (in particular) are not always passive. There may be growth, decay, or change in cloud top height over the time interval being assessed. Further complicating matters is the fact that some clouds do not move with the wind (i.e. wave clouds) while others track with the wind at a level lower than cloud top (i.e. marine cumulus). Therefore it is important to apply robust quality control to remove retrieved DMWs that are in error as a result of these complicating factors (discussed in Section 3.4.2.4).

Clouds grow and decay with lifetimes that vary with their size and location (i.e., land versus ocean). To be effectively tracked, the lifetime of the tracer must be at least as long as the time interval of the image sequence used. The resolution of the imagery is also an important consideration when tracking features in satellite imagery. Merill (1989) and Schmetz et al. (1993) discuss this at length. It is important that the size of the target scene (spatial resolution) is consistent with the temporal resolution of the imagery in order to capture the scale of the intended feature being tracked. For example, estimation of low level winds over land is improved by using smaller target scenes and higher temporal resolution imagery. Early work by Hamada (1983) suggested that the temporal resolution of images should be less than 15 minutes in order to accommodate the short lifetime and rapid deformation of cloudy tracers over land. Shenk (1991) suggested that the temporal resolution needed to properly track low level cumulus over land was in the range of 10 minutes to less than a minute. More recently, Velden et al. (2000) experimented with special GOES-10 rapid scan imagery to determine the optimal temporal resolution to use for different spectral channels. A general finding, that was not unexpected, was that a

higher number of high quality winds can be derived with decreasing time intervals and increasing spatial resolution.

A critical factor that has a significant impact on the quality of the derived winds, especially at higher temporal resolutions, is the image registration; that is, the stability of the image-to-image navigation. If the stability of the image-to-image navigation is poor for an image sequence, the result will be added noise to the tracking process and poor quality DMWs. Furthermore, use of imagery with high temporal resolution, but coarse spatial resolution, can result in poor quality DMWs. This is especially true for small tracer displacements (i.e., low wind speeds) where image registration uncertainties will dominate the resulting true displacements.

Jedlovek and Atkinson (1998) discuss the development of a Tracking Error Lower Limit (TELL) parameter, $\Im$, that provides guidance for understanding the trade-offs between spatial and temporal resolution for varying image registration performances. The TELL parameter is given by:

$$\Im = (\Re + \rho/2)/t \tag{3}$$

where: $\Re$ is the image registration accuracy, ρ is the image spatial resolution, and t is the image separation interval. Figure 2 shows the magnitude of the TELL parameter for various values of the image registration accuracy and image separation.

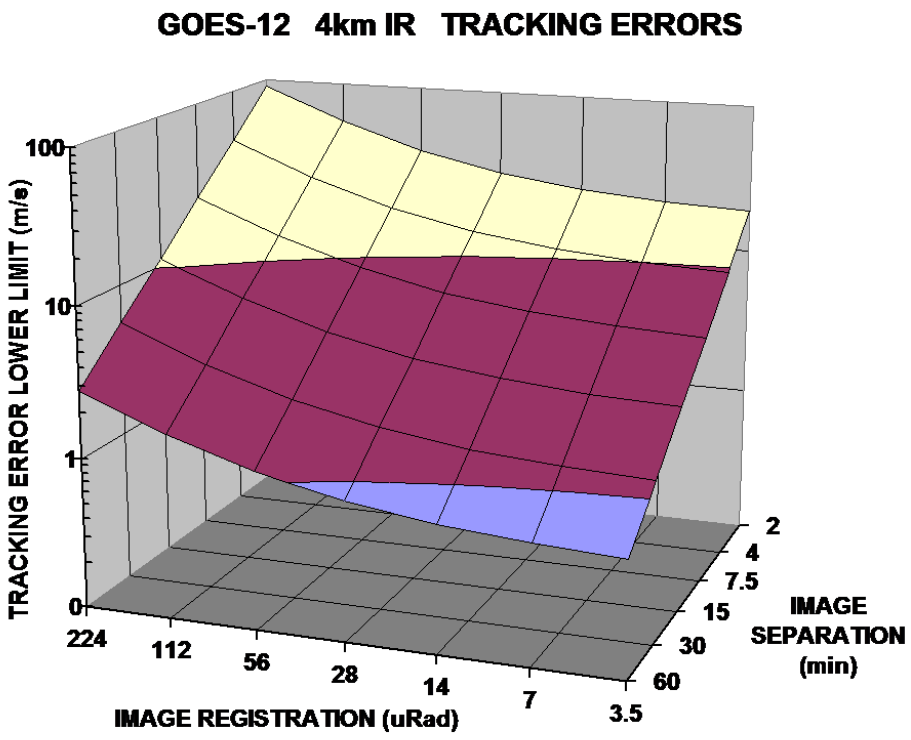

Figure 2. Tracking Error Lower Limit (TELL) is a function of image registration accuracy and image separation time. (Jedlovek and Atkinson, 1998)

Small values of TELL (small wind errors) are achieved with good image registration, high resolution data, and relatively large image separation times. However, for atmospheric applications where trackable features change considerably over a short period of time, large separation intervals are not desirable, making values of image resolution and registration accuracy critical parameters in DMW accuracy.

3.4.1.3 Target Height Assignment

Assigning a representative height to each cloudy target is achieved by processing pixel-level cloud heights, derived via the GOES-R ABI cloud height algorithm, within the target scene. A detailed description of the GOES-R ABI cloud height algorithm can be found in the GOES-R ABI Cloud Height Algorithm Theoretical Basis Document. For clear-sky water vapor targets, NCEP GFS forecast temperature profiles are used as ancillary data and compared to brightness temperatures calculated from the clear-sky water vapor channel brightness temperatures. The pressure height is determined as the level where the brightness temperature fits the forecast temperature.

Target height assignment is considered to be the major source of error for DMWs. A perfectly tracked feature can be rendered useless if it is assigned to the wrong level in the atmosphere. There is also the consideration of how well the final wind actually represents the local wind field at a singular location, height (level) and time. Some clouds do not move with the wind while others follow the wind at a level lower than the cloud top. Additionally, DMWs tend to represent the movement of a layer of the atmosphere, as opposed to the movement of the atmosphere at a particular level (Velden and Bedka 2009).

3.4.2 Mathematical Description

The GOES-R DMWA approach to derive an individual vector consists of the following general steps, each of which is described in detail in the following sections.

- Locate and select a suitable target in second image (middle image; time=t_0) of a prescribed image triplet
- Assign an estimated representative height to the target
- Use a pattern matching algorithm to locate the target in the earlier and later image. Track the target backward in time (to first image; time=t-Δt) and forward in time (to third image; time=t+Δt) and compute corresponding displacement vectors. Compute the mean vector displacement from the two displacement vectors and assign this final DMW to time = t_0.
- Perform quality control procedures on the DMW to edit out or flag suspect vectors. Compute and append quality indicators to each DMW.

3.4.2.1 Target Selection

Targets are selected from the middle image of the sequence. The size of each target scene will depend on the channel being processed and the scale of the motion being estimated. The target scene is traditionally a square with sides of equal length (in pixels). Table 4 summarizes the target scene size and image time separation interval to be employed for each ABI channel used to derive DMWs. It should be noted that the horizontal resolution of the DMW product is driven by the size of the target scene used. Consequently, the horizontal resolution of the wind products derived from the ABI 0.64um band, will be 7.5km, the resolution of the wind products generated from the water vapor bands will be 30km and the resolution of the winds generated with the long wave infrared band will be 38km.

Table 4. Summary of target scene sizes and image time intervals that should be used to derive DMWs for pertinent ABI channels.

Channel Number	*Center Frequency (μm)*	*Target Scene Size (Image lines x elements)*	*Image Time Interval (mins)*
2	0.64	15x15	Full disk: 5 or 15 CONUS: 5 Mesoscale: 5
7	3.90	15x15	Full disk: 5 or 15 CONUS: 5 Mesoscale: 5
8 (cloudy targets) ---------- 8 (Clear targets)	6.15	15x15	Full disk: 5 or 15 CONUS: 5 Mesoscale: 5 ---------- FD, CONUS, Mesoscale: 30
9	7.0	15x15	FD, CONUS, Mesoscale: 30
10	7.4	15x15	FD, CONUS, Mesoscale: 30
14	11.2	19x19	Full disk: 5 or 15 CONUS: 5 Mesoscale: 5

Before the target selection process begins, the brightness temperature gradient magnitude for each pixel location is computed from equation (4).

$$Gradient_{Line,Element} = \sqrt{\{\sum_{k=-2}^{k=2}(W_k)(BT_{Ele\,+\,k,\,Line})\}^2 + \{\sum_{k=-2}^{k=2}(W_k)(BT_{Ele,\,Line\,+\,k})\}^2} \quad (4)$$

where: $W_k = \{-1/12, 8/12, 0, -8/12, 1/12\}$; for k= -2 to 2

BT is the pixel level channel brightness temperature

Ele refers to an image column

Line refers to an image row

Figure 3 shows an example of a brightness temperature gradient image (right side) derived from brightness temperatures (left side) for the GOES-12 imager. The dark areas on the right side of Figure 3 indicate locations where the magnitudes of the brightness temperature gradients are large. These locations exist on the edges of clouds and in the interior of cloud systems where cloud structure exists. It is in these locations where potential acceptable targets are expected to be found. The white boxes shown on the left-side of Figure 3 show the original target scene locations and the yellow dots show the location of the maximum gradient magnitude in each of these target scenes. The center of every target scene is then repositioned at the pixel containing the maximum gradient magnitude. If the same gradient value occurs in multiple pixels within a target scene, then the first occurrence of the maximum gradient value is the one chosen. The repositioned target scenes are shown in green. The intent of repositioning the target scene at the maximum gradient is twofold. First, it focuses the target scene on a strong feature that is expected to be effectively tracked over time. Secondly, it establishes a link between pixels containing the feature being tracked and the pixels contributing to its height assignment (discussed later). Repositioning of the target scenes can result in an irregular spatial distribution of target scenes, and hence, an irregular spatial distribution of the DMW product. The white arrows indicate the direction of the image processing, which begins at the top left of the image and moves left to right along the image and then downwards.

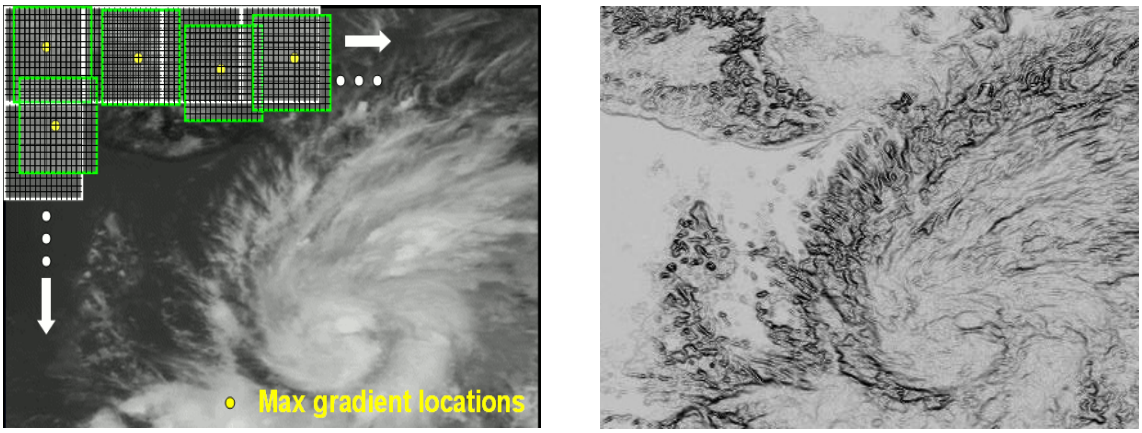

Figure 3. Image of 11um brightness temperature (left) and the 11um brightness temperature gradient (right) from the GOES-12 imager instrument. The white boxes show the target scenes at there original locations. The green boxes show the target scenes which have been repositioned at the pixel location containing the maximum brightness temperature gradient as indicated by the yellow dot.

3.4.2.1.1 Target Selection Tests

All of the potential target scenes undergo a series of quality control tests to determine if the target is a suitable tracer. These 'target selection' tests are described below. If a target fails any one of these tests, the target is determined to be a non-suitable tracer and is flagged. Each failure is associated with a unique "flag" value which is saved in the DMW output file. These values are shown in Table 5.

Table 5. GOES-R ABI Derived Motion Winds Failure Codes.

GOES-R Derived Motion Wind Quality Control Codes	
QC_Flag	**Definition**
0	Good wind
1	Maximum gradient below acceptable threshold
2	Target located on earth edge
3	Cloud amount failure (less than 10% cloud cover for cloud track winds or greater than 0% cloud cover for water vapor clear-sky winds)
4	Median pressure failure
5	Bad or missing brightness temperature in target scene
6	Multiple cloud layers present
7	Target scene too coherent (not enough structure for reliable tracking)
8	Tracking correlation below 0.6 (not used for nested tracking)
9	u-component acceleration greater than 10 m/s (5 m/s for visible)
10	v-component acceleration greater than 10 m/s (5 m/s for visible)
11	u- and v- component accelerations greater than 10 m/s (5 m/s for visible)
12	Derived wind slower than 3 m/s
13	Target scene too close to day/night terminator (visible and SWIR only)
14	Median pressure used for height assignment outside acceptable pressure range (channel dependent)
15	Match found on boundary of search region
16	Gross difference from forecast wind (channel dependent)
17	Median pressure (used for height assignment) of largest cluster for first image pair is too different from median pressure of largest cluster for second image pair – only valid for nested tracking
18	Search region extends beyond domain of data buffer
19	Expected Error (EE) too high
20	Missing data in search region
21	No winds are available for the clustering algorithm
22	No clusters were found
Catastrophic Failures	
Invalid time interval	
Temporal data not available	

Line segment swath too small (must contain at least the same number of lines as target box size, usually 15 lines)
Search region must be larger than target scene

Table 5 describes every possible failure code from the initial target selection step through the final QC process. Because target selection is the first step in the AMV derivation process the tests associated with it are described first. The target selection tests are applied in the following order:

1. Zero gradient check
2. Proximity to day/night terminator check
3. Earth edge test (no space pixels allowed)
4. Fractional cloud cover/clear sky test
   Note: when processing the upper-level water vapor channel for clear-sky tracers pixels with low-level clouds (CTP >= 600 mb) are considered clear.
5. Contrast test – channel dependent
6. Channel validity test

#6 is the extent of target QC for WV processing

Additional target QC performed for visible, SWIR and LWIR winds:

7. Spatial coherence check
8. Multi-layer cloud check

If a target scene fails test #1 the next adjacent target box is processed.
If a target fails any of the 2-8 tests the box is shifted by ½ the width of the target box.

Zero gradient Test

If the maximum gradient found in the target scene is zero the target is discarded and the next adjacent box is processed.

Contrast Test

Each target scene is required to contain sufficient contrast, which is computed from the range of channel measurements (brightness temperature or reflectance percent) within the target scene. The contrast threshold used is channel dependent and is the product of the contrast constant (shown in Table 6) and the ratio of the target scene size used (see Table 4) and the nominal target scene size (7 or 15).

Table 6. Contrast constants and thresholds used for target selection.

Channel Number	*Wavelength Range (µm)*	*Contrast Constant*	*Contrast Threshold*
2	0.59-0.69	12% (reflectance)	12%
7	3.80-4.00	3K	6.43K
8 (clear-sky)	5.77-6.6	1K	1K
8 (cloud-top)	5.77-6.6	2K	2K
9	6.75-7.15	1K	1K
10	7.24-7.44	1K	1K
14	10.8-11.6	4K	5.07K

Earth Edge Test

The earth edge test is applied under the following conditions:

- When channel 2 (0.65um), 7 (3.9um), 8 (6.15um), 9 (7.0um), 10 (7.3um), or 14 (11.2um) is used.

All pixels within the target scene must have valid earth navigation associated with it. If any pixel within the target scene is determined to be located in space (i.e., off the earth edge) the target scene fails, and is flagged. The space mask provided by the framework is used for this purpose. It is assumed that a space mask will be passed down by the framework to the L2 product algorithm level for use by the various algorithms.

Fractional Cloud Cover Test

The fractional cover cloud test is applied under the following conditions:

- When channel 2 (0.65um), 7 (3.9um), 8 (6.15um), 9 (7.0um), 10 (7.3um), or 14 (11.2um) is used.

The clear-sky mask product associated with each pixel is used to classify the target scene as cloudy or clear. When the intent is to track clouds, a minimum threshold of 10% is used to make a determination as to whether the target scene is cloudy or clear. In other words, if at least 10% of the pixels in a target scene are deemed as being cloudy or probably cloudy, then the target scene is classified as cloudy. When the intent is to track clear-sky water vapor features, then a minimum threshold of 0% is used to make a determination as to whether the target scene is cloudy or clear. In other words, every pixel in the target scene must be deemed clear for this target scene to be deemed a suitable clear-sky water vapor target. An exception is made, however, when the upper-level water vapor band (6.15 um) is used to track clear-sky moisture gradient features. Because this band senses radiation only from the middle and upper layers of the atmosphere, any pixel which is clear above a

low-level cloud is considered clear instead of cloudy. In practice, a pressure threshold of 600 hPa is used to identify the low cloud. In other words, a cloudy pixel assigned a cloud-top pressure greater than 600 hPa is considered to be clear instead of cloudy. This exception is made to increase the coverage of these winds.

The cloudy or clear designation given to the target scene has implications on the target selection tests (described in sections 3.4.2.1.1-3.4.2.1.3) and/or thresholds used as well as which algorithm is used to assign a height to the target (described in section 3.4.2.2).

Channel Validity Test

The channel validity test is applied under the following conditions:

- When channel 2 (0.65um), 7 (3.9um), 8 (6.15um), 9 (7.0um), 10 (7.3um), or 14 (11.2um) is used.

The channel brightness temperature or reflectance percent of each pixel in a target scene is checked to ensure its value falls within a valid range. The valid range of reflectance percent for a visible channel is 1-200. For the IR channels, the valid range of brightness temperature is 150-340K. If the channel brightness temperature or percent of any pixel in the target scene falls outside the valid range the target fails and is flagged.

Spatial Coherence Test

The spatial coherence test is applied under the following conditions:

- When channel 2 (0.64um), 7 (3.9um), or 14 (11.2um) is used
- Target scene has been classified as cloudy

Originally proposed by Coakley and Bretherton (1982), the spatial coherence method utilizes the local spatial structure (local mean and standard deviation) of the IR-window radiance field to determine the radiances associated with cloud-free and completely cloud-covered fields of view and to infer the radiances associated with partially filled fields of view. In the context of the DMW algorithm, the method is first used to filter out target scenes that are too uniform to track reliably, and second, to filter out scenes that may contain multiple cloud layers. For both purposes it is necessary to compute the local mean and standard deviation of the radiance field derived from 3x3 sub-regions within the larger target box. The mean and standard deviation values are computed for the entire line segment (with data surrounding the target box). Near the edges these values are computed with however many pixels are available.

After computing the mean and standard deviation radiance values for all possible 3x3 pixel sub-regions in the target box, a standard deviation threshold (1.0 Wm^{-2} sr^{-1} um^{-1}) is applied that results in a "filtered" or coherent sample. The standard deviation threshold value is chosen arbitrarily with consideration given to the range of possible data values expected in the imagery. The resulting "filtered" or coherent sample represents either cloud-free or completely cloud-covered pixels from the less-coherent sample that is likely to include

partially filled fields of view. If more than 80% of the total number of 3x3 pixel sub-regions within the target scene have a standard deviation below the defined threshold, the scene is deemed to be too coherent and it fails to be a viable target for subsequent feature tracking. Target scenes that contain a mixture of cloud-free and cloud-covered pixels exhibit a characteristic arch shape as shown in Figure 4.

Multi-Layer Cloud Test

The multi-layer cloud test is applied under the following conditions:

- When channel 2 (0.64um), 7 (3.9um), or 14 (11.2um) is used
- Target scene has been classified as cloudy

Target scenes that contain multiple cloud layers in them can be difficult to track since clouds at different levels of the atmosphere may be moving in different directions and/or speeds. Furthermore, the assignment of a representative cloud height in these situations is difficult given the existence of clouds at different levels of the atmosphere.

In order to avoid these troublesome target scenes, the filtered sample from the spatial coherence approach described above is used in a cluster analysis approach in order to identify the possible existence of multiple cloud layers. The basic idea behind the method is to use the local mean and standard deviation information to identify clusters of points sharing common characteristics (such as mean radiance and low variance). If more than two clusters (one of which is implicitly assumed to be the surface in clear sky conditions) is found in a target box then the scene is rejected. The key concept of this approach is that peaks in the frequency histogram can be described by Gaussian distribution functions (Simmer et al., 1982; Rossow et al., 1985; Nieman et al., 1993).

Using the filtered sample, the method starts by identifying the peak in the 1-D histogram of local mean IR radiance values. A Gaussian curve is then fitted to the peak of the histogram and all points falling within +/- 3 standard deviations of the peak value are added to the dominant cluster sample. Likewise, a second Gaussian is fitted to the “cold peak” of the histogram and the cold cluster is identified. Lastly, the total number of points falling within the dominant and cold clusters is summed and compared to the total number of points in the filtered sample. If the total number of points from both clusters is less than 80% of the original filtered sample it is assumed that a third, unidentified, cluster exists (in theory representing another cloud layer) and the target is rejected. The example shown in Figure 5 is for a target scene that was partly filled by a single cloud
layer.

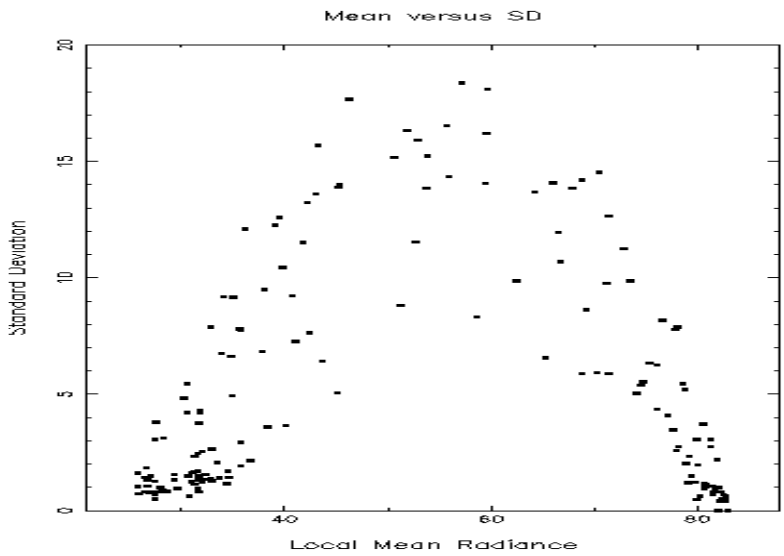

Figure 4. Scatter diagram of window channel IR local mean radiance and standard deviation values for a single target scene. Each point in the figure represents a 3x3 array of pixels constructed from 4-km GOES IR radiance data. The cluster of points near 80 is associated with clear sky while the cluster near 30 is associated with a single cloud layer. The points in the arch represent partly filled fields of view.

The step by step procedure for the above procedure is defined below:

1. Construct histogram of radiance values from 0 to 199 using bin width of 1.

2. Estimate the variance using a two point method (one end point is always the peak frequency) for the three bins closest to the peak (Note: if there is more than one peak the first one is selected) on the LHS with the formula:

$$variance_i = \frac{\left(\overline{x}_i - \overline{x}_{peak}\right)^2}{2\ln\left(\frac{f_i}{f_{peak}}\right)} \tag{5}$$

Where x is the bin value (i.e., radiance), f is the number of points in the bin (i.e., frequency),

$$\overline{x}_i = \frac{x_{i-1} + x_i}{2} \tag{6}$$

and

$$\overline{x}_{peak} = \frac{x_{peak-1}+x_{peak}}{2} \quad (7)$$

NOTE: If f_i is 0 then the variance is set to a value of 0.

3. Average the three variance estimates to obtain the final variance for the LHS half curve.

$$\overline{variance}_{LHS} = \frac{1}{3}\sum_{i=1}^{3} variance_i \quad (8)$$

NOTE: If the computed variance is greater than 25 it is set to a value of 25. Also, only non-zero variance values are used to compute the average. This means any bin having a zero count will not be used in the average.

4. Repeat steps 2 and 3 for the three bins closest to the peak on the RHS of peak frequency.

5. Compute the full Gaussian curve using LHS and RHS variance values. The full Gaussian spans the interval ±5 standard deviations about the peak frequency and is computed using:

$$f_{Gauss} = f_{peak} exp\left[-\frac{(\overline{x}_i-\overline{x}_{peak})^2}{2(\overline{variance}_{LHS,RHS})}\right] \quad (9)$$

NOTE: If the exponent is less than -10.0 it is set to a value of 0.0.

6. Find peak frequency of 5 coldest non-zero clusters and repeat steps 2 to 5 for the cold peak.
7. Total the number of pixels engulfed by the two Gaussian curves according to the following rules:

   ±1 standard deviation of peak, sum up all histogram points
   ±1to3 standard deviations of peak, sum up points in Gaussian histogram (from step 5)
   Do not count pixels outside this range

8. If the total number of points from both clusters is less than 80% of the original filtered sample, it is assumed that a third, unidentified cluster, exists and the target scene is flagged. DMWA assignsQC_Flag=6 to the processed target scene and moves to the next target scene.

Note: If the cold peak corresponds with the overall peak this implies a single cloud layer exists in the target scene. This would be an acceptable target.

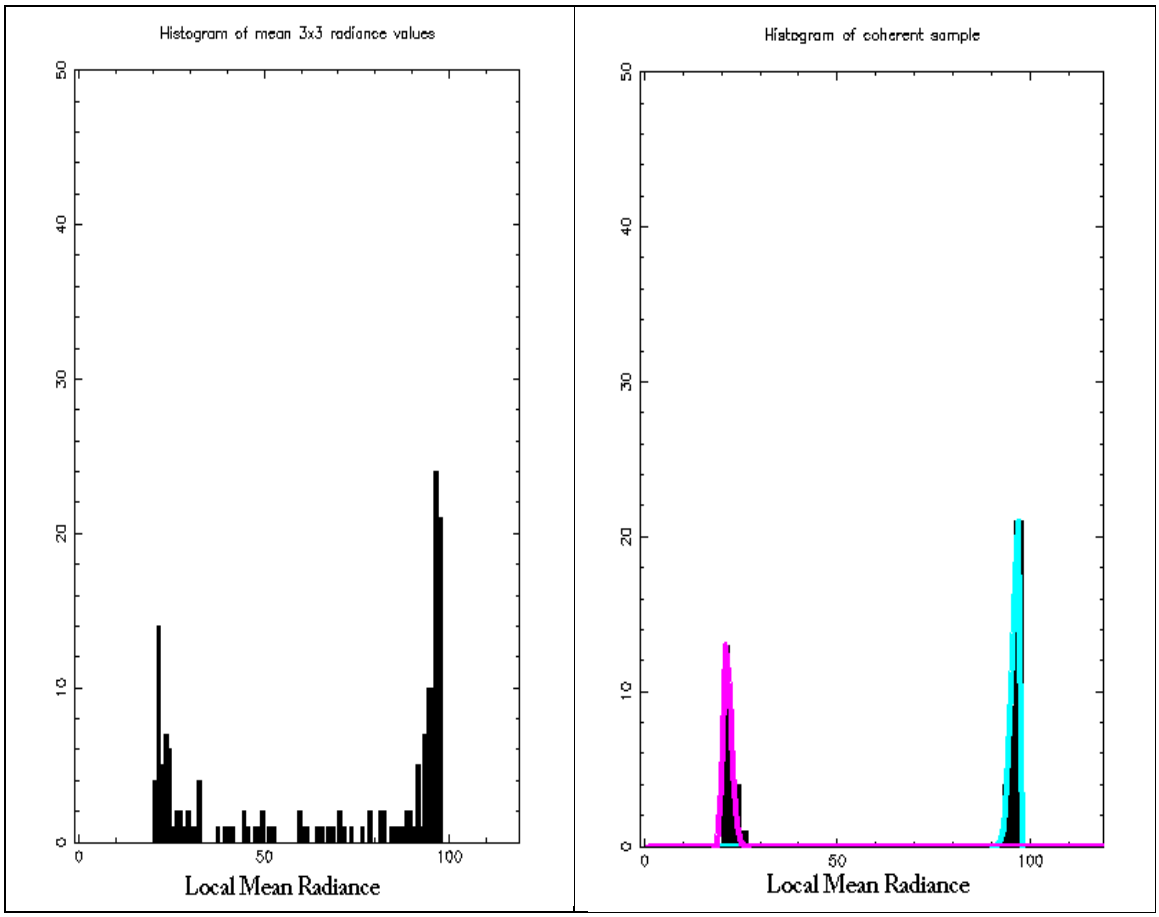

Figure 5. Histogram plots of local mean infrared radiance values for a single target scene: (Left) For the entire target scene, (Right) Filtered sample with Gaussian curves fitted to the peaks. The peak on the left is associated with a single cloud layer.

Day/Night Terminator Test

The Day/Night terminator test is applied under the following conditions:

- When channel 2 (0.65um) or channel 7 (3.9um) is used

When the VIS or SWIR band is being used, a test is invoked in order to avoid the day/night terminator. If the VIS channel is being used, then the solar zenith angle of the center pixel of the target scene must be less than or equal to 80^{o} for the target to be deemed a suitable target. If the SWIR channel is being used, then the solar zenith angle of the center of the target scene cannot be less than 90^{o} or greater than 200^{o} for the target scene to be deemed a suitable target.

3.4.2.2 Feature Tracking

Correlation-based methods are commonly used to track cloud and clear-sky water vapor features in image sequences. A widely used correlation approach to feature tracking is the Sum of Squared Differences (SSD). This correlation method, like all others, aims to locate a target scene, at some time t, in a larger search scene at some earlier or later time. This process is illustrated in Figure 6. A similarity criterion is computed that measures the correlation between the target and search area pixel scenes in the two images. In the DMW algorithm a feature or target is selected from the middle of three images and is tracked backwards and forwards in time, thus generating two displacements. These two displacements are then averaged to generate an average wind vector that is taken to

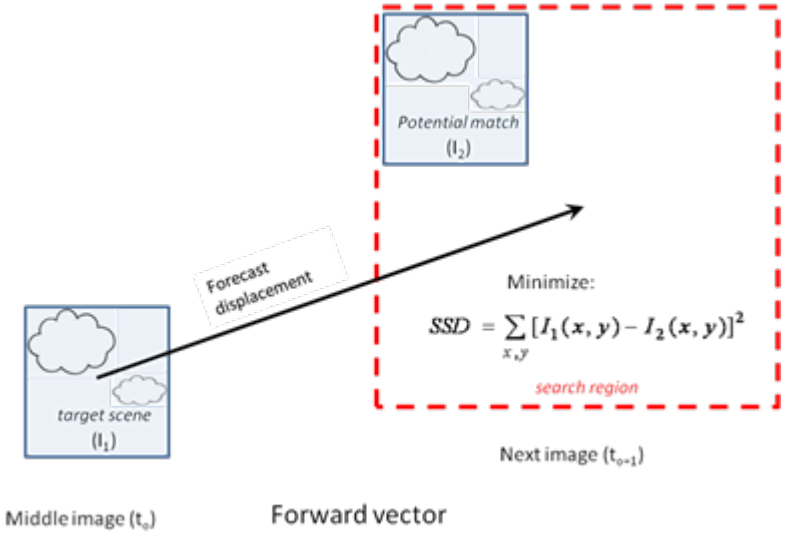

FIG. 6. Schematic showing the basic concepts associated with the feature tracking algorithm. Targets are selected from the middle image of a three-image loop and tracked forward and backward in time via the SSD method. The two displacements are averaged to produce a final motion estimate. Only the forward vector is shown in the figure.

represent the motion of the target over the time interval spanned by the image triplet. This average vector is assigned to the middle image target location. This approach is what we will refer to as the conventional feature tracking approach. This approach is used when tracking clear-sky water vapor features when using the ABI water vapor channels 8 (6.15um), 9 (7.0um), and 10 (7.4um).

When tracking cloud features involving ABI bands 2 (0.64um), 7 (3.9um), 8(6.15um), and 14 (11.2um), however, an approach referred to as nested tracking (Daniels and Bresky, 2010) is used. Nested tracking uses the SSD method to compute local motions nested within a larger target scene together with a clustering algorithm, to arrive at a superior

motion solution for the larger target scene. The details of this approach are described below in Section 3.4.2.2.2.

A short term GFS model forecast wind is used in the feature tracking step to center the location of the search area in the other images. This is done for two reasons. First, it minimizes computational time required for tracking and secondly, minimizes the number of false solutions generated by the SSD method. It should be emphasized that the search region must be sufficiently large to allow for substantial departures from the forecast. It has been shown by Merrill (1989) that the derived wind is inherently constrained to the forecast wind by the following relationship:

$$(u - u_g) \leq \frac{(L-2)x}{2t} \tag{10}$$

where u (m/s) is the east-west component of the satellite wind, u_g (m/s) is the east-west component of the forecast wind, L is referred to as the lag size and is the max displacement of a target scene within a given search box, t is the time interval (in seconds) between images and x is the resolution of the imagery in meters. A similar relationship holds for the north-south component, but is omitted for brevity. For a given image sequence time interval and pixel resolution, the ratio given by the right hand side of equation (10) yields a value that represents the maximum departure of the feature tracking wind solution from the forecast wind. It is important that this ratio be sufficiently large to minimize the dependency of the forecast wind in the tracking step. Furthermore, the magnitude of this ratio must be considered when different size target scenes and/or sequence time intervals are used. For example, for a given image resolution, if smaller image time intervals are desired, then a corresponding reduction in the lag size must be made in order to keep the magnitude of the ratio constant. By specifying a maximum forecast departure of 30 m/s in Equation (10), the equation for keeping the lag size constant is given by:

$$\frac{60}{x}t + 2 = L \tag{11}$$

By specifying the desired time interval between images to use and the resolution of the imagery in Equation 11), the lag size can be computed. Once the lag size is known, the size of the search scene can be computed from:

$$S = T + (L/2) * 2 \tag{12}$$

Where: S is the search scene size in pixels
T is the target scene size in pixels
L is the lag size in pixels

In summary, the step by step procedure for tracking is as follows:

1. Compute forecast displacement, in pixels, using the forecast wind valid at the target lat/lon and interpolated to the initial height estimate.
2. Use forecast displacement to center search box.
3. Fill search box with data from image buffer
4. Find matching scene in the first and third images and compute AMV displacement via the conventional or nested tracking algorithm (displacement is a real value not an integer value).
5. Compute end point of AMV displacement vector in pixel coordinates
6. Compute earth location (lat/lon) of end point
7. Compute U/V components using the beginning (target center pixel) and ending (match location) lat/lon values

3.4.2.2.1 Sum-of-Squared Difference (Euclidean Distance) Method

The sum-of-squared-differences method (SSD) is the correlation routine used by the DMW algorithm. In the SSD routine the following sum is minimized:

$$\sum_{x,y}[I_1(x,y) - I_2(x,y)]^2 \tag{13}$$

where: I_1 is the brightness temperature at pixel (x,y) of the target scene, I_2 is the brightness temperature at pixel (x,y) of the search window, and the summation is performed over two dimensions. In practice, the region over which the search is conducted is substantially larger than the size of the target scene and the above summation is carried out for all target box positions within the search region. The array of positions that the target box can assume in the search region is often referred to as the "lag coefficient" or "lag" array and the field of values is referred to as the correlation surface. The size of the search and lag arrays are given by Equations (11) and (12) in the previous section.

To speed up the search for the minimum SSD value, the tracking algorithm first constructs a table (a square array) of values specifying the order of positions to search within the lag matrix. This is illustrated in Figure 7. The first point in the table corresponds with the middle of the lag matrix, which also corresponds with the center of the search region, which also corresponds with the location predicted by the forecast. The search then "spirals" outward in a clockwise fashion about the central point. By starting the search in the middle of the search region we are hopefully maximizing our chance of finding a match sooner than if we were to start in the top left corner of the search region. The spiral search, when used in conjunction with the practice of terminating the SSD summation early once a current minimum has been exceeded, can significantly reduce the number of computations required during the tracking step of the DMW algorithm.

	7	8	9	10
	6	1	2	11
	5	4	3	12
				13

Figure 7. Table (a square array) of values specifying the order of positions to search within the lag matrix as part of the spiral search algorithm.

A typical correlation surface for the SSD method for the GOES-12 imager is shown in Figure 8. Each pixel in this figure represents a SSD value for a potential matching scene in the search region. The cool colors (blues) indicate minimum values while the warm colors (yellows) indicate relative maxima. The minimum SSD solution value results in a discrete, pixel displacement being identified as a possible DMW tracer. Unaltered, these integer displacements would cause an artificial binning of the satellite derived wind estimates. To avoid this effect, the SSD values of the four points surrounding the minimum SSD are used to linearly interpolate to sub-pixel accuracy. The following equation is used to compute the fractional element displacement:

$$\Delta = \frac{(l_1 - l_3)}{2(l_1 + l_3 - 2l_2)} \tag{14}$$

where l_1 is the lag array value at (x-1, y), l_2 is the lag array value at (x, y) (i.e., the minimum SSD value) and l_3 is the lag array value at (x+1, y).

The fractional value is added to the integer displacement to produce a Real (ie., non-integer) estimate of the displacement..

A similar equation is used for the fractional line displacement, but it uses the lag array values above (x, y-1) and below (x, y+1) the minimum lag location.

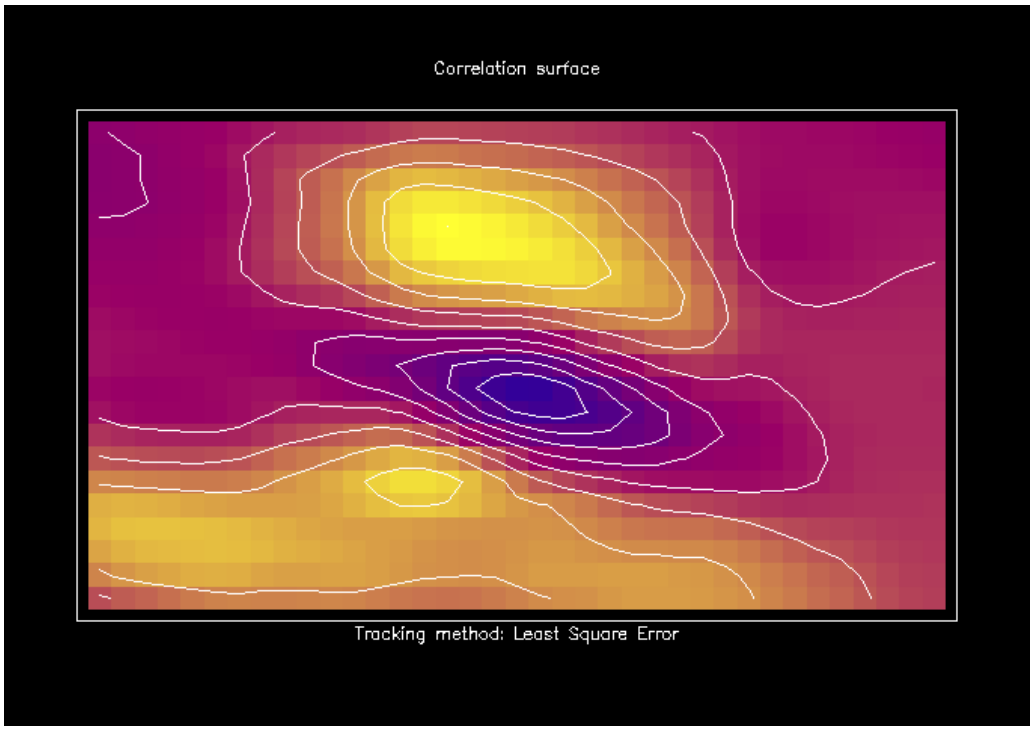

Figure 8. Example of a typical correlation surface for the Sum-of-Squared Difference (SSD) tracking method for the GOES-12 imager. The cool (blue) colors indicate minimum values while the warm (yellows) colors indicate relative maxima.

3.4.2.2.2 Nested Tracking

When tracking cloudy target scenes using ABI channels 2 (0.64um), 7 (3.9um), 8 (6.15um), or 14 (11.2um), a technique referred to as "nested tracking" is employed. This approach involves nesting smaller (5x5 pixels) target scenes within a larger target scene (ie., whose size is specified in Table 4) so that a field of local motion vectors can be derived over the interior pixels.

A schematic of this approach is shown in Figure 9 alongside one example of the vector field produced by the approach. Differences in orientation and magnitude can arise between the local motion vectors if more than one cloud layer is being tracked or if multiple scales of motion are being detected. Outliers vectors – those vectors that differ greatly from most of the sample – can result if the cloud is evolving or if the smaller box is insufficiently large to resolve the true motion. The second contributor to vector outliers is often referred to as the aperture effect and is discussed at length in the field of computer vision (Trucco and Verri, 1998). The red vector shown in Figure 9 makes it clear that averaging conflicting motions within a target scene can produce a slow motion estimate. The challenge is to

derive a dominant motion vector from a subset of all possible solutions that best represents the flow of the larger target scene. This can be accomplished by analyzing all of the local displacements within the larger target scene with a cluster analysis program. More specifically, a cluster analysis of the line and element displacements is done to produce clusters that represent unique displacements.

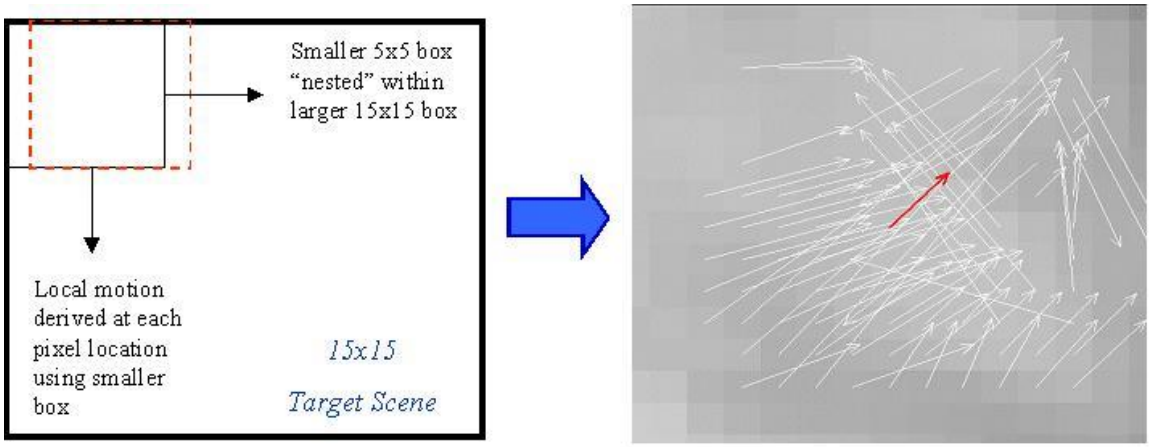

Figure 9. Schematic of the nested tracking approach. The white vectors show the local motion vectors successfully derived for each possible 5x5 box within a larger 15 x 15 target scene. The red vector on the right is the resulting motion vector if one were to take an average of all the successfully derived local motion vectors.

The justification for using a cluster analysis algorithm to analyze the local motion field is twofold. First, as was discussed above, the local motion field can be quite noisy. The field of vectors often reveals motion associated with two or more cloud layers and/or spatial scales. Removing noise and separating the sample into coherent motion clusters can prevent the excessive averaging of motion occurring at multiple levels or for different scales that can lead to a slow speed bias. Second, identifying clusters in the local motion field provides a means for directly linking the tracking step with the height assignment step. In other words, the pixels belonging to the coherent clusters allow us to limit the sample of pixels used for height assignment.

For the DMW algorithm we selected a cluster analysis program called DBSCAN (Ester et. al., 1996), a density based algorithm for identifying clusters in spatial databases with noise. It was selected because it is very effective at identifying clusters of varying shapes and, unlike other methods such as K-means (Lakshmanan et al., 2009a, 2009b, 2003), does not require the user to specify apriori the number of clusters to find. Two parameters must be specified before running DBSCAN: the minimum number of points in a cluster (currently set at 4) and the radius around the point to search for neighbors in the cluster (currently set at 0.5 pixels). Basically, DBSCAN steps through each point (each point being a displacement in line and element space) and classifies it in one of three ways. A "core" cluster point has at least 4 neighbors within its neighborhood (radius). A boundary point has fewer than 4 neighbors but is still connected to a cluster by at least one other point. The

third possibility is that the point does not belong to any cluster and is "noise." Output from DBSCAN consists of a list of clusters found and the number of points in each cluster.

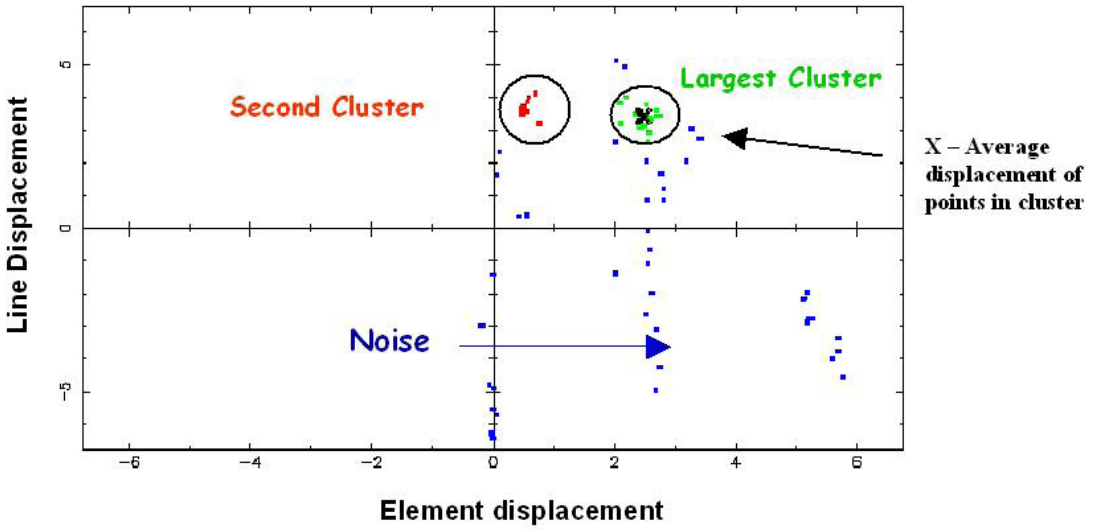

Figure 10. Motion clusters identified by DBSCAN clustering routine. Green dots indicate line and element displacements belonging to the largest cluster. Red dots indicate line and element displacements belonging to the second largest cluster. Blue dots represent incorrect or noisy line and element displacements.

One example of output from DBSCAN is shown in Figure 10. This figure shows that noisy motions have been removed from the scene leaving two distinct motion clusters. The DMW algorithm selects the largest cluster to represent the dominant motion and computes a final derived motion vector by averaging the displacements belonging to the largest cluster. Figure 11 shows the vector field that remains after the analysis is complete.

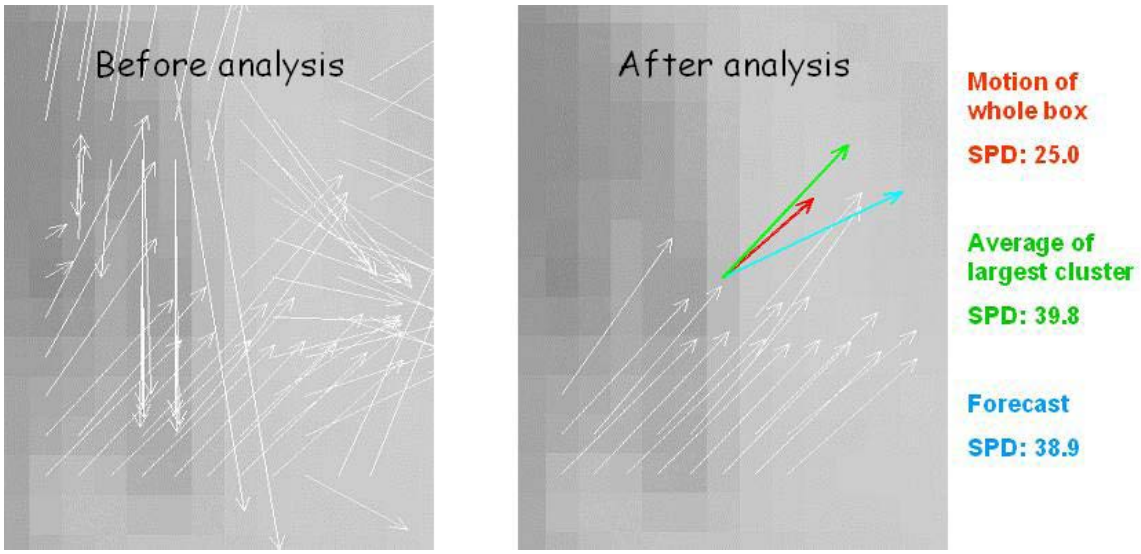

Figure 11. Example of the vector field produced with nested tracking before (left) and after (right) DBSCAN is applied to find the largest cluster. The forecast vector (blue) is shown for comparison.

3.4.2.2.3 Feature Tracking Gross Error Tests

All retrieved wind values undergo a series of quality control tests to determine if the derived wind is valid. This series of tests are described below. If a retrieved wind fails any one of these tests, it is deemed to be an invalid wind and is flagged appropriately. Each failure is associated with a unique "flag" value which is saved in the DMW output file. These unique flag values are listed in Table 6.

The tests are applied in the following order:

a. Match on boundary check
b. Correlation check
c. u-component acceleration check
d. v-component acceleration check
e. u- and v-component acceleration check
f. Slow wind speed check
g. Channel-specific NWP wind speed and direction comparison tests

Correlation Test

As mentioned in Section 3.2, one of two correlation tests is applied when matching the feature of interest to the original target scene. When nested tracking is employed, each matching 5x5 sub-scene must have a correlation score of 0.8 or higher. Otherwise, the displacement associated with the match is discarded and will not be analyzed by the cluster analysis routine. When conventional tracking is used instead of nested tracking, a lower threshold of 0.6 is applied. In this case, the correlation scores of each of the intermediate (i.e., the reverse and forward) matching scenes (derived from the SSD method described in Section 3.4.2.3.1) are checked to see if they exceed the minimum threshold value of 0.60. If either scene fails this correlation test, the DMW product is flagged as unacceptable in the output file.

A higher correlation threshold is used for nested tracking because the scene being matched is much smaller and this increases the likelihood of finding a false positive. The higher threshold is a way of accounting for the higher variance in the estimated displacement and is used to remove gross errors from the matching process.

.

u/v-acceleration Test

If the DMWA is performing as intended, it is reasonable to expect that the wind estimates derived from each image pair of the image triplet will be similar to one another. While real accelerations are certainly plausible, especially in certain weather regimes (near jet

streams, for example) testing for unrealistic accelerations is prudent, especially given the time and space scales we are concerned with. The existence of an unrealistic acceleration in either the u-component or v-component of the DMW is likely to be the result of a false positive in the tracking step. Large, unrealistic u- or v-accelerations are dealt with by imposing an upper limit of 10 m/s on the difference between the two individual u and v-components of DMWs derived for any of the spectral channels except the visible channel, where a 5 m/s limit is imposed. Any DMW that fails the u/v acceleration test is flagged.

Slow Wind Speed Test

The speed of every DMW is checked against a minimum speed threshold of 3 m/s. If any DMW is slower than this speed threshold, then the DMW is flagged.

Correlation Boundary Test

If either of the intermediate matching scenes derived from the SSD method described in Section 3.4.2.3.1 are found on the boundary of the search scene, then the match scene is flagged. This condition may indicate the true matching solution is located beyond the domain of the search scene. In terms of the lag array, this implies that the tracer is rejected if the minimum SSD value is found along the edges of the lag array. Likewise, when nested tracking is used, any matches found on the boundary of the lag array are discarded from influencing the dominant motion calculation.

It should be noted that when tracking the entire target scene with the conventional approach, the correlation boundary test results in a failed tracer. This is not true when nested tracking is employed. In this case, the match is rejected, and the algorithm moves to the next pixel where it attempts to compute another local motion vector.In other words, the small 5x5 sub-target is discarded, not the entire target scene.

NWP Vector Difference Test

An additional quality control component of the derived motion winds is the removal of wind estimates that differ significantly from a short term numerical weather prediction (NWP) forecast wind. The goal of this test is to remove those winds that are grossly different from the forecast due to a poor motion estimate, a poor height assignment, or both. Previously this test examined the difference between the speed and direction components of the wind vector separately but has since been combined into a single vector difference threshold that is band dependent. The threshold was determined, more or less quantitatively, by examining the relationship between the product accuracy (relative to ground truth radiosonde observations), as defined by the mean vector difference and the standard deviation about the mean, and the maximum vector difference. The upper limit was identified as the vector difference value at which the precision specification dropped sufficiently below the requirement (4.2 m/s set forth in the F&PS document) but did not reduce the coverage (i.e., sample size) excessively. The plot used to determine the vector difference threshold for the LWIR winds is shown below in Figure 12.

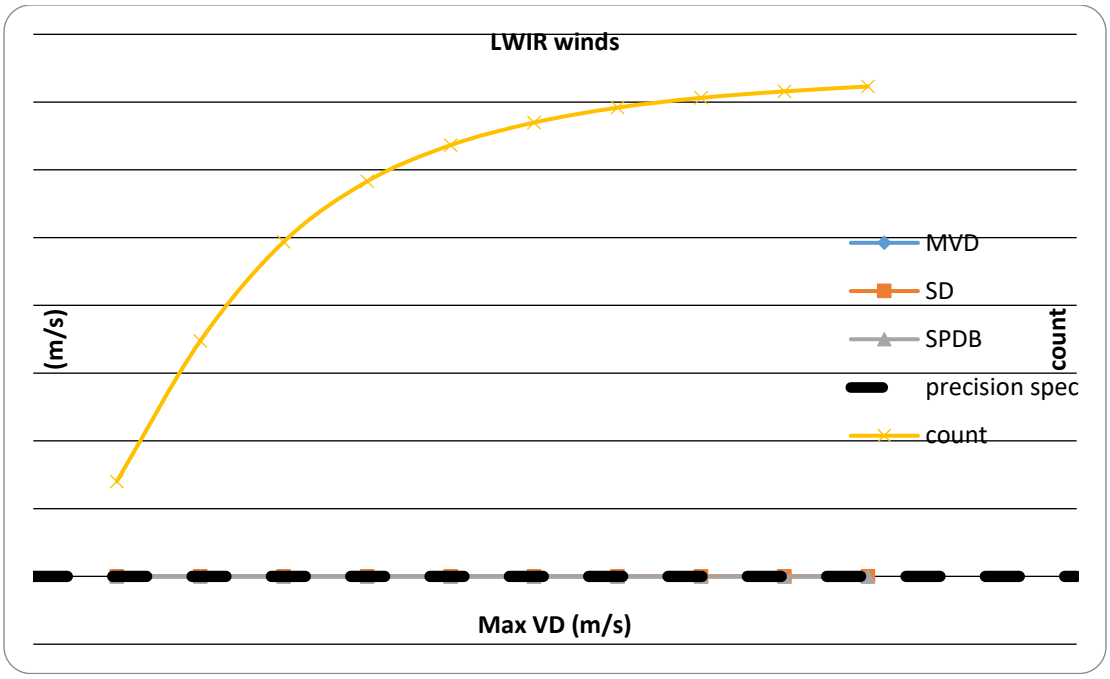

Figure 12. AMV-radiosonde wind verification statistics for the ABI LWIR winds for the period November 1, 2017- January 23, 2018. The Mean Vector Difference (MVD) statistic is used to determine the accuracy of the wind whereas the standard deviation is used to quantify the precision. Note that the accuracy specification (7.5 m/s) is not shown in this figure.

Although the standard deviation curve (red) first dips below the precision specification value when a vector difference threshold of 16 m/s is selected, it is clear from the diagram that the sample size isn't adversely impacted until the limit drops below 10 m/s. For this reason, a threshold of 10 m/s was selected as the upper limit for the LWIR winds, meaning any wind having a vector difference from the forecast of more than 10 m/s is rejected. This threshold is applied as a final check on the AMV before it is classified a good wind. In a similar fashion, vector difference thresholds were determined for all wind product bands. Table 7 summarizes the various band-dependant vector thresholds in current use by the DMW algorithm.

Table 7. Summary of the vector difference thresholds used in the DMW algorithm.

Channel Number	*Tracer Type*	*Vector Difference Threshold (m/s)*
2	Cloud-top	6.0
7	Cloud-top	7.0
8	Cloud-top	10.0
8	Clear-sky water vapor	12.0
9	Clear-sky water vapor	12.0
10	Clear-sky water vapor	12.0
14	Cloud-top	10.0

3.4.2.3 Target Height Assignment

Each suitable target (ie., those passing all of the target selection tests described in Section 3.4.2.1.1) is assigned a height using information from the middle image of the loop sequence. The cloudy or clear designation for each target scene (per the fractional cloud cover test described in Section 3.4.2.1.1) has implications on how a representative height assignment is computed for each target scene.

The process of assigning a representative height to the DMW tracer involves selecting the appropriate sample of pixels from the target scene and using these pixels to compute a representative height for the target scene being processed. The following factors drive the selection of the appropriate sample of pixels to use, as well as the approach, to compute a representative height for each target:

- Target is deemed clear or cloudy
- Channel used to derive the wind
- Whether or not the nested tracking methodology is used

Cloudy Target Scenes

When ABI channels 2 (0.64um), 7 (3.9um), 8 (6.15um, cloud top), or 14 (11.2um) are used to track cloudy target scenes, pixel-level cloud-top pressures provided by the GOES-R cloud height algorithm (see GOES-R ABI Cloud Height ATBD for details) are used to compute a representative height for the target scene. Since the nested tracking approach is used when using these channels, only cloud-top pressures associated with pixels belonging to the largest cluster (as defined in the nested tracking discussion in Section 3.4.2.2.2) are used to derive a representative height. Because two unique large clusters are identified – one for the reverse time step and one for the forward time step – the cloud-top pressure samples from both of these clusters are combined and the median cloud-top pressure value is assigned as the representative height for this target.

A key benefit of this approach is that the assigned height is inherently linked to the tracking solution since the same sample of pixels contributes to each of these derived quantities. Figure 12 highlights the fact that this approach will usually produce a lower height assignment in the atmosphere (higher pressure) than the traditional method of assigning the height based on an arbitrary cold sample (typically 20%) of pixels.

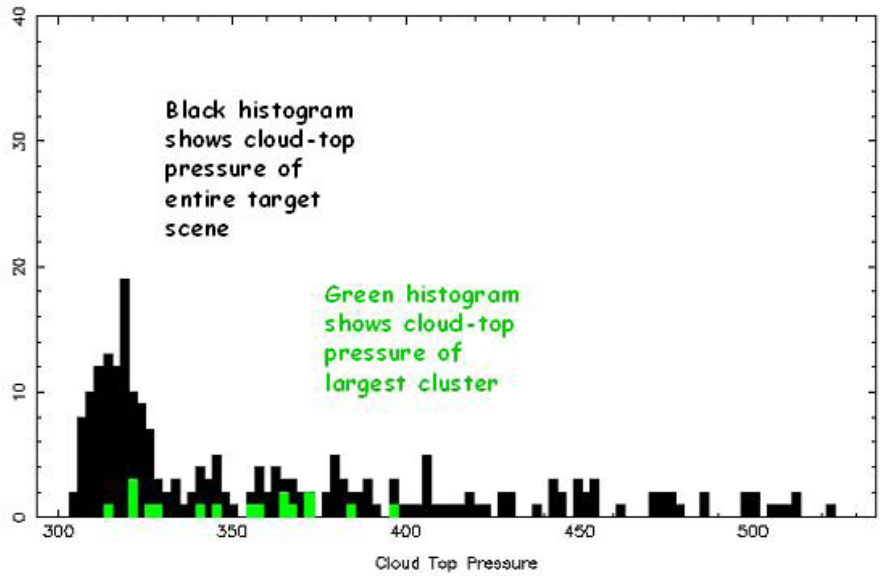

Figure 12. Cloud-top pressure distribution for a single target scene. The values associated with the largest cluster are shown in green.

In situations where a low level cloudy target scene over ocean is partially or totally located in an area experiencing a low level temperature inversion, the DMWA must apply a different approach to compute a representative height assignment to the target scene.
Low-level temperature inversions occur frequently over the ocean in the vicinity of the subtropical high where large-scale subsidence contributes to their formation. These regions are often covered by extensive sheets of marine stratocumulus cloud located at the base of the temperature inversion (see Figure 13). Cloud height algorithms often overestimate the height of these cloud layers by 200 hPa or greater (Gustafsson and Lindberg, 1999). The problem arises when there are two elevations in the temperature profile at which the cloud temperature is reached. In this scenario the actual cloud layer is found at the bottom of the inversion.

The DMWA uses the low-level temperature inversion flag output by the cloud height algorithm to identify those pixels in a target scene where a low level temperature inversion is present. In these situations, the DMWA keeps track of pixels within the largest nested tracking clusters, whose heights are derived at the base of the inversion versus those derived radiometrically via the cloud height algorithm. The DMWA uses only the cloud heights (pressures) belonging to the larger of these two samples to assign a height to the derived wind. The representative height assigned to the derived motion wind is the median pressure of the larger sample.

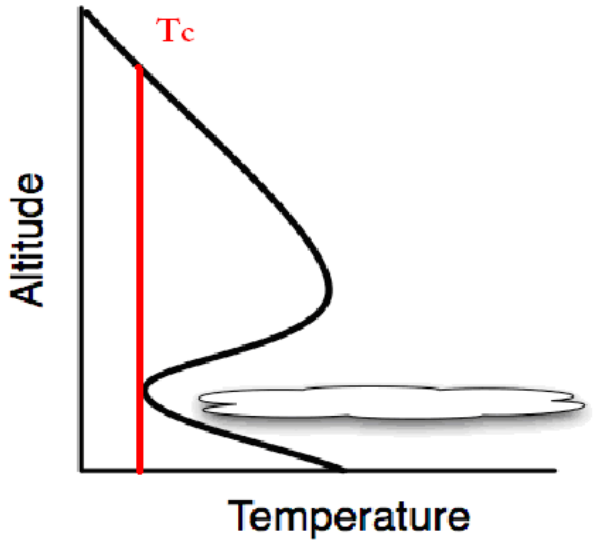

Figure 13. Idealized temperature profile highlighting the cloud height assignment problem posed by low-level temperature inversions.

Clear Target Scenes

When ABI channels 8 (6.15um, clear sky), 9 (7.0um), or 10 (7.4um) are used for targeting clear-sky target scenes (i.e. elevated moisture gradients are being tracked), only clear pixels in the target scene are used. Specifically, a histogram of the target scene brightness temperature values is constructed from all of the clear pixels in the target scene. Next, the 20% coldest pixels of this histogram are identified and the median brightness temperature is calculated. This median brightness temperature is then converted to a height (in pressure) value through linear interpolation of the associated GFS forecast temperatures that bound this brightness temperature.

Initial Cold Sample Height

Regardless of whether nested tracking or traditional tracking is being used an initial "cold sample" height assignment must be computed. The primary purpose of computing an initial height is to use it as a look up index to obtain the forecast wind from a profile. The forecast wind is subsequently used to center the search box in the subsequent (or previous) image. Depending on the channel being processed either a histogram BT values or cloud top temperature values is used to construct a 1-D histogram. The following steps are carried out in constructing the histogram:

1. Loop through each pixel in the target scene and check the cloud mask, temperature (BT or CTT) and low-level inversion flag. For clear sky tracers retain all clear and probably clear pixels. For cloudy tracers retain all pixels having a valid cloud top pressure (not missing). Next, check that the temperature value is in the range 150 –

340 K and exclude those outside of the range. Lastly, determine how many pixels are located in a low-level inversion region (low-level inversion flag=1) and how many pixels are outside a low-level inversion region (low-level inversion flag=0). Determine which sample is larger.

2. Using the larger sample, a histogram is constructed for the range 150 K – 340 K. With a scale factor of 10 the range of the histogram is actually 1500 – 3400. Each CTT or BT from the larger sample is placed in a slot on the histogram rounding up or down to the nearest bin.
3. A point cutoff is computed using the cold threshold:

   Point_Cutoff = NINT(REAL(Histogram_Points) * Cold_Threshold)

   where 'Histogram_Points' is the size of the screened sample from step 1 and Cold_Threshold is:

Band 2	0.25
Band 7	0.25
Band 8	0.20 clear sky, 0.99 cloud top
Band 9	0.20 clear sky, 0.99 cloud top
Band 10	0.20 clear sky
Band 14	0.25

4. Starting from the cold end scan the histogram to find the cutoff slot. One of three conditions must be met:

```
threshold_loop: DO BrtTemp = Lower_Bound, Upper_Bound

  Cold_Sample = Cold_Sample + Histogram(BrtTemp)

  IF (Histogram(BrtTemp) .GT. 0) Number_Of_Bins = Number_Of_Bins + 1

  IF (Cold_Sample .GT. Point_Cutoff .AND. Number_Of_Bins .GT. 1) THEN

    Cold_Sample = Cold_Sample - Histogram(BrtTemp)
    Cold_Slot_Threshold = BrtTemp - 1
    EXIT

  ! Keep at least one histogram bin
  ELSE IF (Cold_Sample .GT. Point_Cutoff .AND. Number_Of_Bins .EQ. 1) THEN

    Cold_Sample = Cold_Sample
    Cold_Slot_Threshold = BrtTemp
    EXIT

  ELSE IF (Cold_Sample .LE. Point_Cutoff .AND. BrtTemp .EQ. Upper_Bound) THEN

    Cold_Sample = Cold_Sample
    Cold_Slot_Threshold = BrtTemp
    EXIT

  ENDIF

END DO threshold_loop
```

Cold sample arrays of BT or CTT, cloud top pressure and cloud top height are created using the cold slot threshold as the highest value allowed

3.4.2.3.1 Derived Motion Wind Height Assignment Quality Tests

All retrieved wind height (in pressure) values undergo a couple of quality control tests to determine if the derived heights are valid. These tests are described below. If a retrieved height fails any one of these tests, it is deemed to be invalid and is flagged appropriately. Each failure is associated with a unique “flag” value which is saved in the DMW output file. These unique flag values are also listed in Table 5.

Acceptable Height Assignment Check

An acceptable height assignment check is done for each derived motion wind that is attempted. The derived height is checked to determine if it falls within an acceptable height (in pressure) range. The minimum and maximum pressures belonging to this range are a function of which channel is being used to derive the wind and shown in Table 8.

Table 8. Acceptable height range to use as a function of channel used and tracer type

Channel Number	*Tracer Type*	*Central Frequency (μm)*	*Acceptable Height Range (hPa)*
2	Cloud-top	0.64	700 - 1000
7	Cloud-top	3.9	700 - 1000
8	Cloud-top	6.15	100 – 350
8	Clear-sky water vapor	6.15	100 - 1000
9	Clear-sky water vapor	7.0	100 - 1000
10	Clear-sky water vapor	7.4	450 - 700
14	Cloud-top	11.2	100 - 1000

Height Consistency Check

When nested tracking is performed, a height consistency checked is performed between the median pressure computed from the largest cluster belonging to the first and second image pairs, respectively. If the difference in these two pressures exceeds 100 hPa, then the derived motion wind is flagged as bad.

3.4.2.4 Product Quality Control

Quality control of the retrieved DMWs is performed in two ways. The first is through the application of target selection, feature tracking, and height assignment error checks as described in the previous sections. The second way involves the calculation of two quality indicators for each of the DMWs using two different, but related, algorithms: the Quality Indicator (QI) (Holmlund, 1998; Holmlund et al., 2001) and the Expected Error (EE) (LeMarshall et al., 2004; Berger et al. 2008).

.

3.4.2.4.1 Quality Indicator (QI) Method

The statistically-based quality indicator (QI) developed at EUMETSAT estimates the reliability of each derived DMW based on several quality control tests (Holmlund, 1998, Holmlund et. al 2001). These tests not only analyze the consistency in space and time of each of the intermediate DMW vector components, but also the height and temperature of the tracers used in the vector determination, the symmetry of vector pairs achieved from tracking tracers between consecutive images, differences with surrounding vectors, and differences from a forecast field (optional). There are a total of seven individual components that contribute to the final QI score that is appended to each DMW. A weighted average value is computed for the final quality test function value $f_i(x)$ for each

vector. In order to combine the results of the different test functions, each result must be normalized into a specific range. This is done using a tanh-based function:

(15)

After normalization of all of the tests, QI values will be distributed from zero (poor quality) to one (perfect quality).

Direction Consistency Check

This calculation is a measure of the direction consistency of the DMW. A quality tracer should provide sub-vectors that are similar in direction. In function space it is calculated as:

Direction: (16)

$D_i(x, y)$, $V_i(x, y)$ are the direction (degrees) and speed (m/s) derived from the first image ($i = 1$) pair (image 1 and image 2) or the second imager ($i = 2$) pair (image 2 and image 3) of an image triplet at location (x, y).

The normalized component used in the software is constructed as such:

$$QI_{dir} = 1 - (\tanh(|D_2(x, y)-D_1(x, y)|/(A*\exp(-vel/B)+C)))**D \quad (17)$$

Where:

$vel = (V_1(x, y) + V_2(x, y))/2$

The values of the constants are:

A	20
B	10
C	10
D	4

Speed Consistency Check

This calculation is a measure of the speed consistency of the DMW. Intermediate DMWs should show agreement in speed. In function space it is calculated as:

Speed: $|V_2(x, y)-V_1(x, y)|/(A*(V_2(x, y)+(V_1(x, y))+B)$ (18)

$V_i(x, y)$ is the speed (m/s) derived from the first image ($i = 1$) pair (image 1 and image 2) or the second image (i = 2) pair (image 2 and image 3) of an image triplet at location (x, y).

The normalized component used in the software is constructed as such:

$$QI_{spd} = 1 - (\tanh(|V_2(x, y)-V_1(x, y)|/(A*vel+B)))**C \quad (19)$$

Where:

$vel = (V_1(x, y) + V_2(x, y))/2$

The values of the constants are:

A	0.2
B	1.0
C	3.0

Vector Consistency Check

This calculation is a measure of the vector consistency of the DMW. This test looks at the vector pairs that make up the final DMW. It should reject acceleration errors, but allow for real acceleration changes (jet entrance and exit regions). In function space it is calculated as:

$$\text{Vector:} \quad |S_2(x, y)-S_1(x, y)|/(A*(V_2(x, y)+(V_1(x, y))+B) \quad (20)$$

$S_i(x, y)$ is the vector (m/s) derived from the first image ($i = 1$) pair (image 1 and image 2) or the second image ($i = 2$) pair (image 2 and image 3) of an image triplet at location (x, y).

The normalized component used in the software is constructed as such:

$$QI_{vec} = 1 - (\tanh(|S_2(x, y)-S_1(x, y)|/(A*vel+B)))**C \quad (21)$$

Where:

$vel = (V_1(x, y) + V_2(x, y))/2$

The values of the constants are:

A	0.2
B	1.0
C	3.0

Spatial Consistency Check (i.e. Best Buddy Check)

This calculation is a measure of the spatial wind consistency of the DMW with its best neighbor. To do this, the DMW values are compared with the DMWs computed at the neighboring grid points.

In function space it is calculated as:

$$\text{Spatial:} \quad |S(x, y)-S(x-i, y-j)|/(A*(|S(x, y)+(S(x-i, y-j)|)+B) \tag{22}$$

Here, $S(x, y) = S_1(x, y) + S_2(x, y)$. $S(x-i, y-j)$ refers to the vectors (m/s) in the surrounding locations. This spatial test is only applied to vectors within a predefined pressure range (50 hPa), and location range (within 1 degree).

The normalized component used in the software is constructed as such:

$$QI_{spatial} = 1 - (\tanh(|S(x-i, y-j)-S(x, y)|/(A*|S(x, y)+(S(x-i, y-j)| +B)))**C \tag{23}$$

The values of the constants are:

A	0.2
B	1.0
C	3.0

Forecast Check

This is currently set as an optional test, and is a measure of the consistency of the satellite DMW with the forecast wind at the height of the satellite DMW. The vector difference of the DMW values and the forecast vector interpolated to the same location and pressure level is computed to calculate it. In function space it is represented as:

$$\text{Forecast:} \quad |S_2(x, y)-F_1(x, y)|/(A*(|S_2(x, y)+(F_1(x, y)|)+B) \tag{24}$$

Where $S_2(x, y)$ is the vector (m/s) from the final DMW at location (x, y). $F_1(x, y)$ is the interpolated forecast vector (m/s) at location (x, y).

The normalized component used in the software is constructed as such:

$$QI_{fc} = 1 - (\tanh(|S_2(x, y)-F_1(x, y)|/(A*fc\_spd+B)))**C \tag{25}$$

In practice, fc_spd is the speed (m/s) of the forecast at the DMW location. The values of the constants are:

A	0.4
B	1.0
C	2.0

U-Component Consistency Check

This calculation is a measure of the DMW's u-component (m/s) consistency from each intermediate vector. In function space it is calculated as:

$$\text{U-component:} \qquad |u_2(x, y)-u_1(x, y)|/((A*|u_2(x, y)+(u_1(x, y)|)+B) \qquad (26)$$

The normalized component used in the software is constructed as such:

$$QI_{uc} = 1 - (\tanh(|u_2(x, y)-u_1(x, y)|/(A*|u_2(x, y)+u_1(x, y)|+B)))**C \qquad (27)$$

The values of the constants are:

A	1.0
B	1.0
C	2.0

V-Component Consistency Check

This calculation is a measure of the DMW's v-component (m/s) consistency from each intermediate vector. In function space it is calculated as:

$$\text{V-component:} \qquad |v_2(x, y)-v_1(x, y)|/((A*|v_2(x, y)+(v_1(x, y)|)+B) \qquad (28)$$

The normalized component used in the software is constructed as such:

$$QI_{vc} = 1 - (\tanh(|v_2(x, y)-v_1(x, y)|/(A*|v_2(x, y)+v_1(x, y)|+B)))**C \qquad (29)$$

The values of the constants are:

A	1.0
B	1.0
C	2.0

To achieve a single QI value to represent the quality of each DMW, a weighted average of each normalized QI component is computed:

$$QI = \Sigma \text{ (Test Weight * Normalized QI Component test)} / \Sigma \text{ Test Weights} \qquad (30)$$

The test weights used for each normalized QI component is shown in Table 9.

Table 9. Test weights used for each normalized QI component test.

Direction Component	1.0
Speed Component	1.0
Vector Component	1.0
Spatial Component	2.0
Forecast Component	1.0
U Component	0.0
V Component	0.0

Figure 14 shows an example of the final (weighted) QI distribution for winds generated from the 12 UTC 04 August 2006 Meteosat-8/SEVIRI proxy dataset. DMWs that possess QI values less than 0.60 are currently flagged as unacceptable quality.

Figure 14. Histogram of the final (weighted) QI values for Meteosat-8 DMWs at 12 UTC on 04 August 2006.

3.4.2.4.2 Expected Error Method

The Expected Error (EE) algorithm, originally developed at the Australian Bureau of Meteorology (LeMarshall et al, 2004) is an extension of the QI algorithm described in the previous section. It is designed to express quality in terms of a physical vector error metric (meters/second, m/s), rather than a normalized score such as the QI. A slightly modified version of the EE algorithm described in Berger et al. 2008 has been adopted for use with the GOES-R DMWA. As shown in (31), the algorithm regresses several DMW variables against the natural logarithm of the EE, which represents the vector difference (in m/s) between a large sample of collocated DMWs and radiosonde winds.

$$a_0 + a_1 x_1 + a_2 x_2 + ... a_9 x_9 = \log(EE + 1) \tag{31}$$

where EE is the expected (or estimated) error, a_0 is a constant, and a_n values are regression coefficients multiplied by their corresponding predictors (x_n). The coefficients are applied in real time to compute and assign an EE to each DMW using:

$$EE = e^{(a_0 + a_1 x_1 + a_2 x_2 + ... a_9 x_9)} - 1 \tag{32}$$

The (-1) term constrains the minimum EE value to be zero. The current predictors are:

1. Constant (spectrally dependent)
2. QI Speed Test
3. QI Direction Test
4. QI Vector Difference

5. QI Local Consistency Test
6. QI Forecast Test
7. DMW Speed
8. Assigned DMW Pressure Level (height)
9. NWP Wind Shear (200 hPa Above – 200 hPa below DMW height)
10. NWP Temperature Gradient (200 hPa Above – 200 hPa below DMW height)

Table 10. Expected Error coefficients and predictors for different Meteosat-8 channels derived from the period August – October 2007.

Predictor	Band-1 (0.60um)	Band-4 (3.9um)	Band-5 (6.2um)	Band-6 (7.3um)	Band-9 (10.8um)
CONST	3.073	3.13	2.42	2.42	2.871
QI Speed Check	0.176	0.003	0.0660	0.0660	-0.0664
QI Direction Check	0.290	-0.171	0.199	0.199	0.1394
QI Vector	-0.101	-0.0471	-0.331	-0.331	-0.176
QI Local Consistency	-0,280	0.244	-0.173	-0.173	-0.252
QI Forecast Check	-0.585	-1.46	-0.552	-0.552	-0.509
DMW Speed	0.014	-3.61×10^{-3}	7.10×10^{-3}	7.10×10^{-3}	6.26×10^{-3}
DMW Pressure	-1.63×10^{-3}	-9.43×10^{-4}	-6.79×10^{-4}	-6.79×10^{-4}	-7.42×10^{-4}
NWP Wind Shear	0.011	0.015	7.80×10^{-3}	7.80×10^{-3}	9.81×10^{-3}
NWP Temp Gradient	0.011	-7.47×10^{-3}	6.89×10^{-3}	6.89×10^{-3}	0.0126

Table 10 shows a set of predictors and their respective coefficients used to calculate EE for different bands from the SEVIRI instrument (proxy to the ABI) onboard the Meteosat-8 satellite, generated from a dataset containing collocated Meteosat-8 DMWs and radiosonde wind observations that covered the period August – October 2007.

Synergistic Use of the EE and QI Quality Indicators

The outputted EE and QI quality indicators associated with each DMW estimate can be used synergistically in order to optimize the quality and geographic coverage of the final DMW dataset passed onto the user community. The synergistic use of these quality indicators is designed to take advantage of the strengths of each. The EE is superior at identifying the quality of relatively slow DMWs, whereas the QI is better at identifying the

quality of relatively fast DMWs. A study conducted under the GOES-R Risk Reduction (Berger et al. 2008) seeked to identify thresholds for each parameter that could serve as a potential starting point for users to use, if so desired, in any process they may have established to select a subset of the highest quality DMWs. Table 11 summarizes what these thresholds are, and shows that they vary as a function of the channel used to derive the DMW and the DMW speed. DMWs whose speeds are slower than the indicated speed thresholds are considered higher quality if their respective EE quality indicators are less then or equal to the EE threshold shown in Table 11. DMWs whose speeds exceed the speed thresholds are considered higher quality DMWs if their respective QI indicators exceed the QI thresholds shown in Table 11.

Table 11. Recommended thresholds for synergistic use of the QI and EE indicators

Channel	EE (m/s) <	OR	(QI >	&	Speed (m/s) >
1 (0.64um)	5.5		95		30
4 (3.90um)	5.0		95		30
5 (6.15um)	5.0		95		30
6 (7.30um)	5.0		95		30
9 (10.8um)	4.5		90		25

In order to validate the established thresholds in Table 11, Meteosat-8 DMWs were generated for an independent dataset covering February 2007 and compared to collocated radiosonde wind observations. The EE values were calculated using the generated coefficients from Table 10, and the QI was calculated as described in the previous section. Table 12 shows an example of DMW-RAOB verification statistics looking at QI > 0.6, QI > 0.8 and the specific EE/QI threshold for IR DMWs from Table 11. The statistics are for all available DMW heights in the dataset. A 0.8 QI threshold produces a lower RMSE, mean vector difference, and standard deviation than the 0.6 threshold (as expected). However, the QI/EE combination threshold results in the lowest RMSE error, mean-vector difference and speed bias of the three quality indicator choices. Use of the combined QI/EE thresholds generally results in the retention of more (less) DMWs when using the QI > 0.8 (0.60) threshold alone. These findings also hold for the other channel DMWs.

Table 12: Comparison statistics (m/s) between DMWs computed from the SEVIRI IR-Window channel (10.8um) and collocated radiosonde winds during Feb 2007.

QC	**QI > 0.6**	**QI > 0.8**	**EE<=4.5 .OR. (QI>90 and Speed>25 m/s**
RMSE	7.62	7.30	6.14
Bias	-1.62	-1.19	-1.02
Number of matches	23692	17501	16861
Mean Vector Difference	6.08	5.82	5.03

Standard Deviation	4.60	4.39	3.53
Avg. DMW Speed	17.16	18.48	17.21

3.4.3 Algorithm Output

Derived motion winds will be generated separately from each of the six ABI bands identified in Table 2. Collectively, the derived motion winds generated from each of these ABI bands contribute are the derived motion wind product. The Mode 3 full disk DMW product has a 60 minutes refresh while the Mode 3 full disk product has a 15 minute refresh. To create these products, the DMW algorithm should be run once an hour and once every 15 minutes respectively. The DMW is considered as a "list" product as it is not output on a grid. The contents of the output of the DMWA are described in the following subsections.

3.4.3.1 Product Output

ID	Description
1	Time of wind from the middle image in image triplet (secs since 1970-01-01 00:00:00) Time
2	Latitude (degrees north) Latitude
3	Longitude (degrees east) Longitude
4	Speed of wind vector (m/s) Wind_Speed
5	Direction of wind vector (degrees) Wind_Dir
6	Pressure assignment of tracer (hPa) MedianPress (hPa)
7	Temperature associated with the pressure assignment of tracer (K) MedianBT
8	Local Zenith Angle (degrees) SatZen
9	Time interval between image pairs (minutes) TimeInterval

3.4.3.2 Diagnostic Information

ID	Description
1	u-component of vector 1 (m/s) [backward in time] UComponent1
2	v-component of vector 1 (m/s) [backward in time] VComponent1
3	u-component of vector 2 (m/s) [forward in time] UComponent2
4	v-component of vector 2 (m/s) [forward in time] VComponent2
5	Speed of forecast wind (m/s) at pressure assigned to satellite wind Fcst_Spd
6	Direction of forecast wind (degrees) at pressure assigned to satellite wind Fcst_Dir
7	Tracking correlation of vector 1 [backward in time] CorrCoeff
8	Tracking correlation of vector 2 [forward in time] CorrCoeff2
9	Standard deviation of cloud top pressure values in target scene (hPa) VariancePress
10	Cold sample counter in brightness temperature histogram PointIndex
11	Latitude of vector 1 (degrees north) [backward in time] LatMatch
12	Longitude of vector 1 (degrees east) [backward in time] LonMatch
13	Latitude of vector 2 (degrees north) [forward in time] LatMatch2
14	Longitude of vector 2 (degrees east) [forward in time] LonMatch2
15	Standard deviation of largest 5x5 cluster (sample 1 – reverse vector) StdDevMVD1
16	Standard deviation of largest 5x5 cluster (sample 2 – forward vector) StdDevMVD2
17	Standard deviation of sample 1 divided by magnitude of average displacement PctOfAvg1
18	Standard deviation of sample 2 divided by magnitude of average displacement PctOfAvg2
19	Number of distinct motion clusters from DBSCAN analysis (sample 1 – reverse vector) NumClusters1
20	Size of largest DBSCAN cluster (sample 1 – reverse vector)

	MaxClusterSize1
21	Number of distinct motion clusters from DBSCAN analysis (sample 2 – forward vector) NumClusters2
22	Size of largest DBSCAN cluster (sample 2 – forward vector) MaxClusterSize2
23	Height assignment of tracer (m) Altitude
24	Date of 1st image (year and Julian day) PriorImageDate
25	Time of 1st image (hour and minute) PriorImageTime
26	Date of 3rd image (year and Julian day) NextImageDate
27	Time of 3rd image (hour and minute) NextImageTime
28	Minimum cloud-top pressure (hPa) in largest cluster MinCTP
29	Maximum cloud-top pressure (hPa) in largest cluster MaxCTP
30	Minimum cloud-top temperature (K) in largest cluster MinCTT
31	Maximum cloud-top temperature (K) in largest cluster MaxCTT
32	Dominant cloud phase of target scene CloudPhase
33	Dominant cloud type of target scene CloudType
34	NWP vertical temperature gradient (K) [+/- 200 hPa about pressure assignment of tracer] TempGrad
35	NWP vertical wind shear (m/s) [+/- 200 hPa about pressure assignment of tracer] Wind_Speed_Shear
36	Land mask LandFlag
37	Low-level inversion flag InversionFlag

3.4.3.3 Product Quality Information

ID	Description

1	Product Quality Flag (0=DMW product passes all quality tests; > 0 DMW product fails quality tests. *(See Table 5 in Section 3.4.2.1.1 for description of DMW failure codes)* Flag
2	Expected Error estimate of derived wind (m/s) ExpectedErr
3	Quality Indicator (QI) of derived wind (0-100, with 100 being the best) QI
4	QI Test 1 value (speed consistency) QISpdFlag
5	QI Test 2 value (direction consistency) QIDirFlag
6	QI Test 3 value (vector consistency) QIVecFlag
7	QI Test 4 value (local consistency) QILocConsistencyFlg
8	QI Test 5 value (forecast consistency) QIFcstFlag
9	Representative height error (hPa) CombinedMedianHgtErr
10	Representative temperature error (K) CombinedMedianTempErr

3.4.3.4 Metadata Information

ID	Description
1	Satellite ID SatID
2	Number of ABI channels NumOfChn
3	ABI channel number AMVChannel
4	Target box size (in pixels) BoxSize
5	Lag size (in pixels) LagSize
6	Nested tracking flag (0=nested tracking disabled, 1= nested tracking enabled) NestedTrackingFlg
7	Target type (0 = clear; 1 = cloudy) Target_Type

8	Number of QC flag values: 23 NumQAVals
9	Percent of targets associated with a QC flag value 0 *Good wind; passes all QC checks* QA_Value_0
10	Percent of targets associated with a QC flag value 1 *Maximum gradient below acceptable threshold* QA_Value_1
11	Percent of targets associated with a QC flag value 2 *Target located on earth edge* QA_Value_2
12	Percent of targets associated with a QC flag value 3 *Cloud amount failure (less than 10% cloud cover for cloud track winds or greater than 0% cloud cover for water vapor clear sky winds)* QA_Value_3
13	Percent of targets associated with a QC flag value 4 *Median pressure failure* QA_Value_4
14	Percent of targets associated with a QC flag value 5 *Bad or missing brightness temperature in target scene* QA_Value_5
15	Percent of targets associated with a QC flag value 6 *More than 1 cloud layer present* QA_Value_6
16	Percent of targets associated with a QC flag value 7 *Target scene too coherent (not enough structure for reliable tracking)* QA_Value_7
17	Percent of targets associated with a QC flag value 8 *Tracking correlation below 0.6 (not used for nested tracking)* QA_Value_8
18	Percent of targets associated with a QC flag value 9 *u-component acceleration greater than 5 m/s (for winds generated from visible channel) or 10 m/s (for winds generated from any other channel)* QA_Value_9
19	Percent of targets associated with a QC flag value 10 *v-component acceleration greater than 5 m/s (for winds generated from visible channel) or 10 m/s (for winds generated from any other channel)* QA_Value_10
20	Percent of targets associated with a QC flag value 11 *u- and v- component accelerations greater than 5 m/s (for winds generated from visible channel) or 10 m/s (for winds generated from any other channel)* QA_Value_11
21	Percent of targets associated with a QC flag value 12 *Derived wind slower than 3 m/s* QA_Value_12

22	Percent of targets associated with a QC flag value 13 *Target scene too close to day/night terminator (visible and SWIR only)* QA_Value_13
23	Percent of targets associated with a QC flag value 14 *Median pressure used for height assignment outside acceptable pressure range (channel dependent)* QA_Value_14
24	Percent of targets associated with a QC flag value 15 *Match found on boundary of search region* QA_Value_15
25	Percent of targets associated with a QC flag value 16 *Gross difference from forecast wind (channel dependent)* QA_Value_16
26	Percent of targets associated with a QC flag value 17 *Median pressure of largest cluster for first image pair is too different from median pressure of largest cluster for second image pair – only valid for nested tracking* QA_Value_17
27	Percent of targets associated with a QC flag value 18 *Search region extends beyond domain of data buffer* QA_Value_18
28	Percent of targets associated with a QC flag value 19 *Expected Error (EE) too high* QA_Value_19
29	Percent of targets associated with a QC flag value 20 *Missing data in search region* QA_Value_20
30	Percent of targets associated with a QC flag value 21 *No winds are available for the clustering algorithm* QA_Value_21
31	Percent of targets associated with a QC flag value 22 *No clusters were found* QA_Value_22
32	Total targets identified NumTargets_Total
33	Mean wind speed (m/s) for all good derived winds WndSpdMean
34	Minimum wind speed (m/s) for all good derived winds WndSpdMin
35	Maximum wind speed (m/s) for all good derived winds WndSpdMax
36	Standard deviation about mean wind speed (m/s) for all good derived winds WndSpdStdDev
37	Number of Atmospheric Layers NumOfAtmosLayers

38	Number of good winds in atmospheric layer 1 *(100 - 399.9 hPa)* NumGoodWnds_Layer1
39	Number of good winds in atmospheric layer 2 *(400 – 699.9 hPa)* NumGoodWnds_Layer2
40	Number of good winds in atmospheric layer 3 *(700 – 1000 hPa)* NumGoodWnds_Layer3
41	Mean height (hPa) assigned to good derived winds in atmospheric layer 1 CldHgtMean_Layer1
42	Standard deviation about mean height (hPa) assigned to good derived winds in atmospheric layer 1 CldHgtStdDev_Layer1
43	Minimum height (hPa) assigned to good winds in atmospheric layer 1 CldHgtMin_Layer1
44	Maximum height (hPa) assigned to good winds in atmospheric layer 1 CldHgtMax_Layer1
45	Standard deviation about mean wind speed (m/s) for all good derived winds in atmospheric layer 1 WndSpdStdDev_Layer1
46	Mean height (hPa) assigned to good derived winds in atmospheric layer 2 CldHgtMean_Layer2
47	Standard deviation about mean height (hPa) assigned to good derived winds in atmospheric layer 2 CldHgtStdDev_Layer2
48	Minimum height (hPa) assigned to good winds in atmospheric layer 2 CldHgtMin_Layer2
49	Maximum height (hPa) assigned to good winds in atmospheric layer 2 CldHgtMax_Layer2
50	Standard deviation about mean wind speed (m/s) for all good derived winds in atmospheric layer 2 WndSpdStdDev_Layer2
51	Mean height (hPa) assigned to good derived winds in atmospheric layer 3 CldHgtMean_Layer3
52	Standard deviation about mean height (hPa) assigned to good derived winds in atmospheric layer 3 CldHgtStdDev_Layer3
53	Minimum height (hPa) assigned to good winds in atmospheric layer 3 CldHgtMin_Layer3
54	Maximum height (hPa) assigned to good winds in atmospheric layer 3 CldHgtMax_Layer3

55	Standard deviation about mean wind speed (m/s) for all good derived winds in atmospheric layer 3 WndSpdStdDev_Layer3
56	Percent good winds generated GoodWndClrCld

4 TEST DATA SETS AND OUTPUTS

4.1 GOES-R Proxy and Simulated Input Data Sets

The data used in the pre-launch phase to develop, test, and validate the ABI DMW products fall into these two categories:

1) ABI proxy data from another observing system
2) ABI simulated data that are derived from use of a radiative transfer model where the atmospheric and earth surface representations are provided by a high resolution numerical weather prediction forecast model

The GOES-R Algorithm Working Group Proxy Data Team is responsible for the generation of the proxy and simulated instrument data sets.

4.1.1 SEVIRI Data

In terms of the ABI proxy data, the Spinning Enhanced Visible and Infra-red Imager (SEVIRI) instrument onboard the European Meteosat Second Generation (MSG) satellite (Schmetz et al, 2002) is being used since it is the best surrogate system for the future ABI. The spectral coverage and pixel level resolution of the SEVIRI instrument is very similar to that expected from the ABI instrument as is the noise level of the various channels. Furthermore, the navigation and registration performance of the SEVIRI instrument is comparable to the expected ABI instrument performance. Finally, the scanning rate of the SEVIRI instrument is similar to the nominal scanning strategies for the ABI instrument. Table 13 lists the SEVIRI bands that are being used in DMWA development and validation pre-launch phase activities. For reference, the corresponding ABI channels are also listed in this table.

Table 13: SEVIRI channels serving as GOES-R ABI proxy data for the GOES-R DMWA.

SEVIRI Band Number	SEVIRI Wavelength Range (µm)	SEVIRI Central Wavelength (µm)	SEVIRI Sensor Noise	ABI Band Number	ABI Wavelength Range (µm)	ABI Central Wavelength (µm)
1	0.56 - 0.71	0.60	0.39@ 5.3 W/m2	2	0.59 - 0.69	0.64

4	3.48 - 4.36	3.90	0.24 K @ 300K	7	3.80 - 4.00	3.90
5	5.35 - 7.15	6.20	0.40 K @ 250K	8	5.70 - 6.60	6.19
6	6.85 - 7.85	7.30	0.48 K @ 250K	10	7.24 – 7.44	7.30
9	9.80 - 11.80	10.80	0.13 K @ 300K	14	10.80 – 11.60	11.20

SEVIRI datasets being used for DMWA product development and validation activities include full-disk Meteosat-8 SEVIRI data for the months of August 2006 and February 2007 and Meteosat-8 SEVIRI rapid-scan data for the period June 1-8, 2008. The temporal resolution of these data, 15 minute for Full Disk and 5-minute for the rapid scan, mimic what is to be expected from the scanning rates of the ABI, making them invaluable for testing and validating the DMWA. Use of these SEVIRI observations enabled an analysis of the performance of the DMWA over a full range of conditions.

4.1.2 Simulated ABI Data

Simulated ABI radiances can be derived using a detailed radiative transfer model over a wide range of atmospheric and surface conditions that originate from short-term forecasts output by a high-resolution numerical weather prediction model. The GOES-R AWG Proxy Data team has created several ABI simulations. This section details work on a CONUS simulation which mimics one of the proposed scan segments on the future ABI (Otkin et al., 2007). Two flexible scanning scenarios are currently under review for the ABI. The first mode allows the ABI to scan the full disk (FD) every 15 minutes, 3 CONUS scenes, and scan a 1000 km x 1000 km selectable area every 30 seconds. A second mode would program the ABI to scan the FD every 5 minutes (Schmit et al. 2005). Figure 15 shows an example of simulated ABI imagery and corresponding actual GOES-12 IR/WV images over the CONUS at 00 UTC 05 June 2005. The simulated data captures the general features and locations well. Some differences can be observed in the cloud structures.

The synthetic GOES-R ABI imagery begins as a high resolution Weather Research and Forecasting (WRF) model simulation. The CONUS simulation was performed at the National Center for Supercomputing Applications (NCSA) at the University of Illinois at Urbana-Champaign by the GOES-R AWG proxy data team. Simulated atmospheric fields were generated using version 2.2 of the WRF model (ARW core). The simulation was initialized at 00 UTC on 04 June 2005 with 1° GFS data and then run for 30 hours using a triple-nested domain configuration. The outermost domain covers the entire GOES-R viewing area with a 6-km horizontal resolution while the inner domains cover the CONUS and mesoscale regions with 2-km and 0.667-km horizontal resolution, respectively.

WRF model output, including the surface skin temperature, atmospheric temperature, water vapor mixing ratio, and the mixing ratio and effective particle diameters for each hydrometeor species, were ingested into the Successive Order of Interaction (SOI) forward radiative transfer model in order to generate simulated top of atmosphere (TOA) radiances. Gas optical depths were calculated for each ABI infrared band using the Community

Radiative Transfer Model (CRTM). Ice cloud absorption and scattering properties were obtained from Baum et al. (2005), whereas the liquid cloud properties were based on Lorenz-Mie calculations.

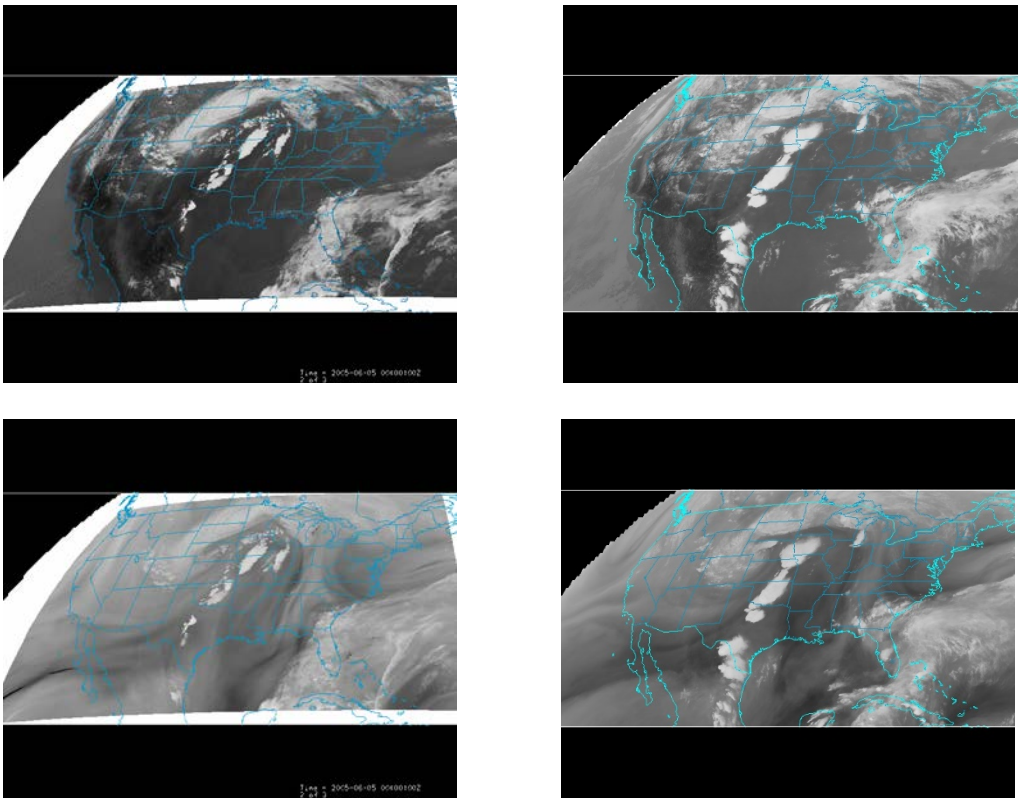

Figure 15. Simulated GOES-R ABI versus actual GOES-12 imager imagery at 00 UTC on 05 June 2005. Top Left: Simulated 11.2 μm imagery from the GOES-R ABI. Top Right: Actual 10.7 μm imagery from the GOES-12 imager. Bottom Left: Simulated 6.19 μm imagery from the ABI. Bottom right: Actual 6.5 μm imagery from the GOES-12 imager.

4.2 Output from Proxy and Simulated Data Sets

4.2.1 Derived Motion Winds Generated from SEVIRI Data

The DMW product has been generated from full disk SEVIRI imagery for the entire month of August 2006 and February 2007 as well as from the rapid-scan SEVIRI imagery for the period June1-8, 2008. Figures 16 and 17 show examples of cloud-drift winds generated from tracking cloud features observed in the SEVIRI 10.8um channel over the full disk and the area covered by the rapid-scans. Figures 18 and 19 show examples of low level (at or below 700 hPa) cloud-drift winds over the full disk generated from tracking cloud features observed in the SEVIRI 0.60um and 3.9um channels, respectively. Figure 20 shows an example of cloud-top water vapor winds over the full disk generated from tracking cloud

features observed in the SEVIRI 6.2um channel. Figure 21 shows an example of clear-sky water vapor winds over the full disk generated from tracking clear-sky moisture features observed in the 6.2um and 7.3um channels.

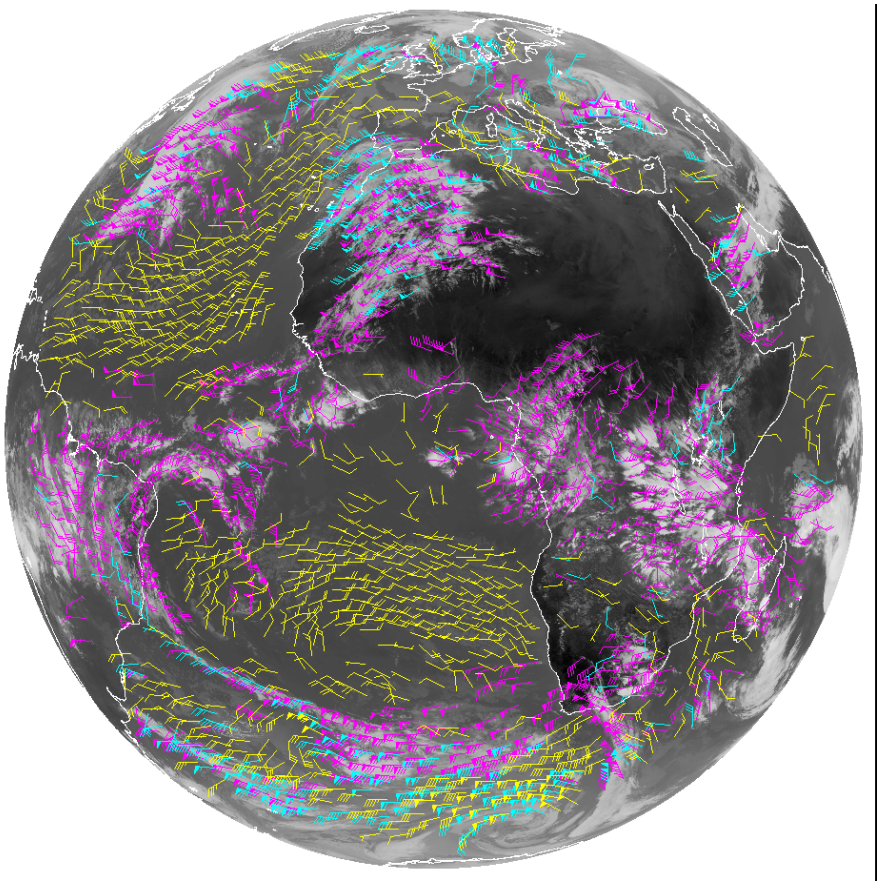

Figure 16. Cloud-drift winds derived from full disk 15-minute Meteosat-8 10.8um SEVIRI data for 12 UTC on 01 February 2007. These winds are derived from tracking cloud features using the 10.8um channel. High level (100-400 hPa) winds are shown in violet; mid-level (400-700 hPa) winds are shown in cyan; and low level winds (below 700 hPa) are shown in yellow.

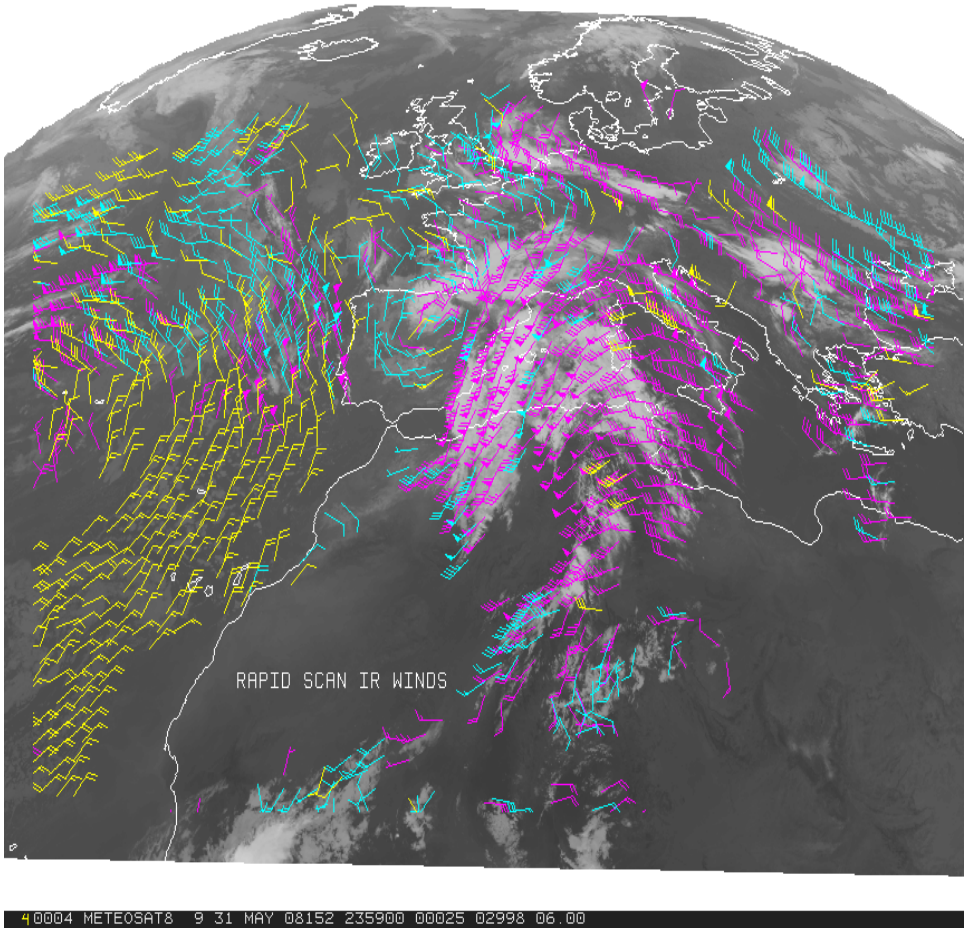

Figure 17. Cloud-drift winds derived from rapid-scan 5-minute Meteosat-8 10.8um SEVIRI data for 2359 UTC on 31 May 2008. These winds are derived from tracking cloud features using the 10.8um channel. High level (100-400 hPa) winds are shown in violet; mid-level (400-700 hPa) winds are shown in cyan; and low level winds (below 700 hPa) are shown in yellow.

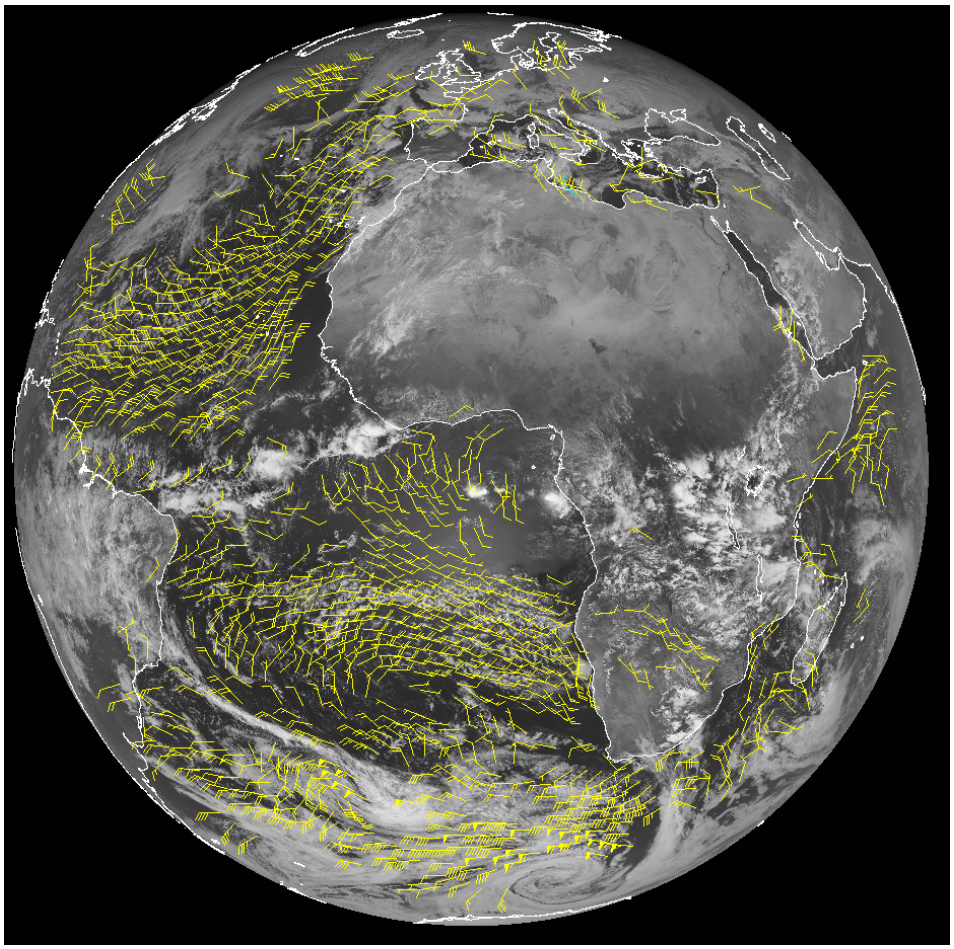

Figure 18. Cloud-drift winds derived from full disk 15-minute Meteosat-8 0.60um SEVIRI data for 12 UTC on 01 February 2007. These winds are derived from tracking cloud features using the 0.60um channel. All winds derived from this channel are at low levels of the atmosphere (below 700 hPa) during the day and are shown in yellow.

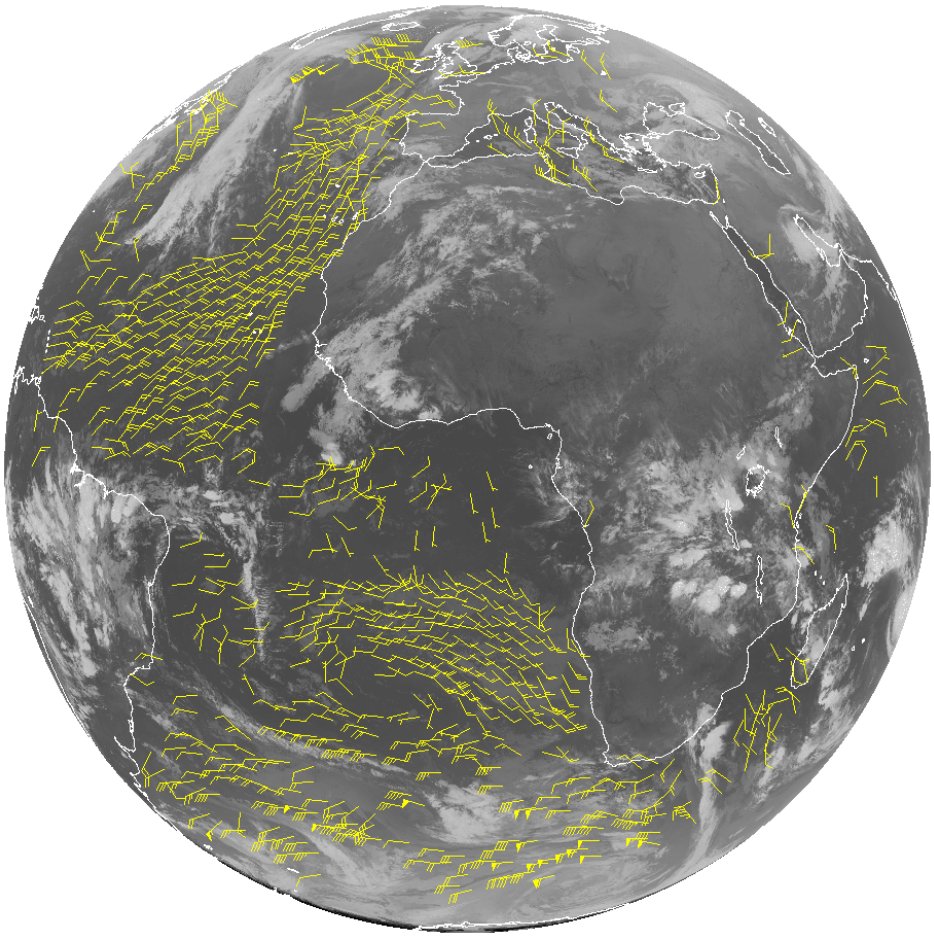

Figure 19. Cloud-drift winds derived from full disk 15-minute Meteosat-8 3.9um SEVIRI data for 00 UTC on 02 February 2007. These winds are derived from tracking cloud features using the 3.9um channel. All winds derived from this channel are at low levels of the atmosphere (below 700 hPa) during the night and are shown in yellow.

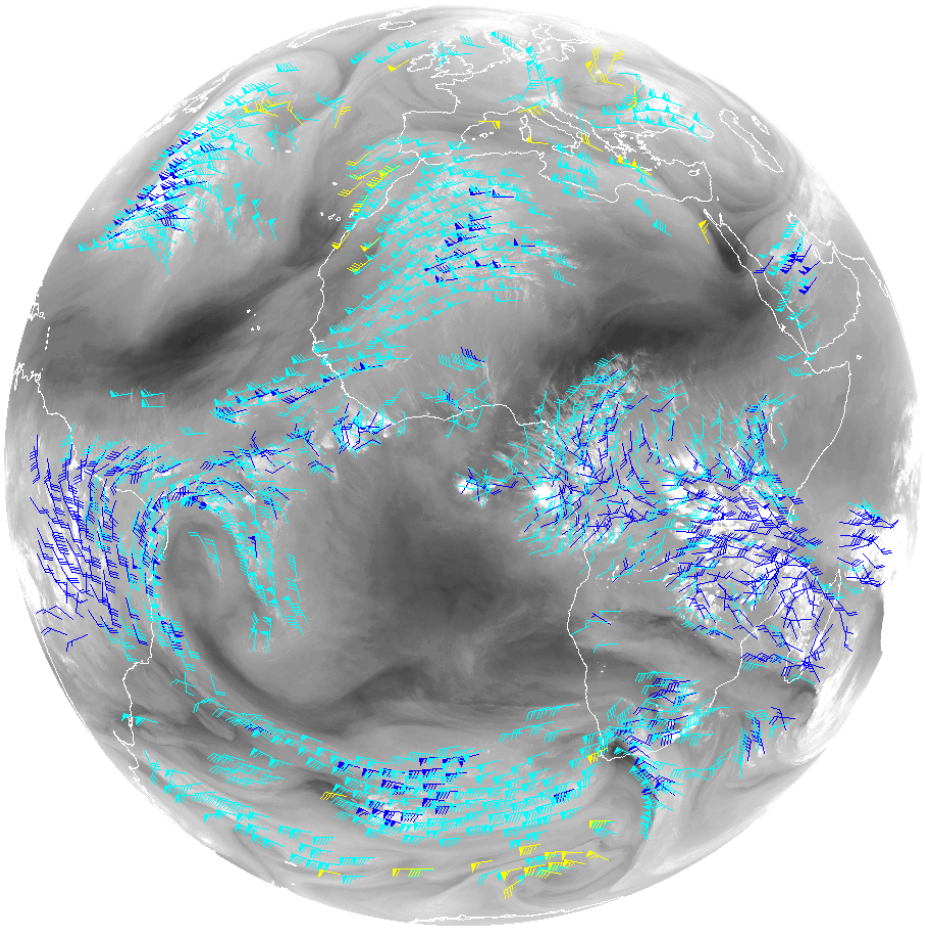

Figure 20. Cloud-top Water Vapor Winds derived from full disk 15-minute Meteosat-8 SEVIRI 6.2um data for 12 UTC on 01 February 2007. These winds are derived from tracking cloud features using the 6.2um channel. In dark blue are winds found in the range 100-250 hPa; in cyan are winds found in the range 250-350 hPa; in yellow are winds in the range 350 – 550 hPa.

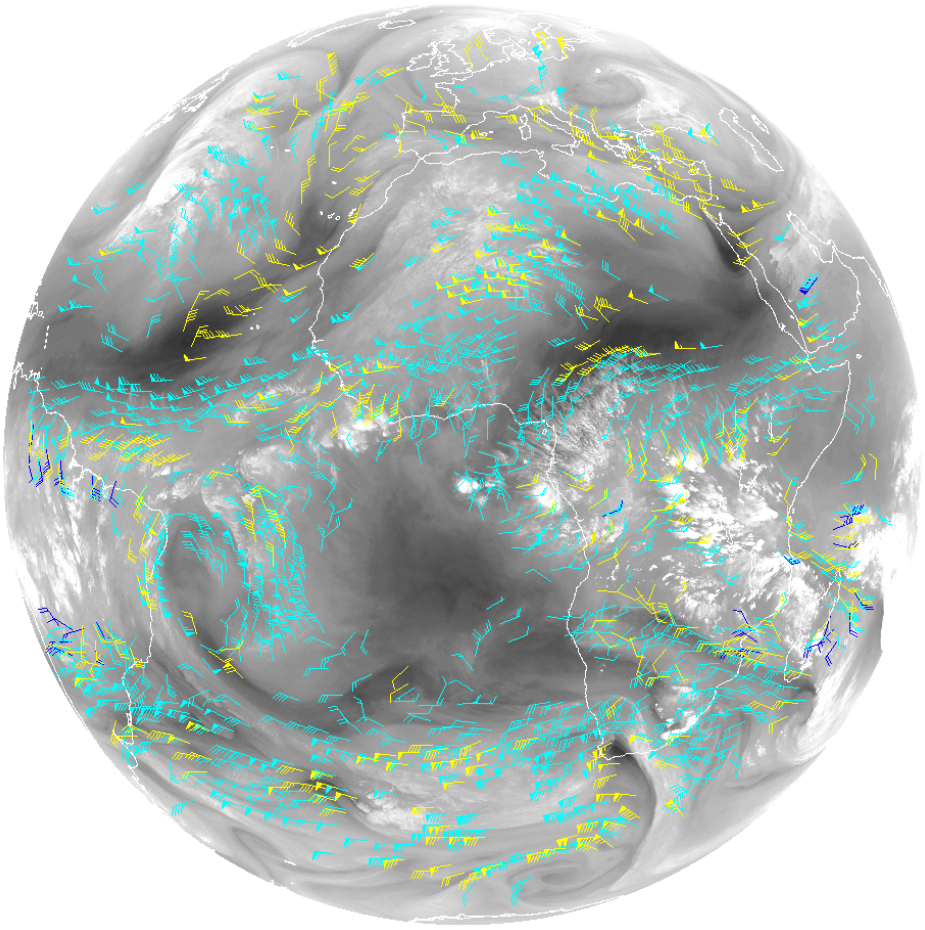

Figure 21. Clear-sky Water Vapor Winds derived from full disk 30-minute Meteosat-8 6.2um and 7.3um SEVIRI data for 12 UTC on 01 February 2007. These winds are derived from tracking clear-sky water vapor features using the 6.2um and 7.3um channels. In dark blue are winds found in the range 100-250 hPa; in cyan are winds found in the range 250-350 hPa; in yellow are winds in the range 350 – 550 hPa.

4.2.2 Derived Motion Winds Generated from Simulated ABI Data

The DMW products can also be generated from simulated GOES-R ABI imagery. Figure 22 shows an example of the IR cloud-drift wind product generated from tracking cloud features observed in simulated 11.2um channel imagery at 00 UTC on 05 June 2005. In this example, an image triplet with a temporal resolution of 5 minutes was used. Figure 23 is an example of clear-sky water vapor winds using a 30-minute time step. Channel 8 (6.19um) and channel 10 (7.34um) are included in the plot. Figure 24 shows the result of tracking channel 2 (0.64 μm), which is the heritage visible channel, at a 5-minute interval.

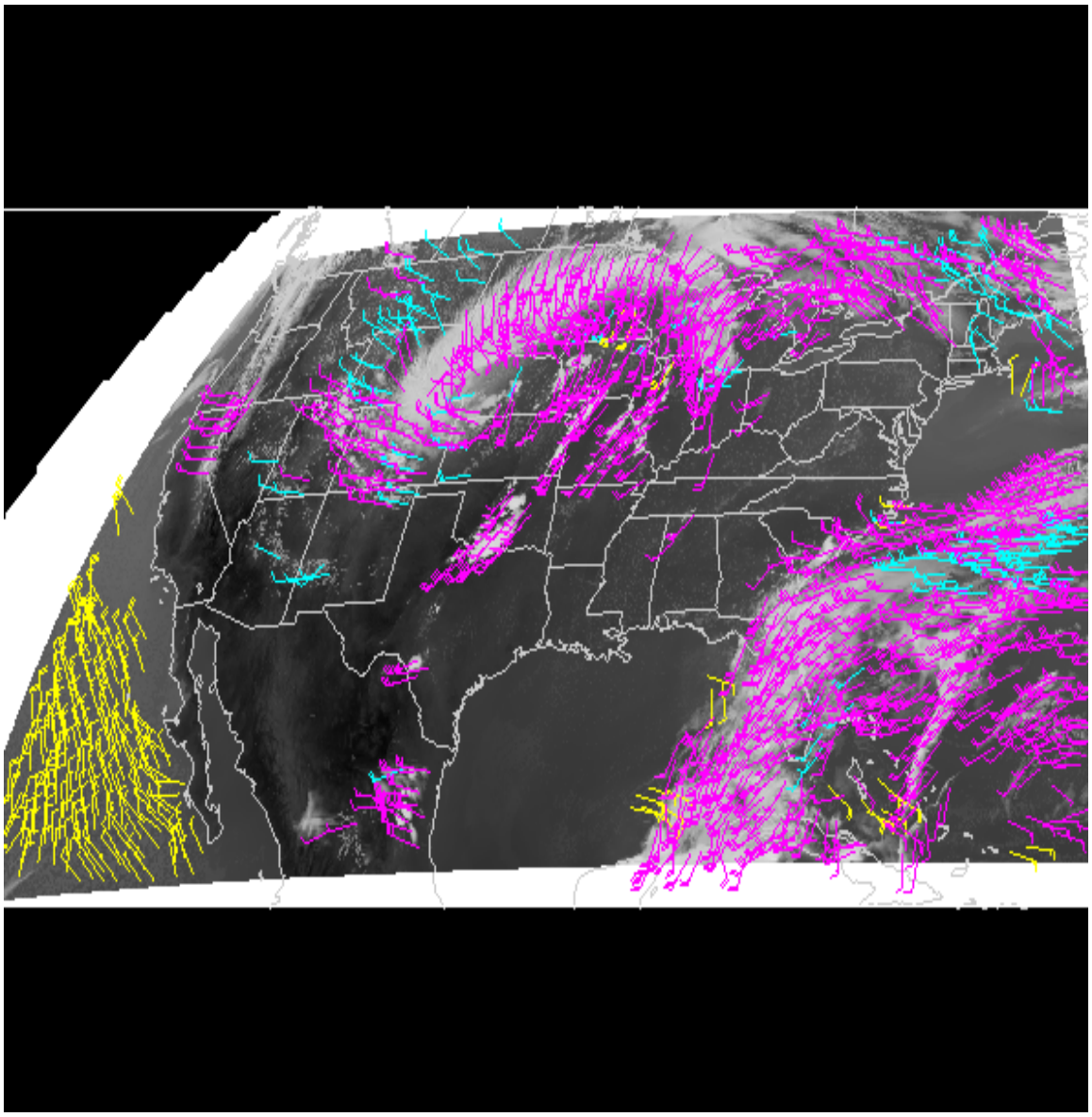

Figure 22. Cloud-drift winds derived from simulated ABI 11um data at 00 UTC on 05 June 2005. The time interval of the image sequence is 5 minutes. High-level (100-400 hPa) winds are shown in violet; mid-level (400-700 hPa) winds are shown in cyan; low-level (> 700 hPa) winds are shown in yellow.

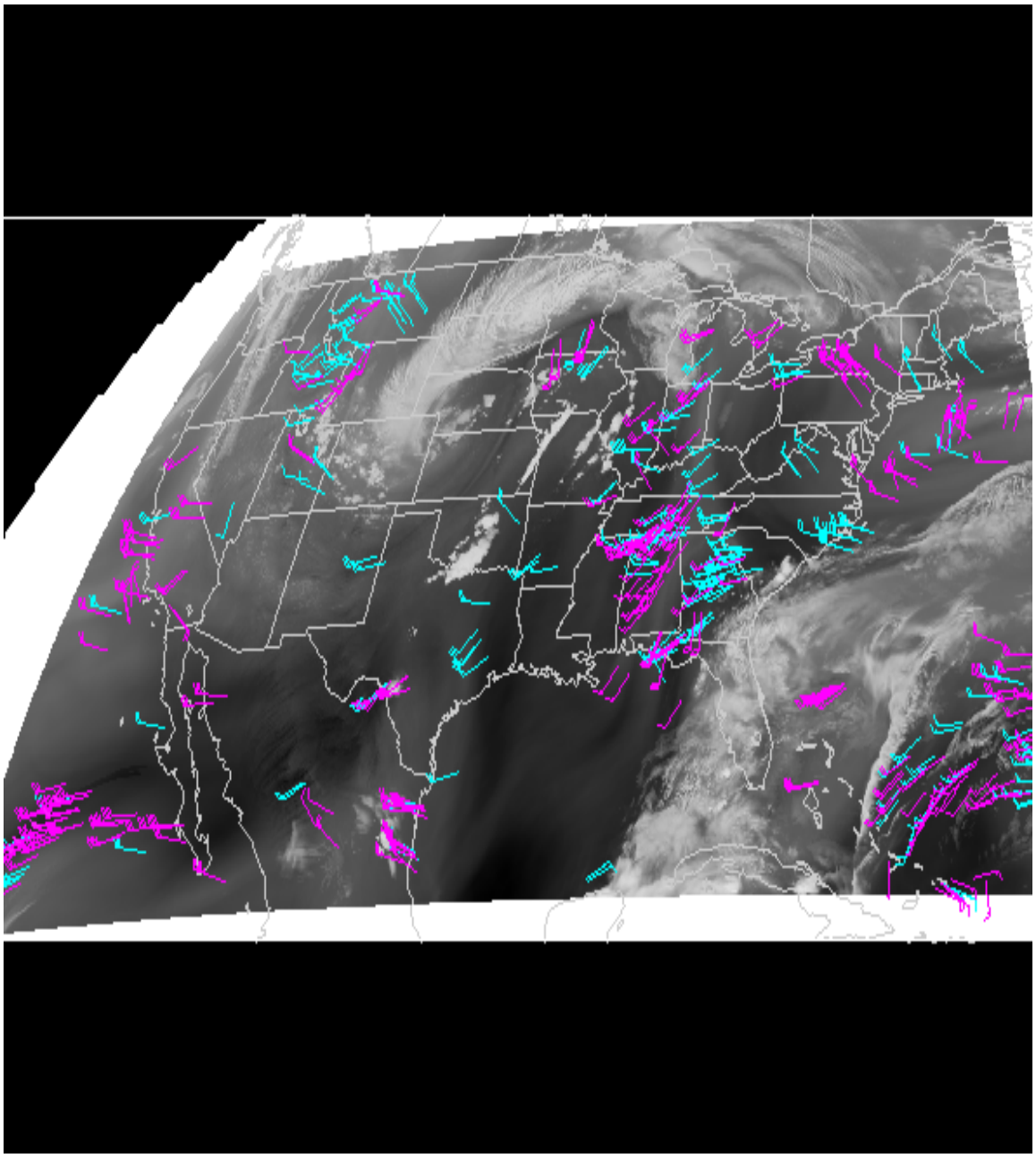

Figure 23. Clear-sky water vapor winds derived from simulated ABI 6.19um and 7.34um data at 00 UTC on 05 June 2005. The time interval of the image sequence is 30 minutes. High-level (100-400 hPa) winds are shown in violet; mid-level (400-700 hPa) winds are shown in cyan.

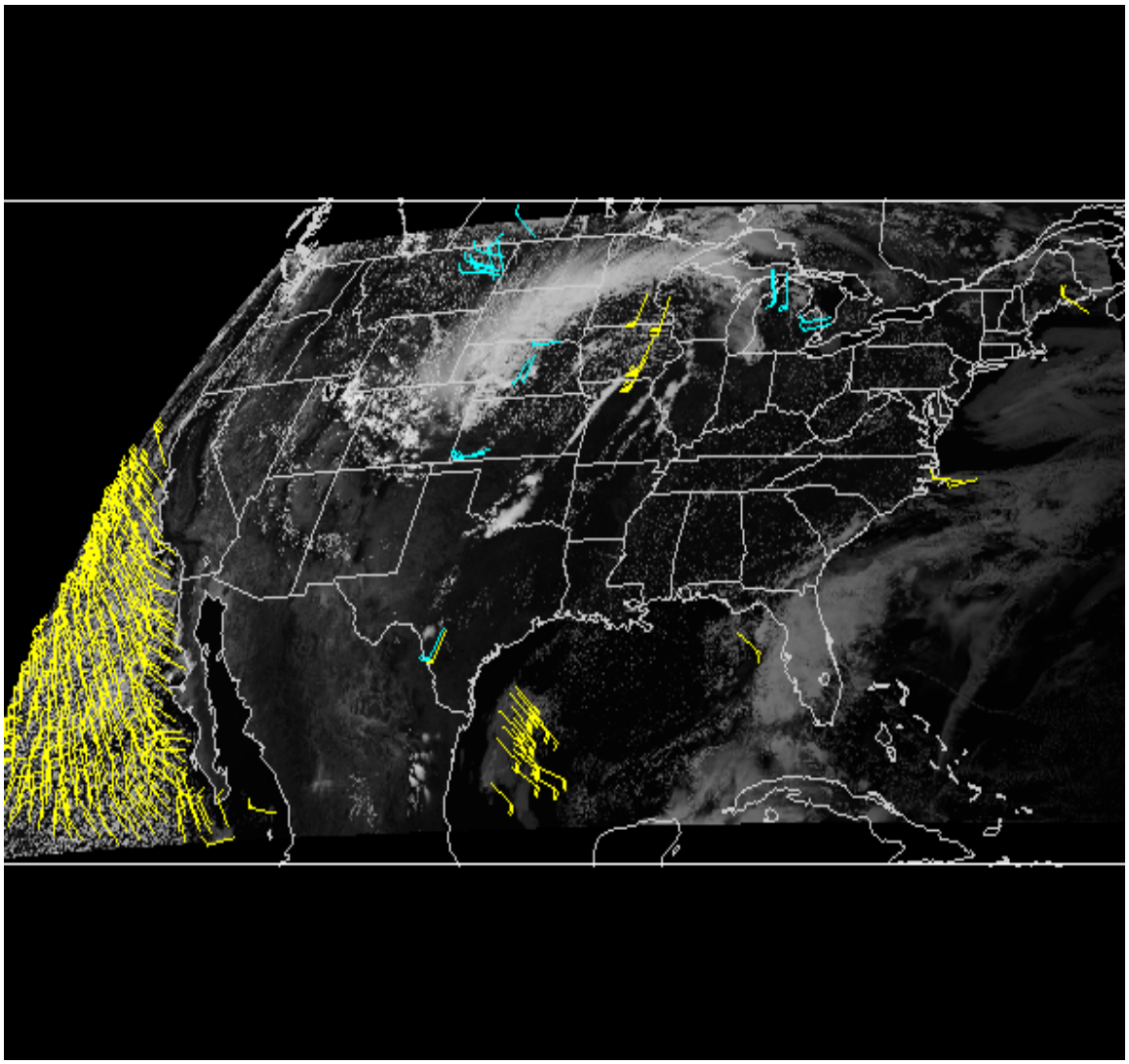

Figure 24. Low-level cloud-drift winds derived from simulated ABI 0.64um data at 2230 UTC on 05 June 2005. The time interval of the image sequence is 5 minutes. Mid-level (600-700 hPa) winds are shown in cyan; low-level (> 700 hPa) winds are shown in yellow.

4.3 Precision and Accuracy Estimates

This section describes the predicted performance and product quality of the DMWA relative to the DMW specifications found within the GOES-R Functional and Performance Specification Document (F&PS). To estimate the precision and accuracy of the DMW product requires coincident measurements of reference ("truth") atmospheric winds values for the full range of observing geometry and environmental conditions that cover multiple seasons.

The reference ("truth") datasets used include radiosonde wind observations and Global

Forecast System (GFS) analyses winds. The radiosonde wind observations are used primarily to validate the DMW product over land and coastal regions. A DMW/radiosonde wind collocation is considered a valid match if the radiosonde observation is within one hour in time within 150km in the horizontal, and within 50 hPa in the vertical of the DMW. The GFS model analysis wind fields are used to measure the performance of the DMW product over oceanic regions. Here, the analysis winds must be within 30 minutes of the DMW, and are spatially (horizontally and vertically) interpolated to the DMW location. An advantage of this approach is that a DMW/Analysis wind collocation match can be generated for every DMW produced.

The accuracy and precision estimates for the DMW products are determined by computing the Mean Vector Difference (MVD) and Standard Deviation (SD) metrics. The mean vector difference between retrieved and reference ("truth") wind representing the *accuracy (average error)* of the GOES-R ABI wind product is computed from:

$$MVD = 1/N \sum_{i=1}^{N} (VD)_i \tag{33}$$

where:

$$VD_i = \sqrt{(u_i - u_r)^2 + (v_i - v_r)^2} \tag{34}$$

u_i = u-component of satellite wind

v_i = v-component of satellite wind

u_r = u-component of the reference wind

v_r = v-component of the reference winds

N = size of collocated sample

The Standard Deviation (SD) about the mean vector difference between the retrieved GOES-R ABI DMW product and the reference wind data represents *the precision (random error)* of the ABI DMW product and is computed from:

$$SD = \sqrt{1/N \sum_{i=1}^{N} [(VD_i) - (MVD)]^2} \tag{35}$$

Certainly, assessment of algorithm performance depends on the validation samples from which the comparison statistics are derived. For example, validation of DMW products performed at different locations, heights in the atmosphere, different wind speeds, or local zenith angle could generate different accuracy and precision values for the same algorithm.

The accuracy and precision of the DMW product will depend largely on a number things that include: (1) Calibration and navigation accuracy of the ABI measurements, (2) ABI band that is used for feature tracking, (3) Height of the DMW in the atmosphere, and (4) Accuracy and precision of the input ABI cloud mask and cloud height products.

Comparisons of DMW Products Derived from Meteosat-8 SEVIRI Imagery to Radiosonde Wind Observations

Tables 14-19 show DMW product validation results as a function ABI band used and AMV height assignment for August 2006 and February 2007 over the earth's full disk when using collocated radiosonde wind observations. These tables include the accuracy and precision metrics and also the speed bias metric which is of particular interest to the NWP user community. Also included in these tables are statistical comparison metrics between NCEP short-term GFS forecast winds (valid at the same time of the satellite winds and at satellite wind height assignment) and radiosonde wind observations. These statistics are included primarily for reference and as a source of information for NWP users of the DMW product.

The comparison statistics for the low level DMWs computed using the visible band are shown in Table 14. The accuracy of these DMWs for August 2006 and February 2007 are 3.26 m/s and 3.10 m/s, respectively, with corresponding precision values of 2.88 m/s and 2.16 m/s. These statistics indicate that these visible DMWs possess some small seasonal dependence, however, this behavior is also evident in the GFS forecast winds. It is interesting to note that the overall performance of the visible DMWs is on par or even slightly better than the GFS forecast winds as measured against collocated radiosonde wind observations. The accuracy and speed bias metrics actually indicate that visible DMWs actually outperform the NCEP GFS forecast winds at low levels of the atmosphere below 700 hPa. This is a very good result and brings high expectations that they can contribute to improving NWP forecast performance when properly assimilated into NWP data assimilation systems.

Table 14. Comparison statistics between DMWs computed using the Visible (0.64um) band from full disk Meteosat-8, NCEP GFS short-term forecast winds, and radiosonde wind observations for the months of August 2006 and February 2007. These estimates were determined from comparisons to collocated radiosonde winds at 00 and 12 UTC.

Low Level *(P > 700hPa)*	***Visible (0.64um) Winds vs. Radiosonde Winds (m/s)***		***GFS Forecast Winds vs. Radiosonde Winds (m/s)***	
	Aug 2006	**Feb 2007**	**Aug 2006**	**Feb 2007**
Accuracy	3.26	3.10	3.29	3.11
Precision	2.88	2.16	2.81	2.07
Speed bias	0.28	-0.01	0.55	0.54
Speed	8.76	9.43	9.02	9.99
Sample	4976	3372	4976	3372

The comparison statistics for the low level DMWs computed using the SWIR band are shown in Table 15. The accuracy of these DMWs for August 2006 and February 2007 are 3.52 m/s and 3.57 m/s, respectively, with corresponding precision values of 2.25 m/s and 2.42 m/s. Like the visible DMWs, the SWIR winds are derived at low levels of the atmosphere below 700 hPa. Their performance in terms of accuracy and precision is very similar to the performance of the visible DMWs. This is an important result as these two datasets are complimentary given that the visible DMWs are generated during daytime and the SWIR DMWs are generated during nighttime. This behavior is very important in terms of their use and potential impact in NWP data assimilation systems.

Table 15. Comparison statistics between DMWs computed using the SWIR (3.9um) band from full disk Meteosat-8, NCEP GFS short-term forecast winds, and radiosonde wind observations for the months of August 2006 and February 2007. These estimates were determined from comparisons to collocated radiosonde winds at 00 and 12 UTC.

Low Level *(P > 700hPa)*	***SWIR (3.9um) Winds vs. Radiosonde Winds (m/s)***		***GFS Forecast Winds vs. Radiosonde Winds (m/s)***	
	Aug 2006	**Feb 2007**	**Aug 2006**	**Feb 2007**
Accuracy	3.52	3.57	3.33	3.41
Precision	2.25	2.42	1.97	2.21
Speed bias	-0.15	-0.07	-0.06	0.29
Speed	9.40	10.89	9.51	11.25
Sample	993	1062	993	1062

The comparison statistics for the DMWs computed using the LWIR band are shown in Table 16. The comparison statistics are shown for all levels of the atmosphere and are also broken down as a function of height in the atmosphere. The overall accuracy of these DMWs for August 2006 and February 2007 are 4.51 m/s and 5.21m/s, respectively, with corresponding precision values of 3.62 m/s and 4.06 m/s. Both sets of DMW metrics indicate some seasonal dependence, but this is not unexpected. This same behavior is also observed with the NCEP GFS forecast winds and reflects the fact that the average wind speeds are higher in February than in August. When the LWIR DMW performance is evaluated as a function of height in the atmosphere, the magnitudes of the accuracy and precision metrics are observed to be smallest in the lower atmosphere and increase with height. This indicates that the performance of the DMWs vary as a function of wind speed. The same is true for GFS forecast winds which also exhibit this same behavior.

Table 16. Comparison statistics between DMWs computed using the LWIR (10.8um) band from full disk Meteosat-8, NCEP GFS short-term forecast winds, and radiosonde wind observations for the months of August 2006 and February 2007. These estimates were determined from comparisons to collocated radiosonde winds at 00 and 12 UTC.

All Levels *(100-1000 hPa)*	***LWIR (10.8um) Winds vs. Radiosonde Winds (m/s)***		***GFS Forecast Winds vs. Radiosonde Winds (m/s)***	
	Aug 2006	**Feb 2007**	**Aug 2006**	**Feb 2007**
Accuracy	4.51	5.21	4.21	4.83
Precision	3.62	4.06	3.04	3.32
Speed bias	0.24	-0.54	0.02	-0.30
Speed	14.56	17.68	14.35	17.92
Sample	13987	15286	13987	15286
High Level *(100-400 hPa)*				
	Aug 2006	**Feb 2007**	**Aug 2006**	**Feb 2007**
Accuracy	5.65	5.94	5.27	5.54
Precision	4.25	4.46	3.48	3.47
Speed bias	0.08	-0.81	-0.05	-0.50
Speed	19.83	21.49	19.71	21.80
Sample	5441	7719	5441	7719
Mid Level *(400-700 hPa)*				
	Aug 2006	**Feb 2007**	**Aug 2006**	**Feb 2007**
Accuracy	4.39	5.25	3.95	4.67
Precision	3.28	3.84	2.59	3.36
Speed bias	0.62	-0.14	-0.15	-0.33
Speed	13.25	16.38	12.48	16.19
Sample	4445	4264	4445	4264
Low Level *(700-1000 hPa)*				
	Aug 2006	**Feb 2007**	**Aug 2006**	**Feb 2007**
Accuracy	3.12	3.39	3.07	3.33
Precision	2.34	2.42	2.31	2.17
Speed bias	0.02	-0.42	0.32	0.19
Speed	8.90	10.32	9.21	10.93
Sample	4053	3249	4053	3249

The comparison statistics for the cloud-top water vapor DMWs computed using the 6.2um band are shown in Table 17. The comparison statistics are shown only for upper levels of the atmosphere above 400 hPa since these winds are only generated above 400 hPa. The accuracy of these DMWs for August 2006 and February 2007 are 5.98 m/s and 6.05 m/s, respectively, with corresponding precision values of 4.45 m/s and 4.36 m/s. Both sets of DMW metrics indicate no seasonal dependence. These statistics indicate that the

performance of these cloud-top DMWs is on par with the performance of the NCEP GFS forecast winds. In fact, these DMWs outperform the NCEP GFS forecast winds in terms of the speed bias metric. This is an extremely good result and brings high expectations that they can contribute to improving NWP forecast performance when properly assimilated into NWP data assimilation systems.

Table 17. Comparison statistics between cloud-top DMWs computed using the Water Vapor (6.2um) band from full disk Meteosat-8, GFS short-term forecast winds, and radiosonde wind observations for the months of August 2006 and February 2007. These estimates were determined from comparisons to collocated radiosonde winds at 00 and 12 UTC.

High Level *(100-400 hPa)*	***Cloud-top Water Vapor (6.2um) Winds vs. Radiosonde Winds (m/s)***		***GFS Forecast Winds vs. Radiosonde Winds (m/s)***	
	Aug 2006	**Feb 2007**	**Aug 2006**	**Feb 2007**
Accuracy	5.98	6.05	5.76	5.65
Precision	4.45	4.36	3.99	3.78
Speed bias	0.04	0.00	-0.27	-0.79
Speed	21.04	22.91	20.73	22.12
Sample	13945	16976	13945	16976

The comparison statistics for the clear-sky water vapor DMWs computed using the 6.2um and 7.3um bands are shown in Tables 18 and 19. The comparison statistics for the 6.2um clear-sky DMWs are shown only for upper levels of the atmosphere above 400 hPa since these winds are only generated above 400 hPa. The comparison statistics for the 7.3um clear-sky DMWs are shown only for the atmospheric layer between 450 hPa and 700 hPa, since this is the layer over which these winds are generated and most representative.

The accuracy of the clear-sky water vapor (6.2um) DMWs for August 2006 and February 2007 are 5.64 m/s and 6.35 m/s, respectively, with corresponding precision values of 4.33 m/s and 5.00 m/s. The clear-sky water vapor (7.3um) DMWs for August 2006 and February 2007 had accuracies of 4.82 m/s and 6.31 m/s, respectively, with corresponding precision values of 3.32 m/s and 4.86 m/s. Both sets of DMW metrics indicate that the performance of the clear-sky DMWs will vary by season with the most challenging season being winter when the atmosphere is much drier. It is clear from these statistics that the clear-sky DMWs are the most challenging to derive. The primary reason for this is that the feature being tracked in these cases is a clear-sky moisture gradient which lacks a sharp radiometric signal typically observed with clouds. Complicating matters further is the fact that the radiometric signal being tracked emanates from a rather broad layer of the atmosphere. Thus, the motion retrieved from tracking clear-sky water vapor features is more representative of the average motion over a broad atmospheric layer. Statistical comparisons of these DMWs versus single level reference/ground truth wind observations like radiosondes, then, reflect this phenomenon with the result being slightly worse performance (e.g., lower accuracy and reduced precision).

Table 18. Comparison statistics between clear-sky DMWs computed using the Water Vapor (6.2um) band from full disk Meteosat-8, GFS short-term forecast winds, and radiosonde wind observations for the months of August 2006 and February 2007. These estimates were determined from comparisons to collocated radiosonde winds at 00 and 12 UTC.

High Level *(100-400 hPa)*	***Clear-sky Water Vapor (6.2um) Winds vs. Radiosonde Winds (m/s)***		***GFS Forecast Winds vs. Radiosonde Winds (m/s)***	
	Aug 2006	**Feb 2007**	**Aug 2006**	**Feb 2007**
Accuracy	5.64	6.35	4.48	4.89
Precision	4.33	5.00	3.24	3.70
Speed bias	-0.25	0.87	-0.55	-0.33
Speed	14.96	18.68	14.67	17.49
Sample	5309	2478	5309	2478

Table 19. Comparison statistics between clear-sky DMWs computed using the Water Vapor (7.3um) band from full disk Meteosat-8, GFS short-term forecast winds, and radiosonde wind observations for the months of August 2006 and February 2007. These estimates were determined from comparisons to collocated radiosonde winds at 00 and 12 UTC.

Mid Level *(450-700 hPa)*	***Clear-sky Water Vapor (7.3um) Winds vs. Radiosonde Winds (m/s)***		***GFS Forecast Winds vs. Radiosonde Winds (m/s)***	
	Aug 2006	**Feb 2007**	**Aug 2006**	**Feb 2007**
Accuracy	4.82	6.31	3.56	4.03
Precision	3.32	4.86	2.26	2.87
Speed bias	0.00	0.86	-0.55	-0.99
Speed	11.50	13.84	10.94	11.99
Sample	3351	1907	3351	1907

Comparisons of DMW Products Derived from Meteosat-8 SEVIRI Imagery to GFS Analysis Winds

Tables 20-25 show DMW product validation results as a function ABI band used and AMV height assignment for August 2006 and February 2007 over the earth's full disk and over

ocean when using collocated NCEP GFS analysis winds. These tables include the accuracy and precision metrics and also the speed bias metric which is of particular interest to the NWP user community. It needs to be noted that use of NCEP GFS analysis winds as the reference/ground truth wind observations leads to smaller magnitudes in the accuracy and precision metrics as compared to the magnitudes of these metrics when using radiosonde wind observations. Two reasons likely contribute to this. First, the horizontal and temporal resolution of the GFS analysis wind field is much coarser than the radiosonde wind observations and second, the GFS analysis wind field is influenced by a number of satellite-derived winds as these are assimilated operationally by NCEP. Despite this, these comparison statistics still provide a useful measure of the performance of the DMWA.

The comparison statistics for the low level DMWs computed using the visible band are shown in Table 20. The accuracy of these DMWs for August 2006 and February 2007 are 2.38 m/s and 2.19 m/s, respectively, with corresponding precision values of 1.60 m/s and 1.55 m/s. These statistics indicate that the visible DMWs possess a very small seasonal dependence which is consistent with what was observed when comparing these winds to radiosonde wind observations.

The comparison statistics for the low level DMWs computed using the SWIR band are shown in Table 21. The accuracy of these DMWs for August 2006 and February 2007 are 2.40 m/s and 2.55 m/s, respectively, with corresponding precision values of 1.61 m/s and 1.56 m/s. Like the visible DMWs, the SWIR winds are derived at low levels of the atmosphere below 700 hPa. Their performance in terms of accuracy and precision is very similar to the performance of the visible DMWs. As previously mentioned, this is an important result as these two datasets are complimentary given that the visible DMWs are generated during daytime and the SWIR DMWs are generated during nighttime. This behavior is very important in terms of their use and potential impact in NWP data assimilation systems.

Table 20. Comparison statistics (ocean only) between DMWs computed using the Visible (0.64um) band from full disk Meteosat-8 and NCEP GFS Analysis winds (valid at 00 UTC and 12 UTC) for the months of August 2006 and February 2007.

Low Level *(P > 700hPa)*	***Visible (0.64um) Winds vs. GFS Analysis Winds (m/s)***	
	Aug 2006	**Feb 2007**
Accuracy	2.38	2.19
Precision	1.60	1.55
Speed bias	-0.17	-0.32
Speed	9.47	9.61
Sample	284269	219746

Table 21. Comparison statistics (ocean only) between DMWs computed using the SWIR (3.9um) band from full disk Meteosat-8 and NCEP GFS Analysis winds (valid at 00 UTC and 12 UTC) for the months of August 2006 and February 2007.

Low Level *(P > 700hPa)*	***SWIR (3.9um) Winds vs. GFS Analysis Winds (m/s)***	
	Aug 2006	**Feb 2007**
Accuracy	2.40	2.25
Precision	1.61	1.56
Speed bias	-0.33	-0.36
Speed	9.68	9.61
Sample	179276	150664

The comparison statistics for the DMWs computed using the LWIR band are shown in Table 22. The comparison statistics are shown for all levels of the atmosphere and are also broken down as a function of height in the atmosphere. The overall accuracy of these DMWs for August 2006 and February 2007 are 3.30 m/s and 3.70m/s, respectively, with corresponding precision values of 2.82 m/s and 3.43 m/s. Conclusions to be drawn from these statistics are similar to those drawn from statistics computed between these winds and radiosonde wind observations. Both sets of DMW metrics indicate some seasonal dependence which reflects the fact that the average wind speeds are higher in February than in August. When the LWIR DMW performance is evaluated as a function of height in the atmosphere, the magnitudes of the accuracy and precision metrics are observed to be smallest in the lower atmosphere and increase with height. This indicates that the performance of the DMWs vary as a function of wind speed.

Table 22. Comparison statistics (ocean only) between DMWs computed using the LWIR (10.8um) band from full disk Meteosat-8 and NCEP GFS analysis winds (valid at 00UTC and 12 UTC) for the months of August 2006 and February 2007.

All Levels *(100-1000 hPa)*	***LWIR (10.8um) Winds vs. GFS Analysis Winds (m/s)***	
	Aug 2006	**Feb 2007**
Accuracy	3.30	3.70
Precision	2.82	3.43
Speed bias	0.01	0.15
Speed	14.31	15.30
Sample	374979	392282

High Level *(100-400 hPa)*		
	Aug 2006	**Feb 2007**
Accuracy	5.16	5.66
Precision	3.76	4.31
Speed bias	0.47	0.65
Speed	23.67	22.46
Sample	86652	138326
Mid Level *(400-700 hPa)*		
	Aug 2006	**Feb 2007**
Accuracy	4.81	4.76
Precision	3.63	3.71
Speed bias	1.13	1.55
Speed	21.93	20.93
Sample	39141	35921
Low Level *(700-1000 hPa)*		
	Aug 2006	**Feb 2007**
Accuracy	2.42	2.28
Precision	1.63	1.56
Speed bias	-0.32	-0.39
Speed	9.85	9.83
Sample	249150	218003

The comparison statistics for the cloud-top water vapor DMWs computed using the 6.2um band are shown in Table 23. The comparison statistics are shown only for upper levels of the atmosphere above 400 hPa since these winds are only generated above 400 hPa. The accuracy of these DMWs for August 2006 and February 2007 are 5.83 m/s and 5.69m/s, respectively, with corresponding precision values of 4.29 m/s and 4.01 m/s. Both sets of DMW metrics indicate no seasonal dependence with respect to the performance of the DMWA when using this channel to track clouds. A positive speed bias ranging from 1.22-1.43m/s is evident from these comparison stats which indicate the DMWs are faster than the GFS analysis. The exact reasons for this are not known. Positive speed biases for these DMWs, however, were not evident in the DMW/radiosonde wind comparison statistics shown in Table 18.

Table 23. Comparison statistics (ocean only) between cloud-top DMWs computed using the Water Vapor (6.2um) band from full disk Meteosat-8 and NCEP GFS analysis winds (valid at 00UTC and 12UTC) for the months of August 2006 and February 2007.

High Level *(100-400 hPa)*	***Cloud-top Water Vapor (6.2um) Winds vs. GFS Analysis Winds (m/s)***	
	Aug 2006	**Feb 2007**
Accuracy	5.83	5.69
Precision	4.29	4.01

Speed bias	1.43	1.22
Speed	26.21	24.38
Sample	190795	254132

The comparison statistics for the clear-sky water vapor DMWs computed using the 6.2um and 7.3um bands are shown in Tables 24 and 25. The comparison statistics for the 6.2um clear-sky DMWs are shown only for upper levels of the atmosphere above 400 hPa since these winds are only generated above 400 hPa. The comparison statistics for the 7.3um clear-sky DMWs are shown only for the atmospheric layer between 450 hPa and 700 hPa, since this is the layer over which these winds are generated and most representative.

The accuracy of the clear-sky water vapor (6.2um) DMWs for August 2006 and February 2007 are 5.21 m/s and 5.52 m/s, respectively, with corresponding precision values of 4.06 m/s and 4.07m/s. The clear-sky water vapor (7.3um) DMWs for August 2006 and February 2007 had accuracies of 4.97 m/s and 5.05 m/s, respectively, with corresponding precision values of 3.85m/s and 3.73 m/s. Both sets of DMW metrics indicate that the performance of the clear-sky DMWs will vary slightly by season with the most challenging season being winter when the atmosphere is much drier. It is clear from these statistics that the clear-sky DMWs are the most challenging to derive. As previously discussed, the primary reason for this is that the feature being tracked in these cases is a clear-sky moisture gradient which lacks a sharp radiometric signal typically observed with clouds. Complicating matters further is the fact that the radiometric signal being tracked emanates from a rather broad layer of the atmosphere. Thus, the motion retrieved from tracking clear-sky water vapor features is more representative of the average motion over a broad atmospheric layer. Statistical comparisons of these DMWs with single level reference/ground truth wind observations like radiosondes or even GFS analysis then, reflect this phenomenon with the result being slightly worse performance (e.g., lower accuracy and reduced precision).

Table 24. Comparison statistics (ocean only) between clear-sky DMWs computed using the Water Vapor (6.2um) band from full disk Meteosat-8 and NCEP GFS analysis winds (valid at 00UTC and 12UTC) for the months of August 2006 and February 2007.

High Level *(100-400 hPa)*	***Clear-sky Water Vapor (6.2um) Winds vs. GFS Analysis Winds (m/s)***	
	Aug 2006	**Feb 2007**
Accuracy	5.21	5.52
Precision	4.06	4.07
Speed bias	1.30	1.30
Speed	15.72	17.57
Sample	103941	76028

Table 25. Comparison statistics (ocean only) between clear-sky DMWs computed using the Water Vapor (7.3um) band from full disk Meteosat-8 and NCEP GFS Analysis winds (valid at 00UTC and 12UTC) for the months of August 2006 and February 2007.

Mid Level *(450-700 hPa)*	***Clear-sky Water Vapor (7.3um) Winds vs. GFS Analysis Winds (m/s)***	
	Aug 2006	**Feb 2007**
Accuracy	4.97	5.05
Precision	3.85	3.73
Speed bias	1.28	1.60
Speed	12.74	14.12
Sample	102526	85434

4.3.1 Error Budget

The GOES-R ABI DMW products are considered validated at the 100% level if the overall accuracy and precision of the wind product satisfy the requirements specified within the F&PS document.

Conformance of DMW Algorithm Performance to F&PS Accuracy and Precision Specifications

This section summarizes the overall accuracy and precision estimates of the DMW product based on the use of ABI proxy data described in Sections 4.1 and the reference data described in Section 4.3. Tables 26 and 27 list the overall DMW product validation results when using collocated radiosonde wind observations and GFS analysis winds, respectively. For each case, the DMWA accuracy and precision metrics are shown relative to the F&PS specifications for each of these metrics. The DMWA accuracy and precision metrics clearly demonstrate that the DMWA meets the F&PS accuracy and precision specifications at the 100% level.

Both sets of validation results demonstrate that both the accuracy and precision estimates for the DMW product meet the F&PS specifications for these metrics at the 100% level.

Table 26. Accuracy and precision estimates of DMWs (whose QI ≥ 60) derived from full disk Meteosat-8 imagery for the months of August 2006 and February 2007. These estimates were determined from comparisons to collocated radiosonde wind observations at 00 and 12 UTC. F&PS accuracy and precision specifications are included in this table for comparison.

F&PS Performance Metric	F&PS Requirement (m/s)	*Validation with Radiosondes*	
		Computed Metric (m/s)	Sample Size
Accuracy	7.5	5.20	65603
Precision	4.2	4.09	65603

Table 27. Accuracy and precision estimates of DMWs (whose QI ≥ 60) derived from full disk Meteosat-8 imagery for the months of August 2006 and February 2007. These estimates were determined from comparisons to collocated GFS analysis winds at 00 and 12 UTC. F&PS accuracy and precision specifications are included in this table for comparison.

F&PS Performance Metric	F&PS Requirement (m/s)	*Validation with GFS Analysis*	
		Computed Metric (m/s)	Sample Size
Accuracy	7.5	4.31	3145211
Precision	4.2	3.70	3145211

5 PRACTICAL CONSIDERATIONS

5.1 Numerical Computation Considerations

The pattern matching performed by the DMWA is the most computationally expensive aspect of the entire derivation process. It is natural then to focus on this step when considering ways to improve the overall performance of the algorithm.

Major efficiency upgrades have recently been made to the tracking portion of the AMV algorithm resulting in a 25% improvement in the processing times. One recent upgrade, the spiral search, terminates the sum-of-squared differences (SSD) calculation early once a current minimum value has been exceeded. The rationale for terminating the summation early is that any additional calculations would simply increase the summation value above the current minimum.

A second implemented upgrade has been to begin the search for the minimum SSD value at the forecast location and "spiral" outwards instead of starting at the top left corner of the search region where the SSD value is typically much larger. This has the effect of establishing a low threshold right from the start so that the SSD calculation can be terminated earlier resulting in fewer calculations.

5.2 Programming and Procedural Considerations

The current version of the DMWA includes a large data buffer that holds information (radiance, brightness temperature, cloud mask, etc) from adjacent line segments (also called swaths). Such a buffer makes it possible for the algorithm to track features that move out of the domain of the middle line segment, which is the only part of the buffer being processed for targets. With each new line segment read in, data in the buffer is shifted upwards so that the “oldest” data is always at the top of the buffer while the new segment data is added to the bottom of the buffer. This involves a substantial amount of copying from one segment of the buffer to another. It is anticipated that future versions of the algorithm will not have this buffer, as it is expected that the processing framework provided by the AIT will take care of this task. This will greatly simplify the algorithm and should significantly improve its performance.

The current version of the algorithm is also limited to processing three images of equal size. These limitations will need to be addressed in future versions. In addition to adding flexibility to the algorithm, having the ability to process images of varying size (mixing and matching) will improve the timeliness of the product.

As required by the AIT, a common variable type declaration statement has been used while writing the AMV algorithm.

5.3 Quality Assessment and Diagnostics

The following information should be monitored/trended for diagnosing the quality of the derived motion wind product:

- Number of total targets attempted
- Number of good winds generated
- Percent of winds retrieved with specified QA flag values
- Mean, Min, Max and StdDev of derived wind speed
- Percent of retrievals with a QA flag value for specified atmospheric layers
- Mean, Min, Max, and StdDev cloud height for specified atmospheric layers

5.4 Exception Handling

Exception handling is required for the development of robust and efficient numerical software. Requirements set forth by the AIT also stress the importance of exception handling. The main modules of the DMW program (target_selection.f90 and feature_tracking_utils.f90) use AIT-provided subroutine for error messaging.

For the most part, the DMWA assumes that all necessary image, forecast and ancillary data are available through the processing framework. The only data that the algorithm explicitly checks for is the temporal brightness temperature data, which is necessary for the tracking portion of the algorithm. If the temporal data is unavailable, the algorithm outputs an error message and control is returned to the processing framework.

As part of the target selection process, the DMWA checks for missing or unrealistic values within both the target and search regions. These values are specified in Section 3.4.2.1.1 (see Channel Validity Test). If either condition is met, the algorithm will flag the scene as bad and proceed to the next adjacent scene.

5.5 Algorithm Validation

Validation of the DMW products requires collocated measurements of reference (“truth”) atmospheric wind values for the full range of ABI observing geometry and environmental conditions. From these collocated measurements, comparison metrics can be calculated that characterize the agreement between the satellite-derived DMWs and the reference values.

During the pre-launch phase of the GOES-R program, the product validation activities are aimed at characterizing the performance and uncertainties of the DMW products resulting from parameterizations and algorithmic implementation artifacts. During this phase, there is total reliance on the use of GOES-R ABI proxy and simulated datasets as described in Section 4.1. Post-launch validation will apply lessons learned to inter-comparisons of actual DMW products generated from real ABI measurements and reference (“ground-truth”) wind observations. Validation methodologies and tools developed and tested during

the pre-launch phase will be automated and applied. More specific details on DMW product validation activities can be found in the Product Validation Document for the DMW product.

6 ASSUMPTIONS AND LIMITATIONS

The following sections describe the limitations and assumptions used in the current version of the DMWA.

6.1 Algorithm Performance

The following assumptions have been made in developing and estimating the performance of the DMWA.

(1) ABI pixel level channel data (for each line segment) from all three images in the sequence are available along with accompanying meta-data (latitude, longitude, solar and local zenith angles, image scan times, quality flags). It is further assumed that the processing framework will handle any preprocessing needed to account for channel imagery whose resolutions may differ

(2) Forecast temperature and wind profiles, surface skin temperature, and surface pressure are available and made available to the DMWA through the processing framework

(3) The pixel level ABI cloud mask, cloud-top pressure, cloud-top temperature, estimated cloud height retrieval error, and cloud height quality flag(s) corresponding to each image in the image sequence are available through the processing framework

(4) DMWA products are validated with reliable ground-based wind measurements and/or winds from a NWP model forecast/analysis

(5) Proxy datasets and simulated ABI radiance fields from NWP models provide a suitable surrogate for estimating the DMWA performance/verification

6.2 Sensor Performance

It is assumed the GOES-R ABI sensor will meet its specifications as documented in the ABI PORD (417-R-ABIPORD-0017).

6.3 Pre-Planned Product Improvements

While development of the baseline DMWA continues, we expect to focus on the following issues.

6.3.1 Improve the Link between Pixels Dominating the Feature Tracking Solution and Target Height Assignment

Target height assignment has been identified as a major source of error for the DMW products. Deriving a representative height that is consistent with, and has ties to, the features being tracked is the goal of an upgraded wind derivation process. Studying and improving the link between the features being tracked and the heights assigned to these features is the major focus of this future effort.

6.3.2 Quality Control Indicators

The quality control indicators attached to each DMW vector are important to the users of these products. Proper interpretation and application of these quality control indicators helps the user community make optimal use of the DMW products. As such, improving these quality control indicators so that they more accurately represent the integrity and accuracy of the DMW product is vital. Of particular interest by the NWP community is a quality indicator that provides information about the estimated accuracy of the height assignment associated with the derived motion wind products. This will be an area of future study.

7 REFERENCES

Baum, Bryan , P. Yang, Yang, Ping; Heymsfield, Andrew J.; Platnick, Steven; King, Michael D.; Hu, Y.-X., and Bedka, Sarah T., 2005: Bulk scattering properties for the remote sensing of ice clouds, part II: Narrowband models. *Journal of Applied Meteorology*, Volume **44**, Issue 12, pp.1896-1911.

Berger, H., C. Velden, J. Daniels and S. Wanzong, 2008: Assessing the 'Expected Error' as a potential new quality indicator for atmospheric motion vectors. 9th International Winds Workshop, Annapolis, MD. Available online at: http://www.eumetsat.int/Home/OldWhoWeAre/Conference_and_Workshop_Proceedings/SP_1217939522789?l=en

Coakley, J.A, and F.P. Bretherton, 1982: Cloud cover from high resolution scanner data: Detecting and allowing for partially filled fields of view. *J. Geophys. Res.*, **87**, 4917−4932.

Daniels, J. and W. Bresky, 2010: A New Nested Tracking Approach for Reducing the Slow Speed Bias Associated With Atmospheric Motion Vectors (AMVS). Proceedings of the 10th International Winds Workshop, Tokyo, Japan.

EUMETSAT, 2005: The EUMETSAT wind vector automatic quality control scheme. EUM/OPS/TEN/05/1747, 10 pp.[Available online at http://www.eumetsat.int/Home/Main/Publications/Technical_and_Scientific_Documentation/Technical_Notes/SP_1124282585834?l=en .

Gustaffson J. and M. Lindberg, 1999: CMW low-level height assignment. Proc. EUMETSAT Satellite Data Users' Conf., Copenhagen, September 1999

Hamada, T., 1983: On the optimal time-interval of satellite image acquisition for operational cloud motion wind derivation. *Meteorology Center of Japan Meteorological Agency Tech. Note 7*, 79–87.

Hansen, M., R. DeFries, J.R.G. Townshend, and R. Sohlberg (1998), UMD Global Land Cover Classification, 1 Kilometer, 1.0, Department of Geography, University of Maryland, College Park, Maryland, 1981-1994.

Holmlund, K., 1998: The utilization of statistical properties of satellite-derived atmospheric motion vectors to derive quality indicators. *Weather and Forecasting*, Volume **13**, Issue 4,pp.1093-1104.

Holmlund, K, C. Velden, and M. Rohn: 2001: Enhanced automated quality control applied to high-density satellite-derived winds. *Monthly Weather Review*, Volume **129,** Issue 3, pp.517-529.

Huang, Allen and M. Goldberg, 2008: Overview of GOES-R Analysis Facility for Instrument Impacts on Requirements (GRAFIIR) planned activities and recent progress. *GOES Users' Conference*, 5th, New Orleans, LA, 20-24 January 2008. American Meteorological Society, Boston, MA, 2008, Manuscript not available for publication.

Jedlovek, G. and R. Atkinson, 1998: The Marshall automated wind algorithm: Error analysis, quality control and climate applications. *Proceedings 3rd International Winds Workshop,* Saanenmoser, Switzerland, pp. 247-254.

Lakshmanan, V., K. Hondl, and R. Rabin. 2009a: An efficient, general-purpose technique for identifying storm cells in geospatial images. J. Ocean. Atmos. Tech., 26, 523-537.

Lakshmanan, V. and T. Smith, 2009b: Data mining storm attributes from spatial grids. J. Ocean. Atmos. Tech, 26, 2353-2365.

Lakshmanan, V., R. Rabin, and V. DeBrunner, 2003: Multiscale storm identification and forecast. J. Atmos. Res., 67, 367-380.

LeMarshall, J. A., A. Rea, L. Leslie, R. Seecamp, and M. Dunn, 2004: Error characterization of atmospheric motion vectors. *Aust. Meteor. Mag.*, **53**, 123-131

Menzel, W.P., 1996: Report from the working group on verification statistics. *Proceedings 3rd International Winds Workshop,* Ascona, Switzerland, 10-12 June 1996, Pages 17-19.

Merrill, R.T., 1989: Advances in the automated production of wind estimates from geostationary satellite imagery. Preprints, *Fourth Conf. on Satellite Meteorology and Oceanography*, San Diego, CA, Amer. Meteor. Soc., 246−249.

Merrill, R.T., W. P. Menzel, W. Baker, J. Lynch, and E. Legg, 1991: A report on the recent demonstration of NOAA's upgraded capability to derive cloud motion satellite winds. *Bull. Amer. Meteor. Soc.*, **72**, 372–376.

Minnis P., P. Heck, D. Young, C. Fairall, and J. Snider, 1992: Stratocumulus cloud properties derived from simultaneous satellite and island-based instrumentation during FIRE. *J. Appl. Meteor*., **31**, 317-339.

Nieman, S.J., W.P. Menzel, C. Hayden, D. Gray, S. Wanzong, C. Velden, and J. Daniels, 1997: Fully Automated Cloud-Drift Winds in NESDIS Operations. *Bull. Amer. Meteor. Soc.*, **78**, 1121–1133

Nieman, S.J., J. Schmetz, and W.P. Menzel, 1993: A comparison of several techniques to assign heights to cloud tracers. *J. Appl. Meteor.*, **32**, 1559−1568.

Otkin, J. A., D. J. Posselt, E. R. Olson, H.-L. Huang, J. E. Davies, J. Li, and C. S. Velden, 2007: Mesoscale numerical weather prediction models used in support of infrared hyperspectral measurements simulation and product algorithm development. *J. Atmospheric and Oceanic Tech.*, 24, 585-601.

Otkin, J. A., and T. J. Greenwald, 2008: Comparison of WRF model-simulated and MODIS-derived cloud data. *Mon. Wea. Rev.*, in press.

Rossow, W.B., F. Mosher, E. Kinsella, A. Arking, M. DeBois, E. Harrison, P. Minnis, E. Ruprecht, G. Seze, C. Simmer, and E. Smith, 1985: ISCCP cloud algorithm intercomparison. *J. Climate Appl. Meteor.*, **24**, 877−903.

Schmetz, J., P. Pili, S. Tjemkes, D. Just, J. Kerkmann, S. Rota, and A. Ratier, 2002: An introduction ot Meteosat Second Generation (MSG). *Bull. Amer. Meteor. Soc.*, **83**, 977-992.

Schmetz, J.K., K. Holmlund, J. Hoffman, B. Strauss, B. Mason, V. Gartner, A. Koch, and L. van de Berg, 1993: Operational cloud-motion winds from Meteosat infrared imagery. *J. Appl. Meteor.*, **32,** 1206-1225.

Schmit, T., M. Gunshor, W.P Menzel, J.Gurka,, J. Li, and A. Bachmeier: 2005 Introducing the next-generation advanced baseline imager on GOES-R. *Bull. Amer. Meteor. Soc.*, Volume **86**, Issue 8, pp 1079-1096.

Shenk, W. E., 1991: Suggestions for improving the derivation of winds from geosynchronous satellites. *Global Planet. Change*, **4**, 165–171.

Simmer, C., E. Raschke, and E. Ruprecht, 1982: A method for determination of of cloud properties from two dimensional histograms. *Ann. Meteor.*, 18, 130-132.

Trucco, Emanuele and Alessandro Verri, 1998: "Introductory Techniques for 3-D Computer Vision", Prentice Hall.

Velden, C.S., and K.M. Bedka, 2009: Identifying the Uncertainty in Determining Satellite-Derived Atmospheric Motion Vector Height Assignments. Weather and Forecasting, Volume 24, Issue 1, pp.76-86.

Velden, C., J. Daniels, D. Stettner, D. Santek, J. Key, J. Dunion, K. Holmlund, G. Dengel, W. Bresky, W.P. Menzel, 2005: Recent innovations in deriving tropospheric winds from meteorological satellites. *Bull. Amer. Meteor. Soc*., 86, 205-221.

Velden, C., D. Stettner, and J. Daniels, 2000: Wind vector fields derived from GOES rapid-scan imagery. *Proc.10th Conf. on Satellite Meteor. and Oceanogr*., Long Beach California, Amer. Meteor. Soc., 20–23.

Appendix 1: Common Ancillary Data Sets

1. LAND_MASK_NASA_1KM

a. Data description

Description: Global 1km land/water used for MODIS collection 5
Filename: lw_geo_2001001_v03m.nc
Origin: Created by SSEC/CIMSS based on NASA MODIS collection 5
Size: 890 MB.
Static/Dynamic: Static

b. Interpolation description

The closest point is used for each satellite pixel:

1) Given ancillary grid of large size than satellite grid
2) In Latitude / Longitude space, use the ancillary data closest to the satellite pixel.

2. SFC_TYPE_AVHRR_1KM

a. Data description

Description: Surface type mask based on AVHRR at 1km resolution
Filename: gl-latlong-1km-landcover.nc
Origin: University of Maryland
Size: 890 MB
Static/Dynamic: Static

b. Interpolation description

The closest point is used for each satellite pixel:

1) Given ancillary grid of large size than satellite grid
2) In Latitude / Longitude space, use the ancillary data closest to the satellite pixel.

3. NWP_GFS

a. *Data description*

Description: NCEP GFS model data in grib format – 1 x 1 degree (360x181), 26 levels
Filename: gfs.tHHz.pgrbfhh
Where,
HH – Forecast time in hour: 00, 06, 12, 18
hh – Previous hours used to make forecast: 00, 03, 06, 09
Origin: NCEP
Size: 26MB
Static/Dynamic: Dynamic

b. Interpolation description

There are three interpolations are installed:

NWP forecast interpolation from different forecast time:

Load two NWP grib files which are for two different forecast time and interpolate to the satellite time using linear interpolation with time difference.

Suppose:

T1, T2 are NWP forecast time, T is satellite observation time, and T1 < T < T2. Y is any NWP field. Then field Y at satellite observation time T is:

$$Y(T) = Y(T1) * W(T1) + Y(T2) * W(T2)$$

Where W is weight and

$$W(T1) = 1 – (T-T1) / (T2-T1)$$
$$W(T2) = (T-T1) / (T2-T1)$$

NWP forecast spatial interpolation from NWP forecast grid points. This interpolation generates the NWP forecast for the satellite pixel from the NWP forecast grid dataset.

The closest point is used for each satellite pixel:

1) Given NWP forecast grid of large size than satellite grid
2) In Latitude / Longitude space, use the ancillary data closest to the satellite pixel.

NWP forecast profile vertical interpolation

Interpolate NWP GFS profile from 26 pressure levels to 101 pressure levels

For vertical profile interpolation, linear interpolation with Log pressure is used:

Suppose:

y is temperature or water vapor at 26 levels, and y101 is temperature or water vapor at 101 levels. p is any pressure level between p(i) and p(i-1), with p(i-1) < p <p(i). y(i) and y(i-1) are y at pressure level p(i) and p(i-1). Then y101 at pressure p level is:

$$y101(p) = y(i-1) + \log(p[i] / p[i-1]) * (y[i] – y[i-1]) / \log (p[i] / p[i-1])$$